

FINAL REPORT

to

DELAWARE RIVER BASIN COMMISSION

25 State Police Drive
PO Box 7360
West Trenton, New Jersey
08628-0360

**SEDIMENTOLOGICAL AND GEOPHYSICAL SURVEY OF THE
UPPER DELAWARE ESTUARY**

by

Christopher K. Sommerfield¹ and John A. Madsen²

¹College of Marine Studies
University of Delaware
700 Pilottown Road
Lewes, Delaware 19958

²Department of Geology
University of Delaware
Penny Hall
Newark, Delaware 19716

October 2003

EXECUTIVE SUMMARY

This document reports the results of a sedimentological and geophysical survey of the upper Delaware Estuary, conducted during 2001–2002 by the University of Delaware (UDel) in cooperation with the Delaware River Basin Commission (DRBC). The purpose of the project was to acquire geologic data pertinent to hydrodynamic and sedimentation models implemented by DRBC to develop a Total Maximum Daily Load (TMDL) for PCBs in the Delaware Estuary. The specific objectives were as follows: (1) to develop an interpretable map of bottom sediment types in the tidal river and estuary; and (2) to quantify recent sedimentation rates at selected depositional sites within the open estuary and fringing tidal marshes. To meet these objectives, the industrialized sector of the river–estuary between Burlington, New Jersey and New Castle, Delaware was systematically surveyed using digital sidescan and chirp sonars. Sidescan sonar provided information on the horizontal distribution of bottom morphologies and sediment types, whereas chirp sonar revealed the vertical extent and continuity of subbottom sedimentary strata and bedrock. A total of 217 kilometers (350 miles) of sonar trackline were collected, covering the estuarine floor at 100 % saturation below the 5-meter isobath. To groundtruth the sonar data, sediment grain-size and porosity measurements were performed on 224 Smith-McIntyre grabs and 25 hydraulically damped cores collected in the survey area. Together, sidescan backscatter patterns and grain-size data were used to render interpretations of bottom sedimentary environment with regard to dominant sediment type and mode of transport. For three open-estuary and six marsh sites (Rancocas Creek, Woodbury Creek, Oldman's Creek, St. George's marsh, Salem River marsh, and Blackbird Creek), sediment chronologies were developed from profiles of the artificial radioisotope Cs-137 ($t_{1/2}=30$ years) to estimate recent sedimentation rates. Chronologies of the natural radioisotope Pb-210 ($t_{1/2}=22.3$ years) were developed for four of the marsh sites for comparison. In addition, sediment inventories of Cs-137 and excess Pb-210 were computed and compared to theoretical values to resolve potential pathways of suspended-particle dispersal and sequestration within the estuary and hydraulically contiguous marshes.

Bottom sediment types in the tidal river and upper estuary area span the full range of grain size, silty clay to gravel, with weight percentages that vary widely both along-

and across-channel, although across-channel variability in sand and mud content clearly increases and decreases, respectively, from DRBC Zone 3 to Zone 5. The down-estuary transition from a dominantly coarse-grained (sand and gravel) to fine-grained (clayey silt to silty clay) bottom occurs near the Zone 4–5 boundary between River Mile 75 and 85. Six general types of sedimentary environments were identified: (1) reworked bottom (three subclasses); (2) fine-grained deposition; (3) coarse-grained bedload; and (4) non-deposition or erosion. By far the most common type is the reworked bottom for which three subclasses (fine grained, mixed grained, and coarse grained) were observed. The process of bed reworking is signified by distinctive bedforms in places, corroborated by non-steady-state distributions of Cs-137 and Pb-210 downcore. Areas of coarse-grained bedload transport, characterized by sandy sediment ripples to waves, are best developed in the tidal river above Philadelphia. Areas of non-deposition or erosion, characterized by patchy bedrock exposures or a coble bottom, are confined to the Tinicum Island–Chester reach. At sites near the Rancocas River mouth and Marcus Hook shoal, an abrupt downcore change from medium-grained sand to estuarine mud was observed, suggesting that transport conditions have changed locally in recent times.

The most significant finding of this study is that fine-grained sediment accumulation within subtidal waters of the upper estuary occurs as discrete depocenters limited to the Marcus Hook–New Castle reach. Historically this segment has been the most sediment-rich of the entire Delaware Estuary and Bay, requiring nearly annual maintenance dredging by the US Army Corps of Engineers (USACE) since about 1945, when the shipping channel was uniformly deepened to 40'. Indeed, the USACE reports that >60% of the *all* the sediment dredged from the Philadelphia–Sea shipping channel is derived from the Marcus Hook–New Castle reach. At the time of the sonar surveys, fluidized mud deposits up to 1-m thick and with a cumulative mass estimated at 3.5×10^5 tons dry weight were present in the shipping channel in the vicinity of Marcus Hook alone. Presence of the short-lived radioisotope Be-7 ($t_{1/2}=53$ days) in cores from this area revealed that these deposits were emplaced rapidly in early 2001. Other fine-grained sediment depocenters were present at the mouth of the Christina River, just south of the Delaware Memorial Bridge.

In addition to its patchy distribution, fine-grained sediment deposition in the subtidal estuary is highly *discontinuous* on decadal timescales as evinced by downcore profiles Cs-137 and Pb-210. Net sedimentation rates estimated from Cs-137 profiles are ≥ 1 cm/yr, yet Be-7 distributions reveal that localized deposition may occur on a seasonal basis at rates approaching centimeters per month. From the sediment chronologies it is concluded that some fraction of material deposited on a seasonal basis is subsequently resuspended and dispersed such that sedimentation rates averaged over longer time spans are considerably lower. In other words, the decadal–centennial sedimentary record of the upper estuary is incomplete, as it archives only a fraction of sediment deposited on shorter timespans. This redistribution process is further evinced by sediment inventories of Cs-137, which are merely 10–14% of the expected post-1954 inventory, and considerably lower than those determined for the tidal marsh sites.

Based on Cs-137 and Pb-210 geochronology, sedimentation rates for the tidal marsh sites ranged from 0.3 to 1.5 cm/yr. Overall, Woodbury Creek, Oldman's Creek, and Rancocas Creek (all freshwater marshes) had the highest sedimentation rates and inventories of Cs-137 and excess Pb-210, revealing that these tributaries are important repositories for fine-grained sediments and adsorbed constituents. In particular, Woodbury Creek appears to be particularly efficient in sequestering suspended matter derived from its watershed, as well as material transported from the open estuary. Detailed studies of sediment transport and deposition within these and other tidal marshes are needed to illuminate their role as sediment sources and (or) sinks in the greater Delaware River-Estuary system.

ACKNOWLEDGEMENTS

A number of individuals contributed to the fruition of this project, which required extensive logistical support in the field and laborious laboratory work. Dr. Thomas Fisklin (DRBC) and Richard Greene (DNREC) were the principal agency contacts who arranged the financial support and oversaw project results as they became available. We appreciate their commitment to the project and flexibility in dealing with the many delays. The sonar surveys aboard the RV *Lear* were facilitated by a generous contribution of boat time by EPA Region III. We thank Charles Apt for making the *Lear* available to the project, and William Muir, James Gougas, and Leonard Mangiaracina who aptly skippered (and repaired) her during the survey. Wayne Spencer of Spencer Oceanographic, Inc. provided indispensable technical expertise during the sidescan and chirp sonar surveys. Dr. Jonathan Sharp of the College of Marine Studies graciously provided sampling time on his RV *Cape Henlopen* cruises during which essential coring and sidescan sonar data were obtained. The following graduate students at the College of Marine Studies made significant contributions to this project: David Walsh, Andrew Klingbeil, Elyse Scileppi, and Tim Cook. Stacey Cochiera, a 2002 undergraduate intern, performed grain-size analyses. In addition, we thank the many Department of Geology undergraduate and graduate students who volunteered on the *Cape Henlopen* research cruises, with special thanks to Lyndon Brown. We are grateful to the captain and crew of the RV *Cape Henlopen* (cruises CH01-28 and CH02-09) who assisted with sediment sampling and seafloor mapping in their characteristically professional manner.

This study, supported by DRBC, was conducted in parallel with a Delaware Sea Grant project that provided considerable resources through grant R/ME-30 (to C. Sommerfield and J. Madsen). The authors gratefully acknowledge the Delaware Sea Grant Program for their support.

TABLE OF CONTENTS

EXECUTIVE SUMMARY	1
ACKNOWLEDGEMENTS	4
1. INTRODUCTION	9
1.1. <i>Study Objectives</i>	9
1.2. <i>Study Area and Previous Work</i>	10
2. SONAR SURVEYS	15
2.1. <i>Sidescan Sonar</i>	16
2.1.1. <i>Principles of Operation</i>	16
2.2. <i>Chirp Sonar</i>	18
2.2.1. <i>Principles of Operation</i>	18
2.2.2. <i>Chirp Instrumentation</i>	20
2.3. <i>Single-Beam Echosounder</i>	20
2.4. <i>Data Reduction and Presentation</i>	20
3. SEDIMENT SAMPLING	21
3.1. <i>Hydraulically Damped Cores</i>	21
3.2. <i>Smith-McIntyre Grabs</i>	22
4. ANALYTICAL METHODS	23
4.1. <i>Water Content and Porosity</i>	23
4.2. <i>Grain-Size Analysis</i>	23
4.3. <i>Radioisotope Measurements</i>	25
5. RESULTS AND INTERPRETATION	27
5.1. <i>Sonar and Bottom Sampling Coverage</i>	27
5.2. <i>Sidescan Backscatter</i>	40
5.3. <i>Sediment Physical Properties</i>	42
5.3.1. <i>Porosity</i>	42
5.3.2. <i>Grain Size</i>	42
5.4. <i>Sedimentary Environments</i>	48
5.5. <i>Subbottom Observations</i>	62
5.5.1. <i>Features of Note</i>	62
5.6. <i>Radioisotope Profiles and Sedimentation Rates</i>	70
5.6.1. <i>Reconnaissance Cs-137 Measurements</i>	70
5.6.2. <i>Seasonal Deposition in the Estuary</i>	73

5.6.3. <i>Marsh and Floodplain Sediment Accumulation</i>	74
5.6.4. <i>Radioisotope Inventories</i>	77
6. CONCLUSIONS	81
7. REFERENCES	84
APPENDIX A. SONAR TRACKLINE DATA	88
APPENDIX B. GIS DATABASE ON CD-ROM	91
APPENDIX C. SEDIMENT SAMPLING STATIONS	95
APPENDIX D. WATER CONTENT AND POROSITY DATA	104
APPENDIX E. GRAIN SIZE DATA	111
APPENDIX F. CS-137 AND PB-210 ACTIVITIES	118

LIST OF TABLES

TABLE 1.	Timeline of Major Tasks.....	10
TABLE 2.	Backscatter Mosaic Names and Locations.....	40
TABLE 3.	Sedimentary Environments Classification.....	49
TABLE 4.	Push Core Locations.....	72
TABLE 5.	Sediment Accumulation Rates and Radioisotope Inventories.....	79

LIST OF FIGURES

Figure 1.	Location map of the study area	11
Figure 2.	Schematic of the sidescan sonar method.....	17
Figure 3.	Schematic of the chirp sonar method.....	19
Figure 4.	Sediment grain-size classification.....	24
Figure 5.	Survey Area Map 1.....	28
Figure 6.	Survey Area Map 2.....	29
Figure 7.	Survey Area Map 3.....	30
Figure 8.	Survey Area Map 4.....	31
Figure 9.	Survey Area Map 5.....	32
Figure 10.	Survey Area Map 6.....	33
Figure 11.	Survey Area Map 7.....	34
Figure 12.	Survey Area Map 8.....	35
Figure 13.	Survey Area Map 9.....	36
Figure 14.	Survey Area Map 10.....	37
Figure 15.	Survey Area Map 11.....	38
Figure 16.	Survey Area Map 12.....	39
Figure 17.	Sidescan sonar coverage map.....	41
Figure 18.	Downcore porosity profiles.....	43
Figure 19.	Results of grain-size analysis	44
Figure 20.	Photographs of cores C-3A and C-11B.....	46
Figure 21.	Plots of grain-size trends	47
Figure 22.	Sedimentary Environments Map 1.....	50
Figure 23.	Sedimentary Environments Map 2.....	51
Figure 24.	Sedimentary Environments Map 3.....	52
Figure 25.	Sedimentary Environments Map 4.....	53
Figure 26.	Sedimentary Environments Map 5.....	54
Figure 27.	Sedimentary Environments Map 6.....	55
Figure 28.	Sedimentary Environments Map 7.....	56
Figure 29.	Sedimentary Environments Map 8.....	57
Figure 30.	Sedimentary Environments Map 9.....	58
Figure 32.	Sedimentary Environments Map 11.....	60
Figure 33.	Sedimentary Environments Map 12.....	61
Figure 34.	Sonar Line 103	63
Figure 35.	Sonar Line 39	65
Figure 36.	Fluid-mud distribution map.....	66
Figure 37.	Sonar Line 122	67

Figure 38. Sonar Line 34	68
Figure 39. Bedrock occurrence map	69
Figure 40. Locations of cores analyzed for radioisotopes.	71
Figure 41. Cs-137 activity profiles for estuary and marsh cores	75
Figure 42. Cs-137 and Be-7 activity profiles.....	76
Figure 43. Profiles of excess Pb-210 activity	78

1. INTRODUCTION

1.1. Study Objectives

In cooperation with the Delaware River Basin Commission (DRBC), Delaware Department of Natural Resources and Environmental Control (DNREC), and Environmental Protection Agency Region III (EPA), a sedimentological and geophysical study of the upper Delaware Estuary was conducted during 2001–2002 by researchers from the College of Marine Studies and the Department of Geology, University of Delaware. The overarching objective of this project was to assist DRBC in identifying sediment depositional zones within the upper estuary, and to quantify rates of accumulation, ultimately to help constrain the loading history of toxic compounds from point and non-point sources (DRBC, 1998). The specific goals were to: (1) generate a comprehensive map of sedimentary environments with respect to bottom morphology and sediment type, and (2) develop sediment chronologies for select muddy depositional sites revealed through sonar observations or otherwise specified by DRBC. To accomplish these goals, extensive sidescan and chirp sonar surveys and sediment sampling of the estuarine floor and shallow subbottom were conducted aboard the RV *Cape Henlopen* (University of Delaware) and the RV *Lear* (EPA) between April and December of 2001. Sidescan and chirp sonars were used to obtain acoustic remote sensing data on bottom sedimentary environments and identify regions of fine-grained sediment deposition, i.e., possible pollutant depocenters. Downcore distributions of the radioisotopes Cs-137 and Pb-210 were measured at these sites to estimate recent sedimentation rates.

Initial radioisotope measurements at several sites within the subtidal estuary revealed that the most recent sedimentary record is incomplete and therefore unable to yield unambiguous sediment chronologies. As a substitute, selected tidal marsh and river-floodplain sites in Delaware and New Jersey assumed (and later confirmed) to be amenable to radioisotope geochronology were visited between March and July 2002 for push-core sampling. Interim results of this study were presented at the 2002 Geological Society of America meeting (Sommerfield and Madsen, 2002), as well as at the 2002 TMDL Symposium in Philadelphia. A timeline of the field and laboratory components of this study is provided in Table 1.

Table 1. Timeline of major tasks

Task (2001–2002)	J	A	S	O	N	D	J	F	M	A	M	J	J	A	S	O	N	D	
CH0103&7 coring	X																		
Sonar surveys		X		X		X													
CH01-28 coring					X														
Marsh coring								X	X	X	X	X	X						
Labwork	X	X	X	X	X	X	X	X	X	X	X	X	X						
Sonar data analysis							X	X	X	X	X	X	X	X	X				
Grain size analysis											X	X	X	X	X				
Reporting															X	X	X	X	

1.2. Study Area and Previous Work

The Delaware Estuary between Crosswicks Creek, New Jersey, southward to the Smyrna River, Delaware, was the area targeted for study (Figure 1). This region falls within DRBC Zones 2–6, between river miles (RM) 133.4 and 48.2 relative to the Bay mouth (RM 0). The sidescan and chirp sonar surveys were limited to subtidal waters of Zones 2–5, the industrialized corridor between Burlington, New Jersey, and New Castle, Delaware. Sediment coring was conducted within a broader range of subtidal estuarine, intertidal marsh and floodplain settings.

The northern boundary of the survey area falls within a transition from purely fluvial to estuarine sedimentary environments. The Burlington–Philadelphia reach is tidal freshwater (0–0.5 PSU), whereas oligohaline conditions (0.5–5 PSU) prevail between Philadelphia to New Castle. Accordingly, in this report "tidal river" refers to the region between Trenton and Philadelphia, whereas "upper estuary" denotes the Philadelphia to New Castle segment. The estuarine turbidity maximum, a quasi-stationary zone of elevated suspended-sediment concentration, typically extends from the Zone 4–5 boundary near Chester to the lower estuary off the Cohansey River, New Jersey. The mean tidal range at Burlington and New Castle is 1.6 m and 2.2 m, respectively, relative to mean lower low water (MLLW). Maximum tidal-current velocities in the tidal river and upper estuary are on the order of 1–1.5 m/s (C. Sommerfield, unpublished data).

The morphology and sedimentology of the modern Delaware Estuary floor

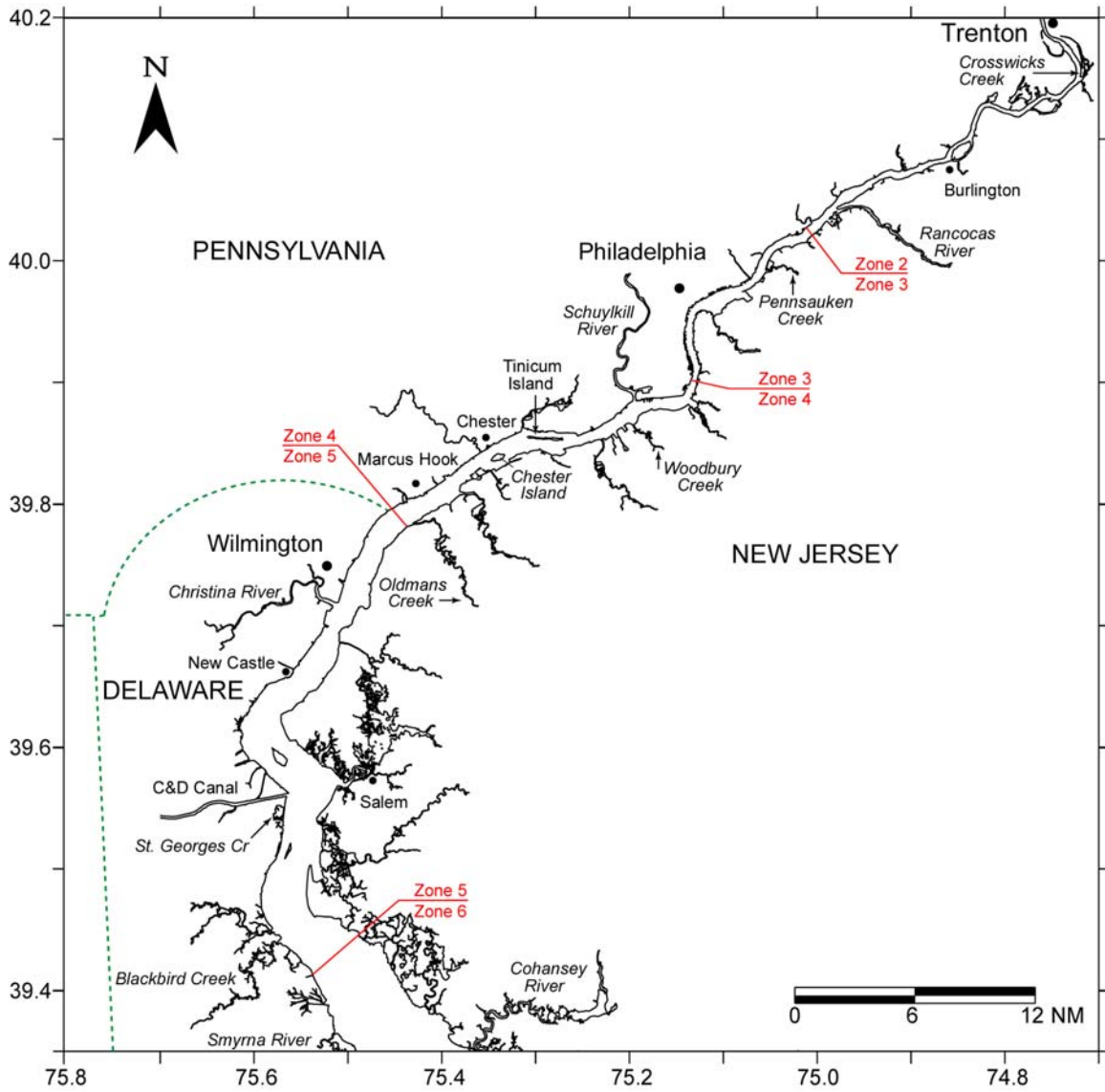


Figure 1. Location map of the study area showing geographic features and DRBC zones.

reflects both the geologic framework of the ancestral river valley, as well as fluvial–estuarine sedimentation during the Holocene Epoch (past 10,000 years). From Trenton to Wilmington the Delaware River flows along the Fall Line, the geologic boundary between Piedmont Lowland and Atlantic Coastal Plain physiographic provinces to the northwest and southeast, respectively (Parker et al., 1964). The river deeply incises consolidated and unconsolidated sedimentary strata and crystalline rocks of the broader Delaware River valley, cut and filled during multiple sea-level regression–transgression cycles since Miocene times (Newell et al., 1998; Owens and Denny, 1979). The most recent cycle was associated with the Wisconsinan glacial, reaching its maximum 18,000 years ago, and continental flooding during the ensuing deglaciation. The most recent phase of fluvial–estuarine sedimentation commenced about 8,000 years ago when rising seas began to inundate lowlands adjacent to the ancestral Delaware River near the modern Delaware Bay mouth (Fletcher et al., 1990).

Modern (Holocene) sediments in the Delaware River and Estuary are derived from three major sources: (1) tributary discharge from the Pennsylvania–Delaware and New Jersey sides of the river, (2) erosion of subaqueous Pleistocene–Cretaceous strata and crystalline bedrock, and (3) up-estuary transport of suspended particles from the bay and Atlantic Ocean. An estimated 1.4 million metric tons of suspended silt and clay enter the Delaware Estuary from rivers on an annual basis; bedload delivery of sand and gravel is far more difficult to quantify but may comprise 10–15% of the total suspended load (Mansue and Commings, 1974). Modern bottom sediments are generally <10 m thick and overlie the Cape May Formation, late Pleistocene marginal-marine sediments comprising the greater volume of Delaware River valley fill (Newell et al., 1998). The Cape May Formation is composed of multiple subunits of gravel, sand, clayey silt, and peat, material that accumulated in former estuarine, beach and inner-shelf environments. The thickness of this formation increases down estuary from <5 m at Burlington, New Jersey, to ~30 m at the upper Delaware Bay, where it extends laterally into New Jersey (Newell et al., 1998). The late Pleistocene deposits unconformably overlie unconsolidated Cretaceous non-marine strata including the Magothy, Raritan, and Potomac Formations in descending order. The Cretaceous strata, composed of alternating beds of gravel, sand, silt and clay, are truncated along the width of the greater

river valley, and dip to the southeast toward the Atlantic Ocean. Cretaceous formations lap on to crystalline rocks of the Pennsylvanian Piedmont and are known to crop out locally in the upper estuary. Piedmont bedrock of the Wissahickon Formation (schist) is present 2–3 m below the riverbed adjacent to the mouth of the Rancocas River and at Petty Island. Along a 50 km reach between Tinicum Island and Marcus Hook, Wissahickon and Wilmington Complex rocks (gabbro) are present at, or within 10 m of, the estuary floor (Duran, 1986; Lyttle and Epstein, 1987; Mansue and Commings, 1974; Schenck et al., 2000).

The bottom morphology of the tidal river and upper estuary is a compound, steep-sided channel flanked by relatively flat subtidal shoals. The channel bottom ranges in depth from 6–12 m MLLW at the thalweg to 5.5–6 m at the channel–shoal transition. The shore-to-shore width of the estuary increases from ~336 m at RM 120 (Burlington) to ~2,288 m at RM 72 (New Castle), and the overall mean water depth in this region is ~6.5 m. The shoals extend from 0 to 6 m water depths and have gentle bottom slopes (1:20–1:1200) that generally steepen with distance upriver of Philadelphia. Of the total 103 km² shore-to-shore surface area between Burlington and New Castle, the subtidal shoals and natural channel comprise 36.1 km² (35.1 %) and 55.1 km² (53.6 %), respectively. The total length of shoreline in this reach is 177.7 km, 135.6 km (76.3 %) of which is bulkheaded.

The shipping channel maintained by the Philadelphia District of the U.S. Army Corps of Engineers (USACE) incises the natural estuarine channel and is dredged to a nominal depth of 12.2 m (40') MLLW. The shipping channel between Burlington and New Castle occupies a surface area of 11.6 km², 11.2 % of the 103 km² total. Between Philadelphia and New Castle the channel infills so rapidly that continual maintenance dredging is required to render it navigable. On an annual basis over 60 % of *all* of the sediment dredged between Trenton and Delaware Bay mouth is derived from the Philadelphia–New Castle reach (USACE, 1973). From results of hydrographic studies in the late 1960's, the USACE concluded that the rapid shoaling within this reach is caused by deposition of suspended sediment transported from down-estuary erosional sources, rather than from virgin sediment supplied annually from the watershed (USACE, 1973); however, the relative contributions of these sources and the actual trapping mechanisms

were not identified. At the time of the UDel sonar survey in August 2001, the shipping channel was clear in places, infilled in others, and USACE dredging operations were underway between Wilmington and New Castle.

Although bottom sediment types in the Delaware Estuary have been examined previously, the overall sampling coverage is generally spotty, and the methods of grain-size analysis are inconsistent among studies (USACE, 1973; Oostdam, 1971; Biggs and Beasley, 1988). Between the Rancocas River and Marcus Hook, bottom sediments are mapped simply as "sand" and "silt" (Duran, 1986; USACE, 1973), whereas from Marcus Hook to New Castle the bottom is described as "clay" (Duran, 1986) and "mud" (Biggs and Beasley, 1988). A gradual transition from fluvial sands and gravels to dominantly muds (<63 μm grain size) is reported to occur between Philadelphia and Chester (USACE, 1973), a change that may manifest particle aggregation (flocculation) and rapid deposition within the turbidity maximum (Biggs et al., 1983). An aim of the present study was to build on the previous work by performing a systematic, high-resolution characterization of the bottom based on sonar mapping data, sediment sampling and analysis, and a regular classification scheme.

Sedimentation rates for subtidal environments of Delaware Estuary have been determined locally, but the published data are sparse in comparison to neighboring estuaries of the Mid-Atlantic region (Olsen et al., 1993). In part this is due to coarse grain size and intense tidal resuspension in the Delaware, factors that limit the utility of traditional sediment chronometers such as Pb-210, Cs-137, and Pu-239,240. Another complication is the extent of dredging, which since the early 1900's has removed much the historical sedimentary record in the vicinity of the shipping channel, and which may have had far-field impacts on the river-estuary system. For example, it is well known that by increasing the cross-sectional area of the estuarine channel, dredging has indirectly increased the native tidal range at Philadelphia by ~ 0.3 m and 1.3 m at Trenton (Nichols, 1988; DiLorenzo et al., 1993).

Considerably more information on sedimentation rates is available for fringing tidal marsh and floodplain environments of the Delaware Estuary. Based on Pb-210 and Cs-137 geochronologies for four New Jersey freshwater marshes, Orson et al. (1992) reported sediment accumulation rates ranging from 0.7 to 2.2 cm/yr. These rates are

somewhat higher than the 0.20–0.68 cm/yr reported for southern Delaware salt marshes (Church and Lord, 1981; Kraft et al., 1992; Kim et al., 1997; Nikitina et al., 2000), perhaps as a consequence of different sediment supply and depositional conditions.

2. SONAR SURVEYS

Three types of acoustic mapping tools were used to image the estuarine floor and shallow subbottom: (1) sidescan sonar; (2) chirp sonar; and (3) single-beam echosounding. Sidescan sonar provided information on the lateral distribution of bottom types and morphologies, chirp sonar resolved the thickness and horizontal continuity of subbottom sedimentary strata and bedrock, and the echosounder provided accurate bottom depths relative to the water surface. The sidescan and chirp towfish were towed in tandem from the vessel ~3–4 m below the water surface at speeds of 3–5 knots, whereas the echosounder transducer was pole-mounted to the stern.

A total of 350 miles of sonar data were collected along 122 tracklines during 17 days between August and December 2001, though most of the work was completed between August 13th and 24th. The survey was conducted aboard the RV *Lear*, a 35' vessel maintained by EPA Region III for aquatic sampling. The tracklines were established at 100 m intervals regularly spaced along-river and approximately 2 km apart across-river to cover the bottom at 100 % saturation with sidescan, which was configured for a 200-m wide swath. In this manner the same area of bottom was covered twice, once on the inner and again on the outer lanes of adjacent survey tracks. As a result, a continuous record of acoustic backscatter was obtained in the study area for water depths in excess of 5 m. Shallower waters posed multiple hazards to navigation and therefore were not mapped. Details on individual sonar tracklines data are tabulated in Appendix A.

Geographic position (i.e., latitude and longitude) during the sonar survey was determined using a Leica MX412B Differential Global Positioning System (DGPS) receiver interfaced with the three sonars. Position data were logged by the sonar acquisition software at one-second intervals and are considered accurate to within ± 5 m. During survey operations Nobeltec™ navigation software was used to display real-time vessel position relative to predetermined survey tracklines.

2.1. Sidescan Sonar

2.1.1. Principles of Operation

The main purpose of sidescan sonar is to provide high-resolution acoustic images (sonographs) of the seafloor that can be interpreted to glean information on geologic properties (Johnson and Helferty, 1990). Sidescan sonars emit a fan-shaped beam of sound to either side of a towfish, the sound source and receiver (Figure 2). The beam is wide in the across-track direction, typically 3–10 times the survey water depth, and narrow along-track. The beam geometry allows for broad areas of the bottom to be imaged in a single pass, an asset in regional seafloor studies. Sidescan sonars detect sound that is backscattered (i.e., diffracted) from the bottom, not reflected as with echosounders or subbottom seismic profilers. The amplitudes of acoustic returns are recorded as variations in transducer voltage and then translated into pixel values and corresponding greyscale tones on sonographs. The amount of outgoing acoustic energy reradiated back in the direction of the transducers varies in a complex manner with the amount penetrating the seafloor as a function of the sound frequency, bottom hardness, and microtopography, a property generally known as “roughness”. Bottom roughness is actually a composite of elements that may range in scale from single grains (millimeters) to bedforms such as sand waves (meters). All other factors equal, rough bottoms are more efficient backscattering mediums than smooth bottoms and elicit higher amplitude returns at the sidescan receiver.

Sidescan backscatter conveys information on bottom geologic properties at two distinct spatial scales. At scales of several decimeters to a few meters, bedforms such as sediment waves and lineations provide information on local hydrodynamics and sediment type. On multi-kilometer scales, backscatter intensity typically tracks bottom roughness related to geologic structure, grain-size trends, and bed morphology. Together, small- and large-scale backscatter patterns can be interpreted to characterize bottom sedimentary environments with regard to dominant sediment type, transport mode, and dispersal pathways.

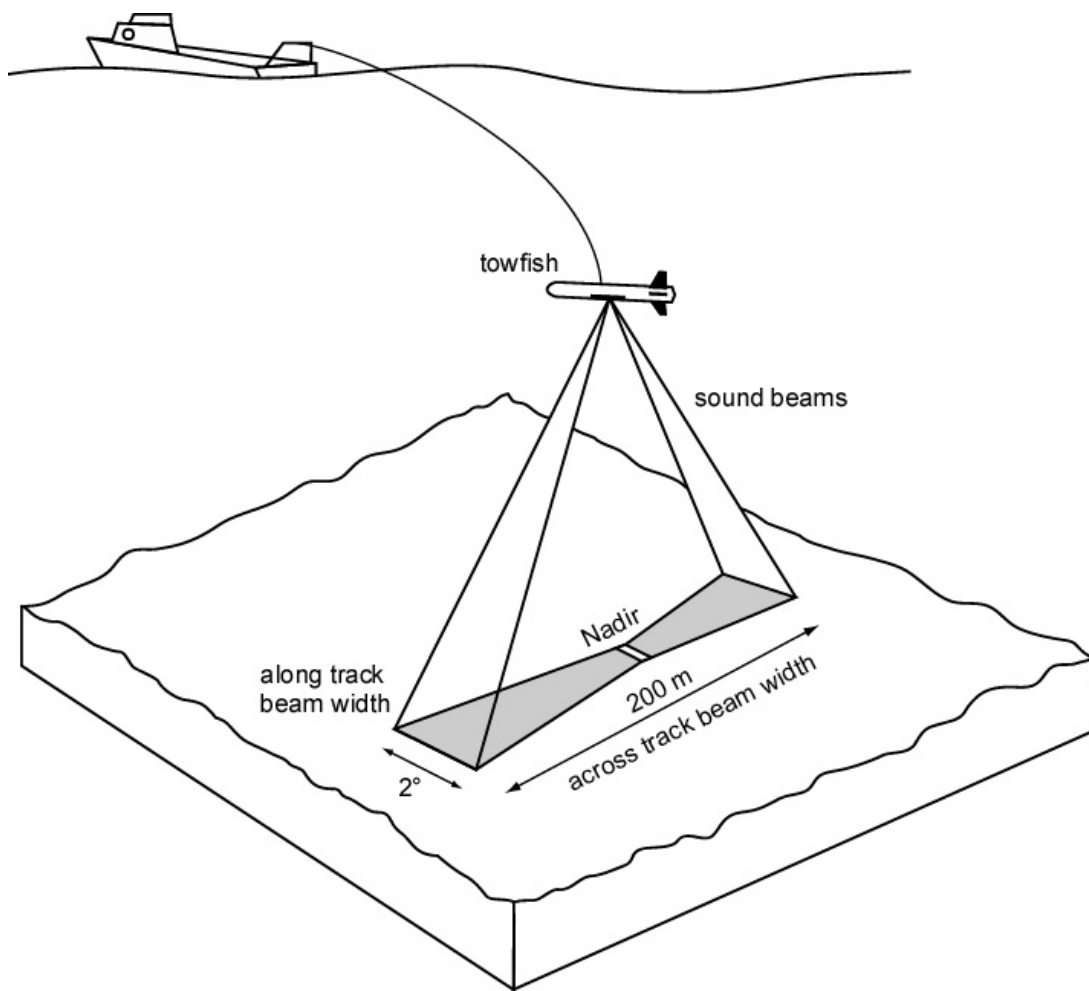


Figure 2. Schematic of the sidescan sonar method.

2.1.2. Sidescan Instrumentation

The major components of sidescan systems include: a sound source and receiver (towfish), a communications cable and tow member, a topside data-acquisition and processing computer, and a printer for generating sonograph hardcopies. The system used for the Delaware Estuary survey was an Edgetech DF1000 towfish and an EdgeTech 516D topside computer module running Triton Elics Isis sonar acquisition software. The DF1000 is a digital, dual-frequency system (100 and 500 kHz) that automatically corrects for vessel speed and slant range, referencing sonar recordings to geographic position using integrated differential geographic positioning (DPGS) data. Time-varied gain and a beam-angle correction applied in Isis effectively removes the sonar-beam pattern and greatly improves clarity and resolution of the sonographs. The side-looking range was set to 100 m for a total cross-track swath of 200 m. At a maximum vessel speed of 5 knots, this configuration yielded a theoretical along-track resolution of ~30 cm, i.e., objects greater than 30 cm apart were resolved. Hardcopies of the 100 kHz sonographs were printed on thermal film during acquisition using an EPC HSP-100 thermal plotter. All sidescan data were recorded digitally on CD ROM for post-survey processing, reproduction, and archival.

2.2. Chirp Sonar

2.2.1. Principles of Operation

Chirp seismic profilers generate high-resolution cross-sectional images of the seafloor subbottom to depths of ~5–30 m. The chirp is a wide-band FM sound pulse, linearly swept over a full spectrum frequency range between 2 and 12 kHz. The transmitted sound pulses travel through the water column and seabed, reflecting back toward the source when the pulse encounters changes in acoustic impedance, the product of sonic velocity and sediment bulk density (Figure 3). Reflected sound pulses are recorded digitally by the profiler as a function of their two-way travel time. Because acoustic reflecting boundaries almost always occur at interfaces between different geologic materials, so-called seismic discontinuities, spatial changes in the continuity and geometry of discontinuities can be used to interpret subbottom structure and stratigraphy. The theoretical minimum vertical resolution of chirp (based on the 12 kHz frequency) is about five centimeters, although 2–3 decimeters is more typical in practice.

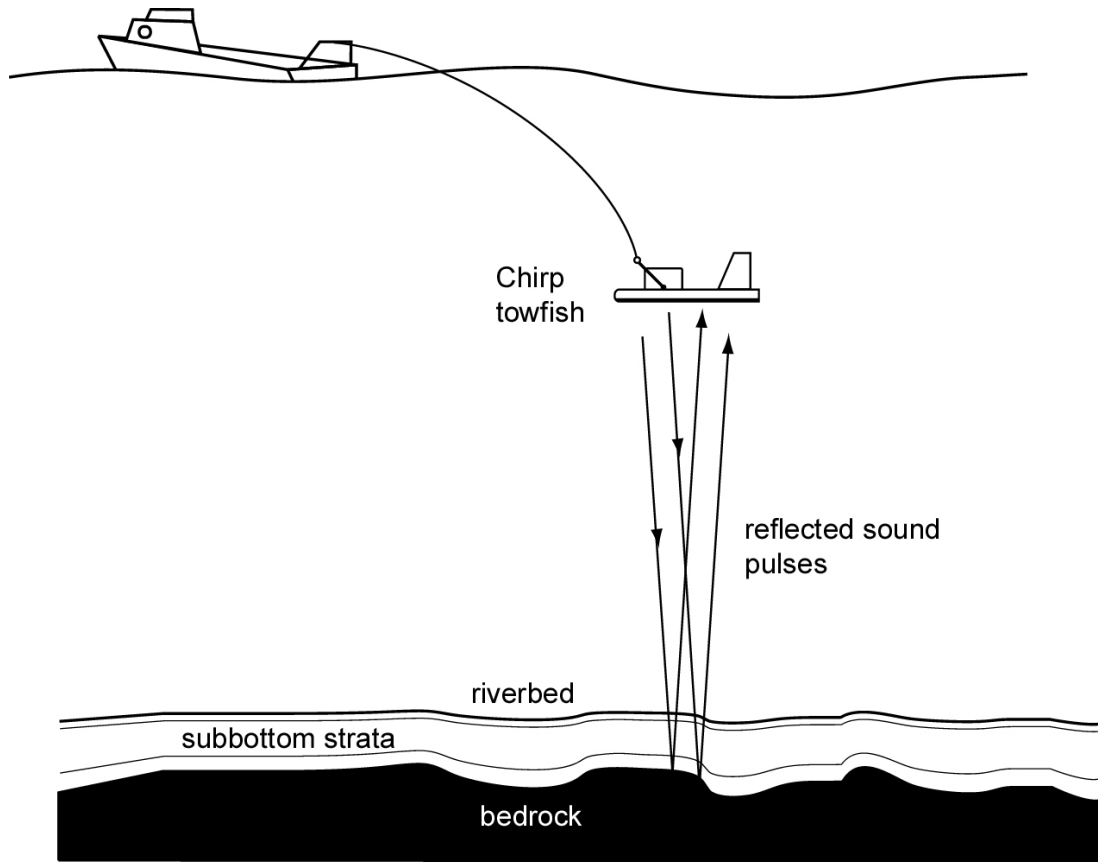


Figure 3. Schematic of the chirp sonar method.

2.2.2. Chirp Instrumentation

An Edgetech X-STAR sonar system with a SB-216S towfish was used to collect chirp profiles of the subbottom. The SB-216S was towed ~10 m aft on the starboard side of the R/V *Lear*, whereas the sidescan towfish was towed from the port side. The SB-216S was configured to emit a sound pulse with a frequency of 2–12 kHz frequency at an interval of 8 cycles per second. At an average vessel speed of 3–5 knots, this sampling frequency yielded a theoretical trace resolution (i.e., layer thickness) on the order of 20–30 cm. In terms of subbottom range, sonar reflections from material interfaces were observed to a maximum depth of ~10 m below the riverbed in places. All data were recorded with co-registered with DPGS positional data on DAT tape and later printed on thermal paper.

2.3. Single-Beam Echosounder

Accurate bathymetric data (water depth) were collected during the survey to aid navigation of the towed instrumentation and subsequently to augment interpretation of the chirp profiles and sidescan sonographs. A Knudson 320 B/P dual-frequency (25/200 kHz) echosounder integrated with a DGPS signal was used during the entire survey to record geographically referenced bathymetric data at a sampling frequency of 100 milliseconds. The data were recorded digitally and stored on CD ROM for further processing. Although the echosounder provided essential hydrographic information during survey operations, because the soundings were not tide-corrected at the time of this writing, they are not presented herein. Alternatively, a complete set of National Ocean Service depth soundings for the study area (NOS, 1998) are included in the data CD accompanying this report.

2.4. Data Reduction and Presentation

Sidescan data reduction involved the following standard procedures: 1) slant-range correction, 2) beam-angle correction, 3) contrast normalization, and 4) creation of an acoustic backscatter mosaic. The software package Sonar Web Pro™ was used to process the sidescan data and mosaic the sonographs. The data were processed at a horizontal resolution of 1 m, sufficient to resolve small bedforms. Overall, twelve individual georeferenced backscatter mosaics in GeoTIFF format were created. These images were then exported to ARC MAP, a geographic information system (GIS)

platform, in which they were merged to create a composite backscatter mosaic (for the entire survey area) on which other types of data may be displayed. A description of the GIS database that accompanies this report is provided in Appendix B.

A default sonic velocity of 1500 m/s was used by the chirp processing software to convert acoustic travel time to linear depth. However, it should be noted that velocities of 1600–1700 m/s are in fact more representative for shallowly buried marine strata in general. The chirp profiles were interpreted by manually tracing seafloor and subbottom reflections along their lateral extent. Because seismic profiling datasets are notoriously difficult to display in report format, only a selection of subbottom profiles are presented herein.

3. SEDIMENT SAMPLING

A suite of bottom sediment samples were collected at subtidal estuarine sites to (1) determine the physical basis for mapped patterns of acoustic backscatter, and (2) develop downcore sediment chronologies with Cs-137 and Pb-210, where applicable. Additional cores were collected at selected marsh site for sediment geochronology. The geographic locations and collection dates of all cores and sediment grab samples are tabulated in Appendix C and are also displayed in the GIS database.

3.1. Hydraulically Damped Cores

A hydraulically damped corer (HDC) was used to collect undisturbed sediment cores in the estuary for chronological studies. The HDC works by advancing a 1-m long, 15-cm diameter polycarbonate barrel into the bed under 350-kg of weight at a rate controlled by a hydraulic piston. Typical cores lengths are 25–50 cm in fine- to medium-grained sands, 50–70 cm in muds. The slow rate of entry reduces disturbance to the sediment-water interface, thereby preserving the stratigraphic integrity of low-density deposits.

A total of 21 HDC samples were collected in April and June 2001 during RV *Cape Henlopen* cruises CH0401 and CH0701, respectively, between Pennsauken Creek and New Castle. An additional 46 HDC samples were recovered farther down-estuary during cruise CH01-28 in November 2002. Upon recovery, the core barrels were capped, labeled, and stored cold. In the laboratory, the cores were extruded vertically and

sectioned in continuous, 2-cm thick intervals using stainless-steel spatulas. Sediment in contact with core liner was trimmed and discarded to avoid material potentially pushed downward during the coring process, and the spatulas were cleaned of mud after each slice to prevent cross-contamination. Roughly half of each sample (~100 grams wet weight) was placed in a labeled plastic bag and frozen for PCB analysis, whereas the other half was processed for radioisotope measurements at the College of Marine Studies.

3.2. Smith-McIntyre Grabs

A Smith-McIntyre grab sampler was used to obtain bed material for grain-size analysis; grab sampling is a rapid way to collect surficial sediments when stratigraphic preservation is not necessary. The Smith-McIntyre samples a 30x30 cm area and removes a semi-circular scoop of bed sediment, ~20-cm deep, using spring-loaded buckets. A seal at the top of the device prevents sample washout upon ascent from the bottom. During cruise CH01-28, a total of 163 bottom-grab samples were collected between the Pennsauken Creek and New Castle, and an additional 94 grabs were collected between New Castle and Port Mahon, Delaware, during cruise CH02-09 in June 2002. The CH01-28 grabs were collected along 36 cross-river transects, spaced about 2 km apart, to determine the along- and across-estuary variability in sediment grain size. Upon recovery of the sampler, a 1-liter volume of sediment was removed, photographed, and stored in a plastic jar until analysis in the laboratory.

3.3. Push Cores

Simple push cores were used to collect marsh and floodplain deposits for radioisotope geochronology during six separate trips between February and August 2001. Small-boat and on-foot excursions were required access the coring sites. At each site a 4-inch diameter PVC tube was affixed with a piston hung from a tripod and winch assembly and then pushed or hammered into the ground. The piston minimized shortening of the sediment column as the core tube penetrated the ground, whereas the winch facilitated extraction. Cores 70–100 cm in length were easily recovered in this manner. Cores were capped and labeled in the field and transported upright to the laboratory, where they were extruded and sectioned as described above. Sediment subsamples not immediately processed for radioisotope measurements were placed in sterile plastic bags and stored in a freezer.

4. ANALYTICAL METHODS

4.1. Water Content and Porosity

Water content and porosity were determined gravimetrically on core subsamples as part of the processing protocol for radioisotope measurements. Approximately 200 g of wet sediment from each 2-cm core interval was weighed, oven dried at 100° C for 24 hours, and reweighed. Water content (W_c) in percent was determined from:

$$W_c = \left(\frac{W_w}{W_s + W_w} \right) \cdot 100\% \quad (1)$$

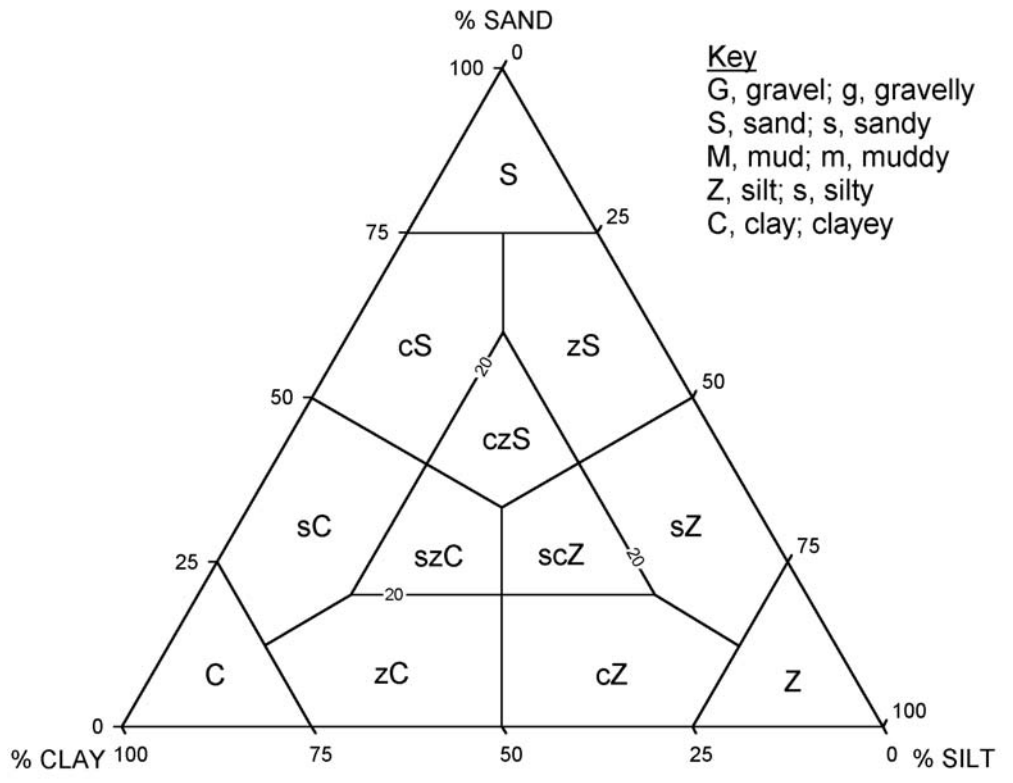
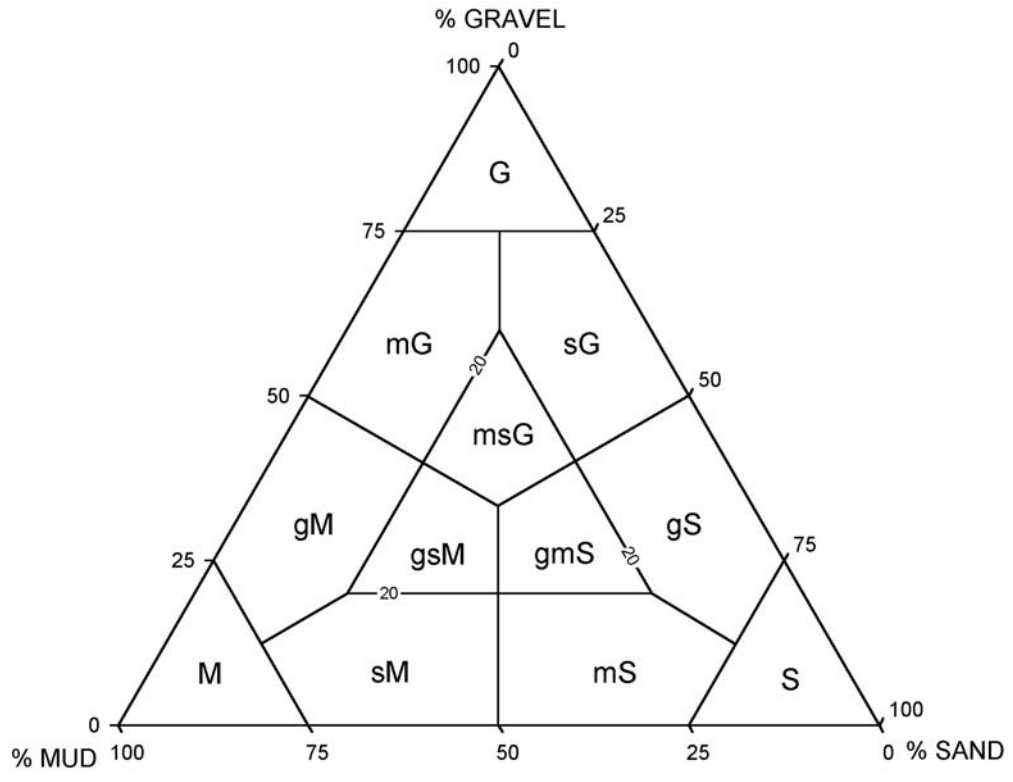
where W_w and W_s are the wet weight and dry sediment weights (corrected for salt content), respectively. Porosity (ϕ) was computed from fractional water content ($W_c/100$) and measured values of water (ρ_w) and mineral density (ρ_s) from:

$$\phi = \left(\frac{(W_c \rho_s)}{(W_c \rho_s) + (1 - W_c) \rho_w} \right) \cdot 100\% \quad (2)$$

4.2. Grain-Size Analysis

Sediment grain-size analysis was carried out on the grabs to determine the lateral variability of bottom types. Weight percentages of gravel, sand, and mud (silt+clay) were determined using a combination of standard techniques described in (Folk, 1974). First, 25 g of sediment was wet-sieved through nested 2 mm and 63 μ m sieves using a solution of deionized water and sodium metaphosphate dispersant, separating gravel (>2 mm diameter), sand (<2mm but > 63 μ m diameter), and mud (<63 μ m diameter). Gravel and sand fractions were dried in an oven at 110° C for 24 hours and weighed. Next, the sediment and wash water that passed through the 63 μ m sieve was collected in a 1000 ml graduated cylinder, and a standard pipette analysis was performed to determine the relative amounts of silt and clay. The results of the sieving and pipette analyses were combined to determine weight percentages of individual size fractions relative to the total dry weight of the sample.

Two ternary schemes following Trefethen (1950) were used to group the grain-size data into sediment-type classes: (1) weight percent gravel, sand, and mud, and (2) weight percent sand, silt, and clay for samples devoid of gravel (Figure 4).



Key
 G, gravel; g, gravelly
 S, sand; s, sandy
 M, mud; m, muddy
 Z, silt; s, silty
 C, clay; clayey

Figure 4. Sediment grain-size classification.

Note that very large grains (>6 cm diameter) were removed by hand prior to analysis to prevent biasing of grain-size weight percentages and corresponding classifications. This practice was also required in places where a scattering of large pebbles (>6 cm diameter) or cobbles (>13 cm) were present atop a dominantly sandy or muddy substrate. At sites where the sampler recovered cobble or rock fragments too large for grain-size analysis, the bottom was classified as rock (R).

4.3. Radioisotope Measurements

Sediment accumulation rates were estimated from downcore profiles of the artificial radionuclide Cs-137 ($t_{1/2}$ =30 years), a product of nuclear fission. The penetration depth of Cs-137 in the sediment column relative to its well-known source function may be used estimate net accumulation rates averaged over the past several decades. Cesium-137 fallout was first detected in the environment around 1954, peaked in 1963–1964, and thereafter dropped to insignificant levels by 1980 (Monetti, 1996). Whereas marsh surfaces collect Cs-137 through precipitation and dry deposition, Cs-137 scavenged by suspended particles in the estuarine water column is delivered to bottom sediments via deposition. Another source of Cs-137 to estuarine waters is erosion from watershed soils, the so-called "wash-in" effect. Overall, Cs-137 distributions in estuarine sediments reflect both the regional fallout history and local sedimentary processes. Effective across a wide range of aquatic environments (Ritchie and McHenry, 1990), the Cs-137 technique has been successfully employed in estuaries throughout the Mid-Atlantic region (Olsen et al., 1993).

A sediment accumulation rate representative for the past several decades can be computed from Cs-137 activity-depth profiles using:

$$S = \frac{L}{T_2 - T_1} \quad (3)$$

where S (cm/yr) is the sediment accumulation rate, L (cm) is the depth of measurable Cs-137 activity below the sediment-water interface (or land surface), T_1 (yr) is the year of Cs-137 onset (1954) or peak fallout (1964) in the environment, and T_2 (yr) is the date of

core collection. This method assumes that Cs-137 is chemically immobile within the sediment column, and that the first appearance of Cs-137 is concordant with 1954.

Where applicable, sedimentation rates were also estimated from excess activity profiles of Pb-210 ($t_{1/2}=22.3$ years), a natural radioisotope of the U-238 decay series. Lead-210 is produced via Rn-222 decay in the atmosphere and deposited on the continents and surface water in the form of precipitation and dry deposition. Lead-210 is also produced in aquatic waters through *in situ* decay of Rn-222; because U-238 is enriched in seawater relative to freshwater, the standing crop of Pb-210 in marine and brackish waters is typically much larger than in lakes and rivers. In addition, relatively low (background) levels of Pb-210 are produced in the sediment column via decay of Rn-222 *in situ*, known as the "supported" activity. Dissolved Pb-210 scavenged by fine-grained particles in the water column is deposited at the seafloor and concentrated in the uppermost sediment column relative to the supported activity. This "excess" Pb-210 activity decays to background at a rate determined by its 22.3 yr half-life. At steady state, the profile of excess Pb-210 activity with sediment depth represents a balance between the Pb-210 depositional flux and radioactive decay. Accordingly, a sedimentation rate can be estimated from the excess activity profile from the following:

$$S = \frac{\lambda z}{\ln(A_0/A_z)} \quad (4)$$

where S is the linear sedimentation rate (cm/yr), λ is the decay constant for Pb-210 ($0.0311 \text{ years}^{-1}$), A_0 is the specific activity (dpm/g) at the top of the profile, and A_z is the specific activity at depth z . This simple model assumes the following: (1) the specific activity of Pb-210 reaching the bed is constant through time (steady state), (2) Pb-210 is neither desorbed nor chemically mobile in the sediment column, and (3) sedimentation is the dominant process governing the activity-depth profile, i.e., post-depositional physical or biological mixing is negligible. Because the steady-state condition is rarely met in dynamic subtidal environments, the Pb-210 technique is best suited to intertidal flat and supratidal marsh environments where the sedimentary record is relatively complete (e.g., Orson et al, 1992; Church and Lord, 1981).

Total Pb-210 and Cs-137 activities were measured non-destructively via gamma spectroscopy of the 46.5 and 661.6 keV photopeaks, respectively (Cutshall et al., 1983). Supported Pb-210 was determined by measuring the activity of its parent radioisotope, Bi-214, using the 609.3 keV photopeak. Approximately 25–50 g of dry sediment from each 2-cm core interval was ground to a fine powder, placed in a 60 ml plastic screw-lid jar, and counted for 48 hours on a Canberra Instruments Model 2020 low-energy Germanium detector (LEGe). Detector efficiencies were computed based on measured versus registered activities of NISST Standard Reference Material 4357B (a.k.a. Ocean Sediment). For each subsample the supported activity of Pb-210 was subtracted from the total activity to compute excess activity.

Spot measurements of the natural radioisotope Be-7 ($t_{1/2}=53$ days) were made on HDC samples from two sites in the estuary where fresh deposition was presumed at the time of sampling. Beryllium-7 is produced in the atmosphere by cosmic ray spallation of nitrogen and oxygen and delivered to the earth's surface through precipitation and dry deposition. In turbid estuaries Be-7 is rapidly adsorbed to particles and serves as a tracer of short-term deposition (or mixing) when present in bottom sediments (Olsen et al., 1986). Samples for Be-7 measurements were processed and gamma counted as per Cs-137 and Pb-210, and the activities were quantified from the 477.7 keV photopeak following the method of Larsen and Cutshall (1981).

5. RESULTS AND INTERPRETATION

5.1. Sonar and Bottom Sampling Coverage

Sonar tracklines and sediment sampling stations are presented together in a series of 12 maps scaled at approximately four-by-four nautical miles (Figures 5–16). Plotted are the actual tracks of the survey vessel as recorded by DGPS, numbered 1–122 following the order in which they were completed in the field. Note that each line has a corresponding sidescan, chirp and echosounder record. Due to a problem with the data cable, chirp data were not collected along Tracklines 11–14. Geographic positions of bottom grab and HDC sampling stations shown in Figures 5–16 are tabulated in Appendix D and presented in the accompanying GIS database.

Total Pb-210 and Cs-137 activities were measured non-destructively via gamma spectroscopy of the 46.5 and 661.6 keV photopeaks, respectively (Cutshall et al., 1983). Supported Pb-210 was determined by measuring the activity of its parent radioisotope, Bi-214, using the 609.3 keV photopeak. Approximately 25–50 g of dry sediment from each 2-cm core interval was ground to a fine powder, placed in a 60 ml plastic screw-lid jar, and counted for 48 hours on a Canberra Instruments Model 2020 low-energy Germanium detector (LEGe). Detector efficiencies were computed based on measured versus registered activities of NISST Standard Reference Material 4357B (a.k.a. Ocean Sediment). For each subsample the supported activity of Pb-210 was subtracted from the total activity to compute excess activity.

Spot measurements of the natural radioisotope Be-7 ($t_{1/2}=53$ days) were made on HDC samples from two sites in the estuary where fresh deposition was presumed at the time of sampling. Beryllium-7 is produced in the atmosphere by cosmic ray spallation of nitrogen and oxygen and delivered to the earth's surface through precipitation and dry deposition. In turbid estuaries Be-7 is rapidly adsorbed to particles and serves as a tracer of short-term deposition (or mixing) when present in bottom sediments (Olsen et al., 1986). Samples for Be-7 measurements were processed and gamma counted as per Cs-137 and Pb-210, and the activities were quantified from the 477.7 keV photopeak following the method of Larsen and Cutshall (1981).

5. RESULTS AND INTERPRETATION

5.1. Sonar and Bottom Sampling Coverage

Sonar tracklines and sediment sampling stations are presented together in a series of 12 maps scaled at approximately four-by-four nautical miles (Figures 5–16). Plotted are the actual tracks of the survey vessel as recorded by DGPS, numbered 1–122 following the order in which they were completed in the field. Note that each line has a corresponding sidescan, chirp and echosounder record. Due to a problem with the data cable, chirp data were not collected along Tracklines 11–14. Geographic positions of bottom grab and HDC sampling stations shown in Figures 5–16 are tabulated in Appendix D and presented in the accompanying GIS database.

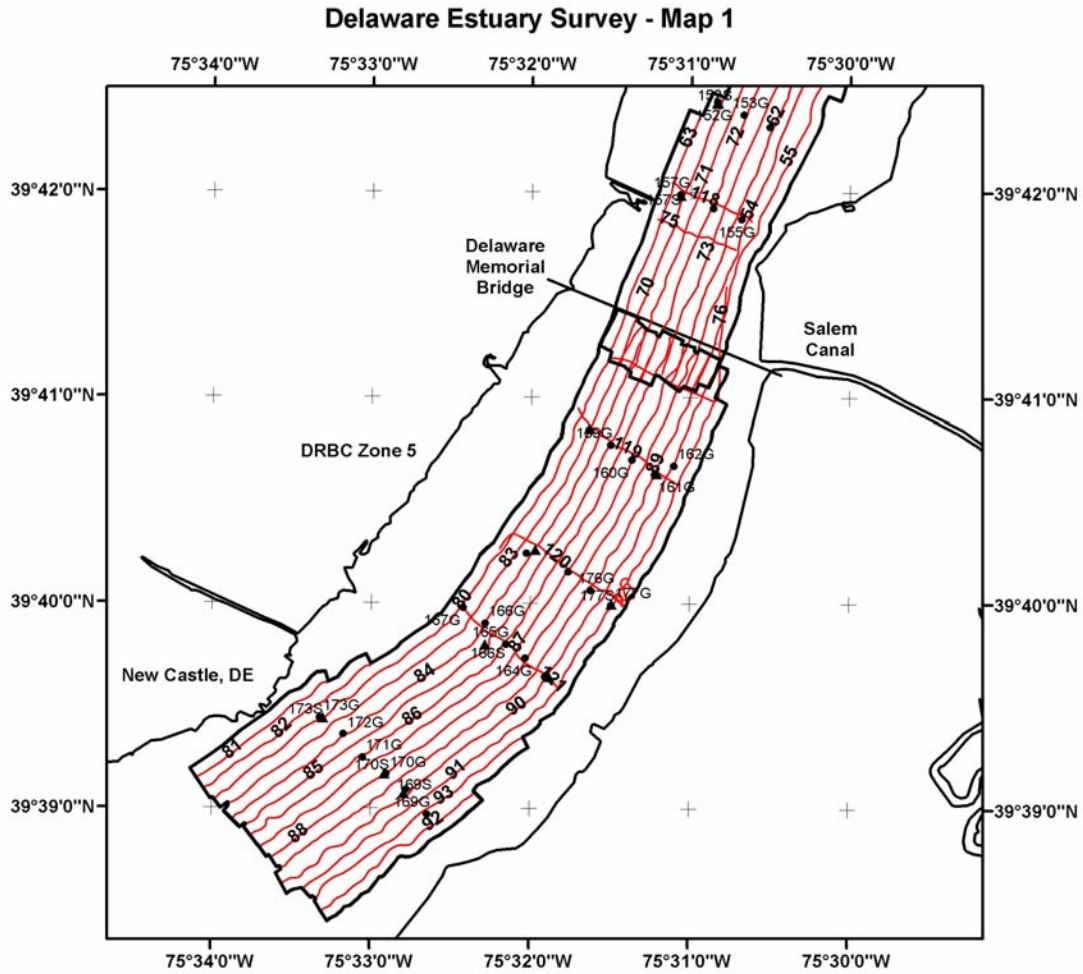


Figure 5. Survey Area Map 1. The entire survey area is presented in Maps 1–12 of Figures 5–16. Bold-numbered lines (red) are vessel tracklines along which sonar data were collected. Circles and triangles denote sediment-grab (G) and HDC stations (S), respectively. The thick black line represents the areal extent of sidescan sonar coverage.

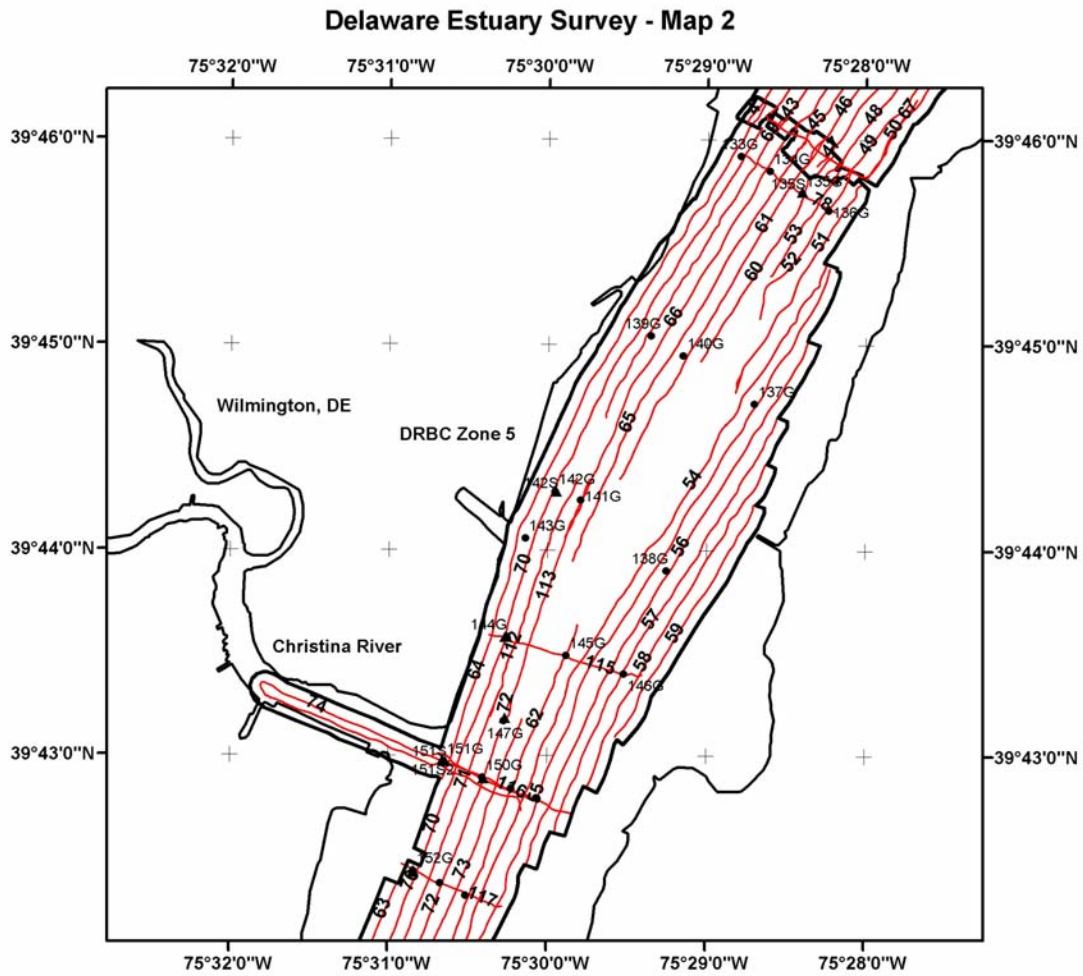


Figure 6. Survey Area Map 2. See Fig. 5 for details.

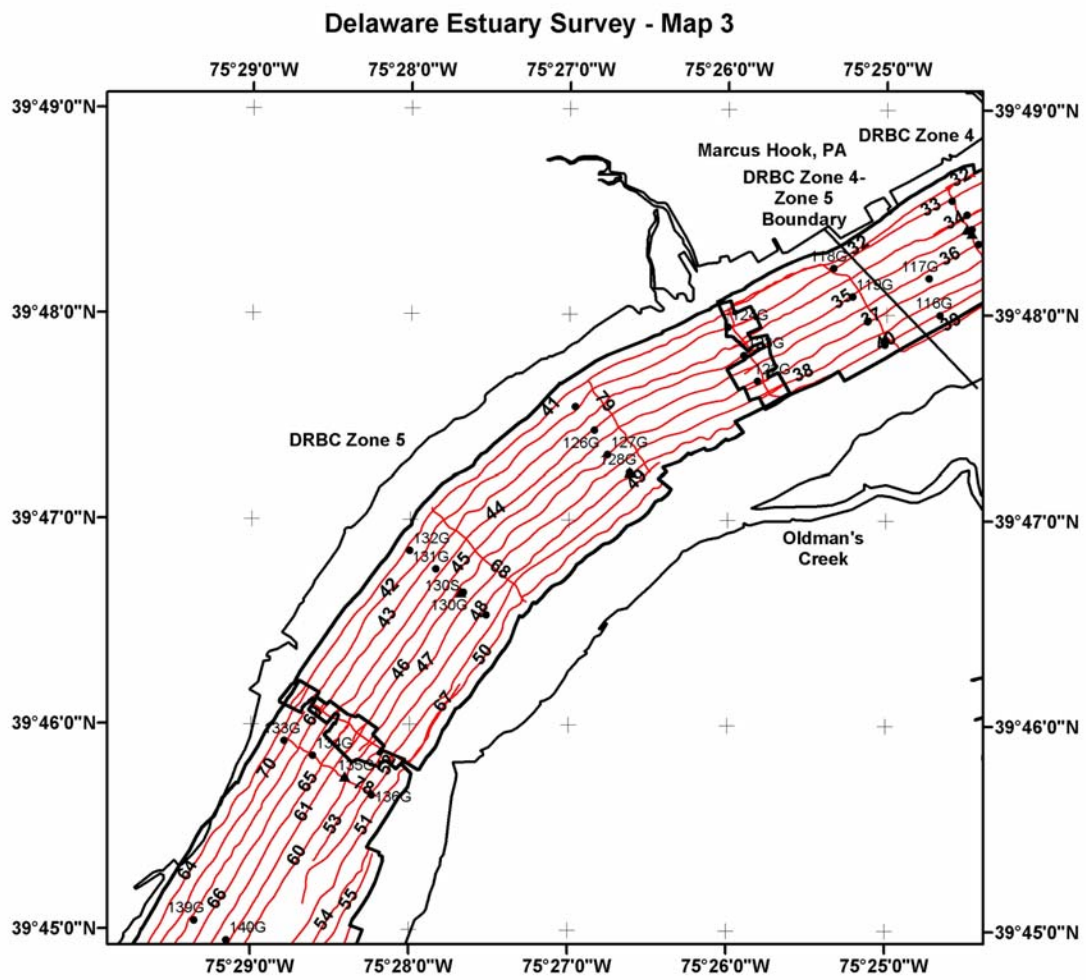


Figure 7. Survey Area Map 3. See Fig. 5 for details.

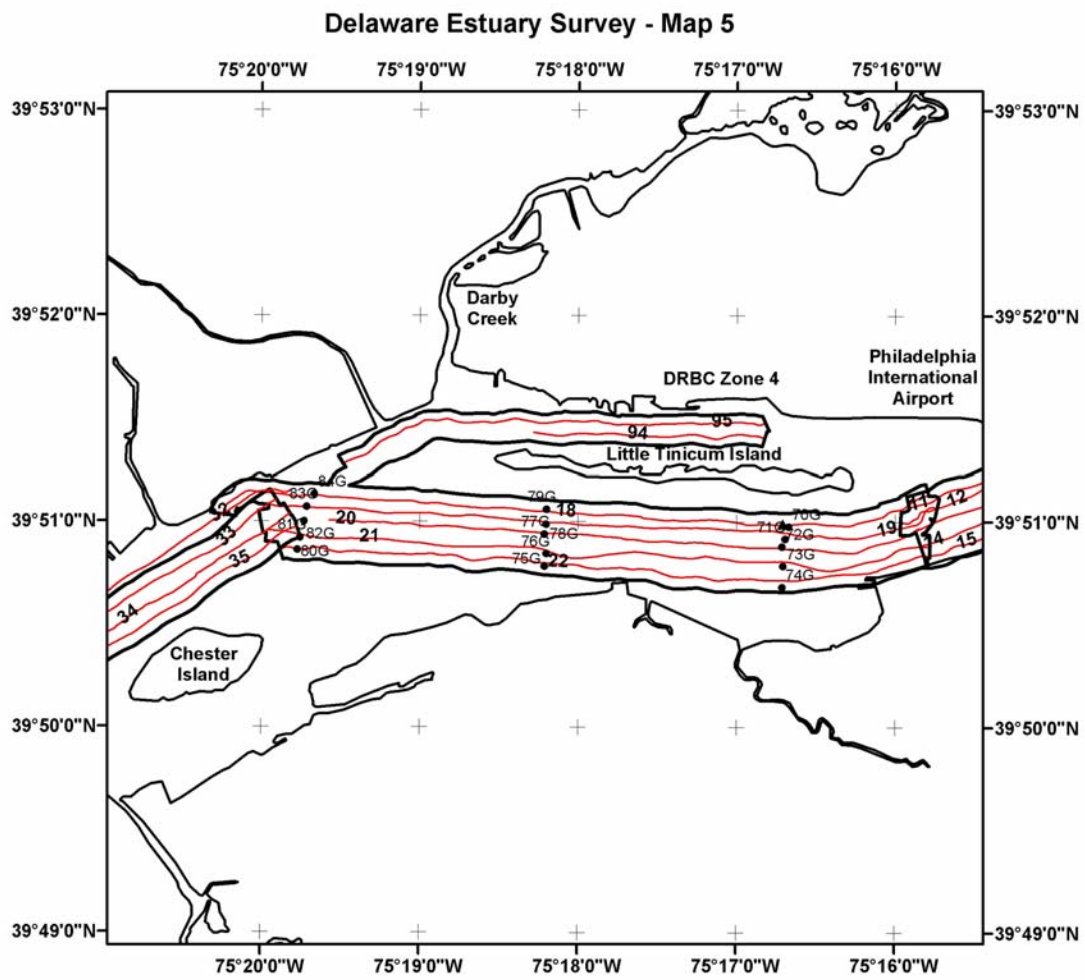


Figure 9. Survey Area Map 5. See Fig. 5 for details.

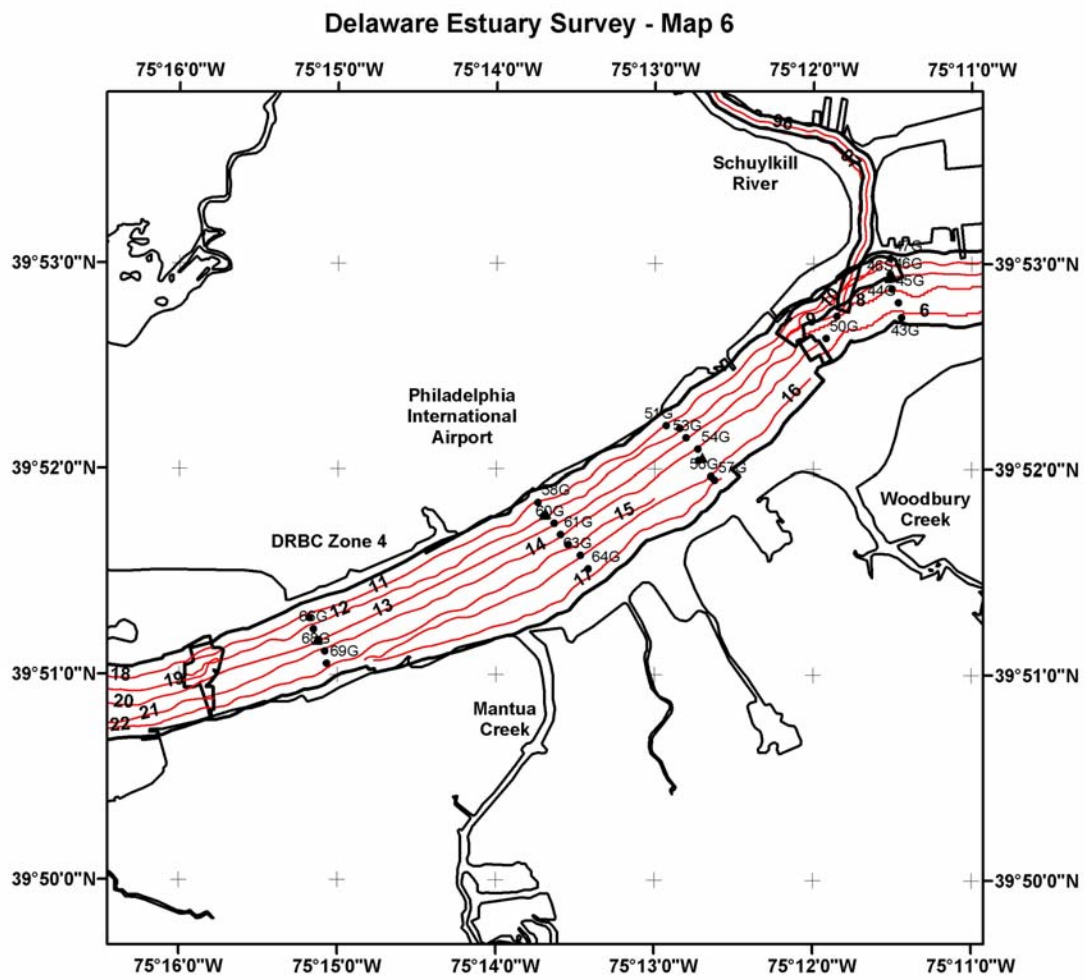


Figure 10. Survey Area Map 6. See Fig. 5 for details.

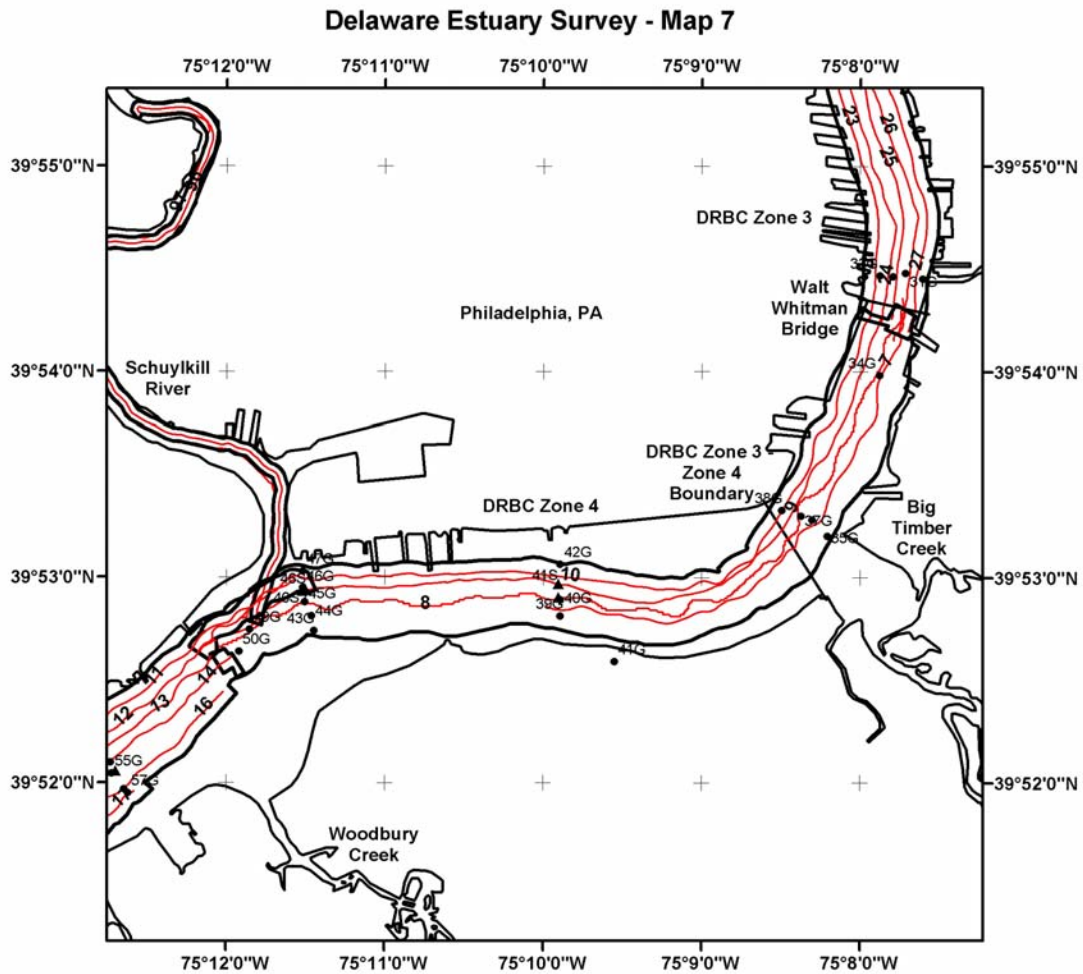


Figure 11. Survey Area Map 7. See Fig. 5 for details.

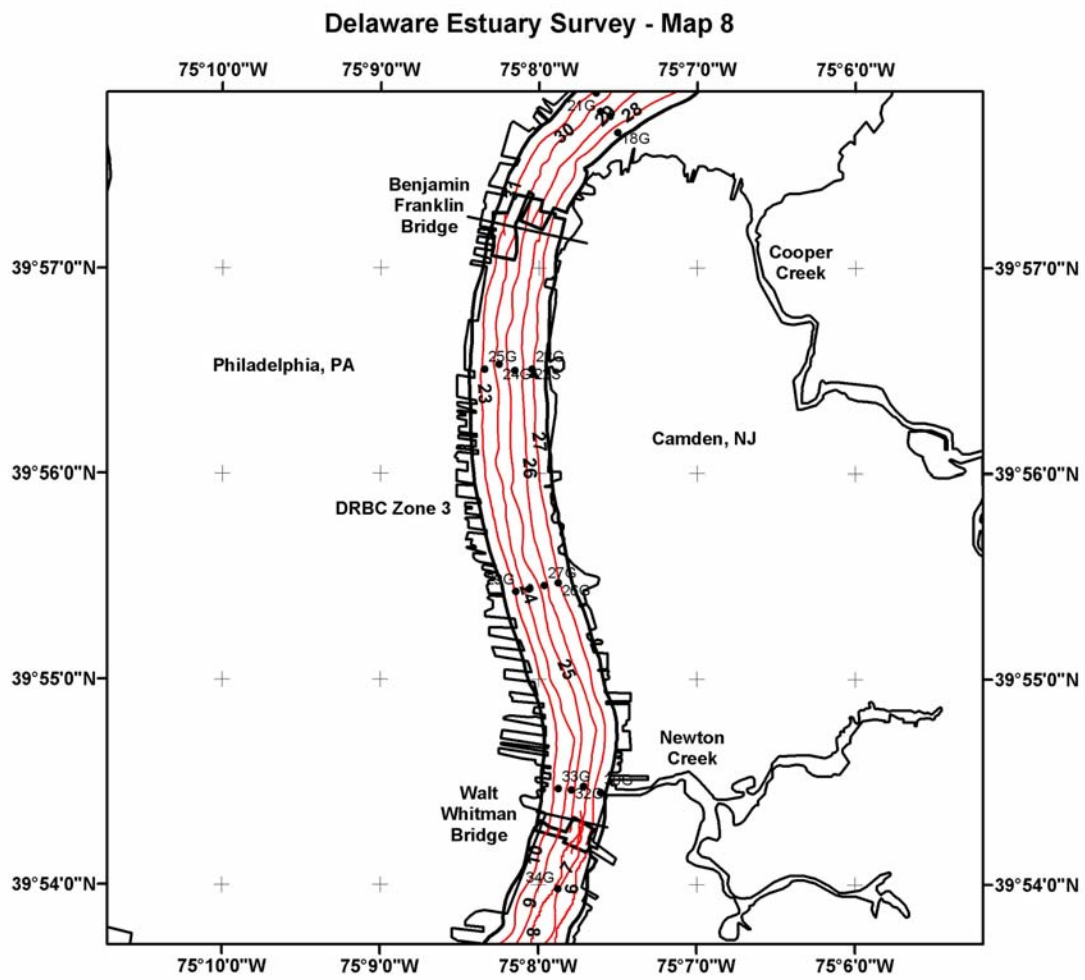


Figure 12. Survey Area Map 8. See Fig. 5 for details.

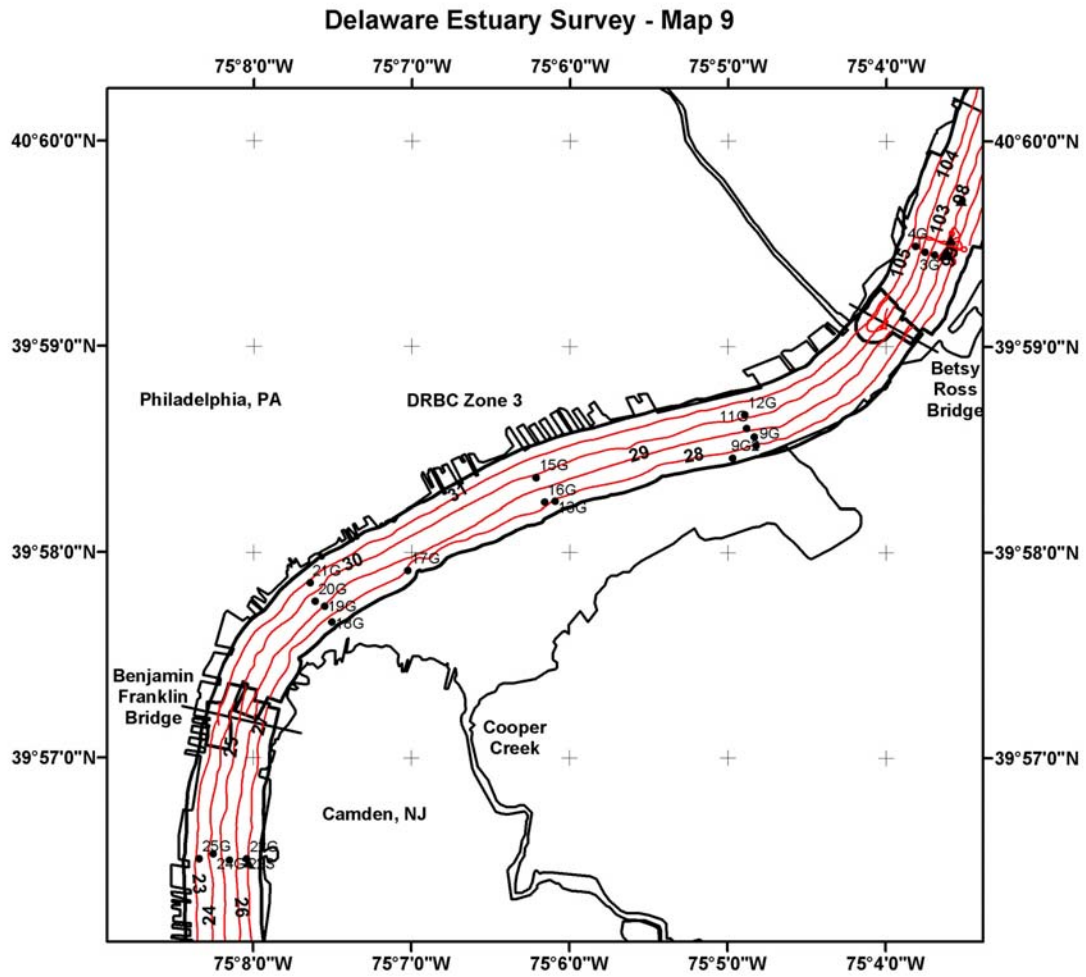


Figure 13. Survey Area Map 9. See Fig. 5 for details.

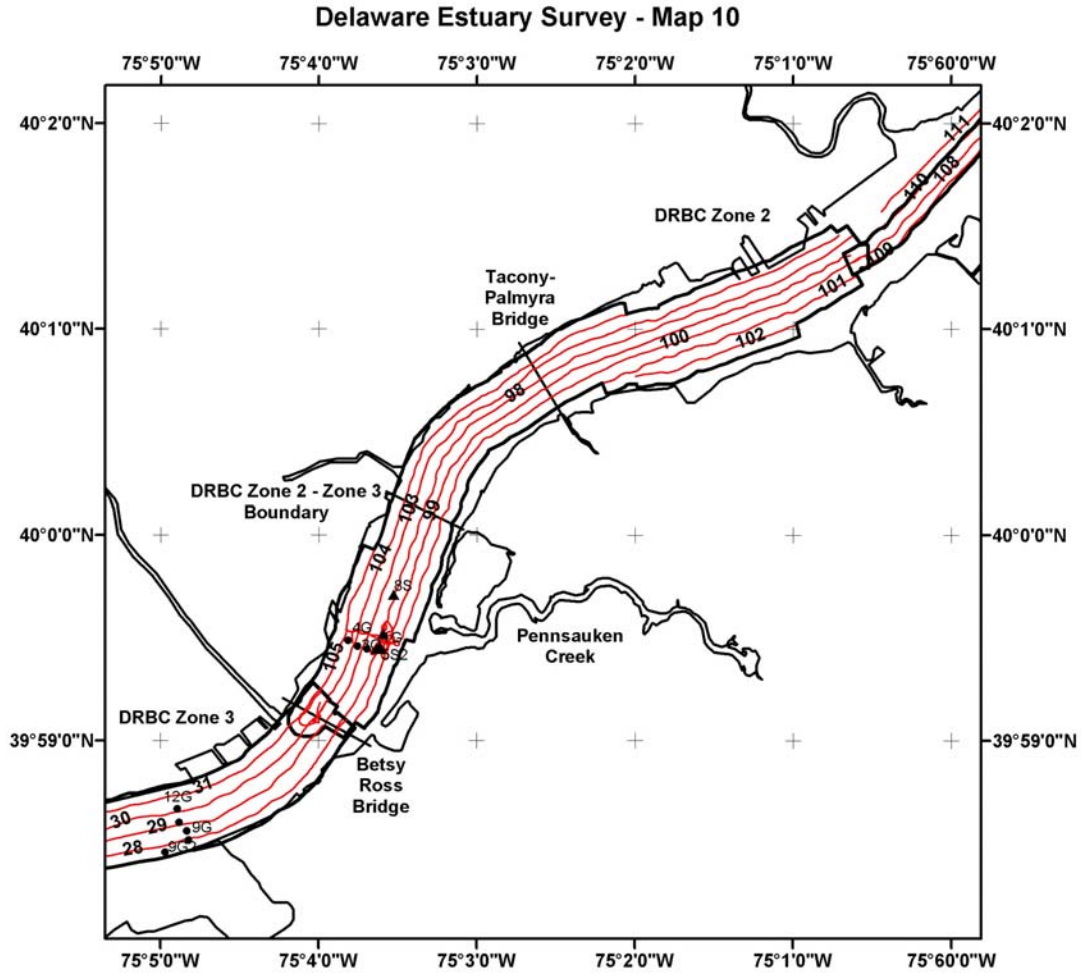


Figure 14. Survey Area Map 10. See Fig. 5 for details.

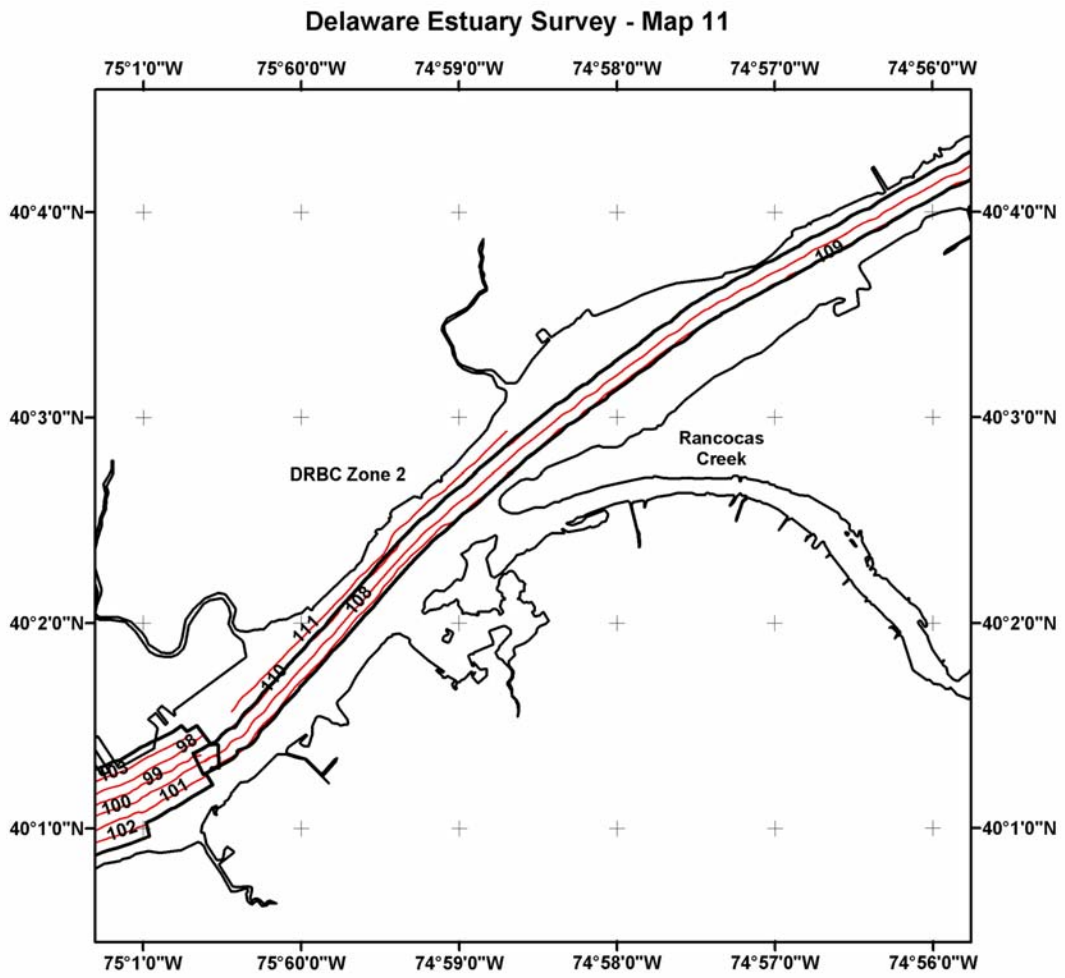


Figure 15. Survey Area Map 11. See Fig. 5 for details.

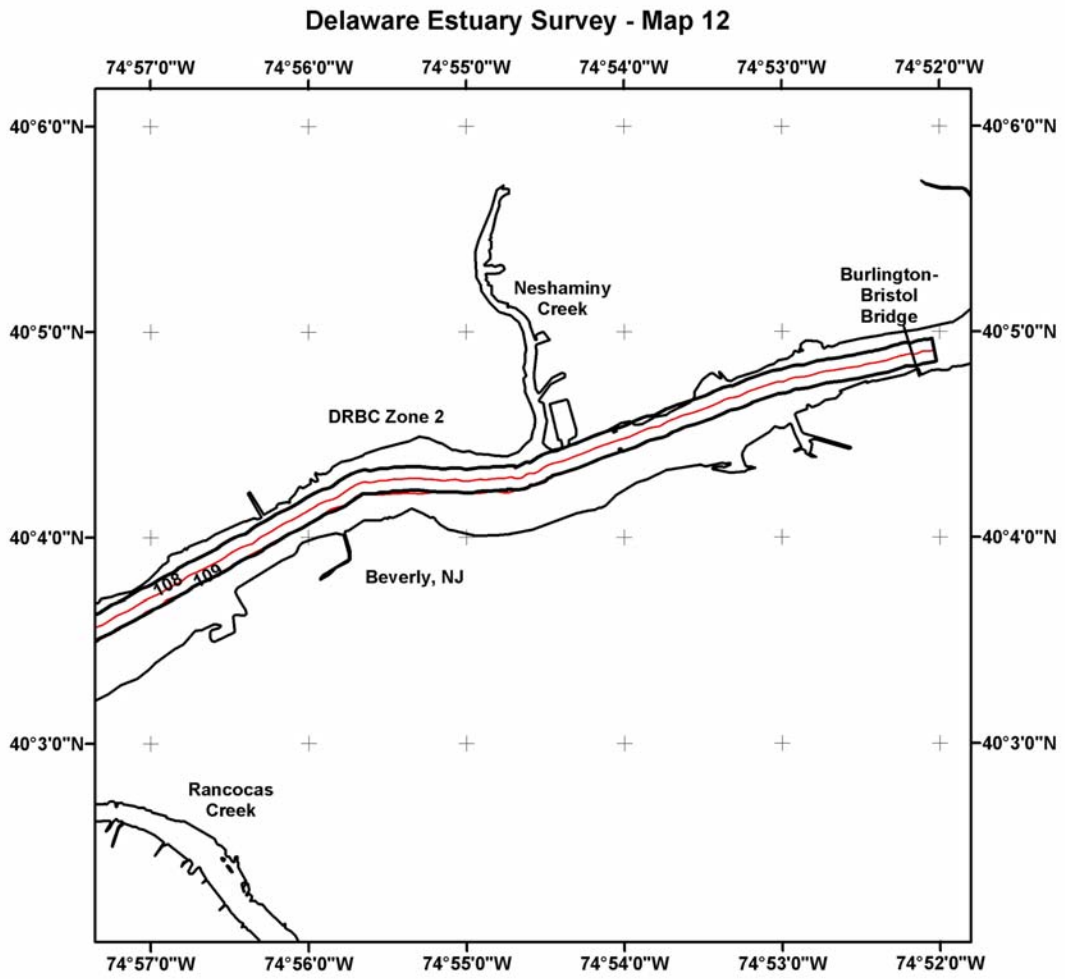


Figure 16. Survey Area Map 12. See Fig. 5 for details.

The total area of the bottom imaged by sidescan was 68.6 km², roughly 65 % of the total subaqueous area of the estuary between Burlington and New Castle, 80 % of the area below the 6-m isobath. Most of the remaining area (31.4 km²) consists of shoals that were too shallow to be mapped without risking damage to the towed instrumentation. Though both sidescan sonar frequencies (100 and 500 kHz) were used to characterize the bottom, the backscatter mosaic was constructed from 100 kHz data because it provided more horizontal range.

5.2. Sidescan Backscatter

Because a detailed analysis of sidescan backscatter at the bedform scale was beyond the scope of this study, only the regional patterns are elaborated herein. The 12 backscatter mosaics are presented together in a large-scale map to illustrate the cumulative coverage (Figure 17; see Table 2 for details), and the individual 1-m resolution mosaics on which the sedimentary environments maps were based are presented as a composite GIS layer.

Table 2. Backscatter mosaic names and locations

DRBC Zone	Mosaic Name	Report Figure
5	New Castle	22
5	Christina	22, 23
5	Marcus Hook Bar	24
4–5	Marcus Hook	25, 26
4	Tinicum	26
4	Airport	27
4	Schuylkill	27, 28
3–4	Navy Yard	28
3	Camden	29
3	Petty Island	30
2–3	Palmyra	31
2	Burlington	32, 33

The spatial distribution of acoustic backscatter intensity exhibits a general along-estuary pattern that mirrors the predominant bed morphology and sediment type (Figure 17). For purposes of interpretation, backscatter intensity was divided into three categories: (1) *strong* (black to dark gray grayscale tones); (2) *moderate* (dark gray to light gray tones); and (3) *weak* (light grey to white tones). Backscatter intensity was

The total area of the bottom imaged by sidescan was 68.6 km², roughly 65 % of the total subaqueous area of the estuary between Burlington and New Castle, 80 % of the area below the 6-m isobath. Most of the remaining area (31.4 km²) consists of shoals that were too shallow to be mapped without risking damage to the towed instrumentation. Though both sidescan sonar frequencies (100 and 500 kHz) were used to characterize the bottom, the backscatter mosaic was constructed from 100 kHz data because it provided more horizontal range.

5.2. Sidescan Backscatter

Because a detailed analysis of sidescan backscatter at the bedform scale was beyond the scope of this study, only the regional patterns are elaborated herein. The 12 backscatter mosaics are presented together in a large-scale map to illustrate the cumulative coverage (Figure 17; see Table 2 for details), and the individual 1-m resolution mosaics on which the sedimentary environments maps were based are presented as a composite GIS layer.

Table 2. Backscatter mosaic names and locations

DRBC Zone	Mosaic Name	Report Figure
5	New Castle	22
5	Christina	22, 23
5	Marcus Hook Bar	24
4–5	Marcus Hook	25, 26
4	Tinicum	26
4	Airport	27
4	Schuylkill	27, 28
3–4	Navy Yard	28
3	Camden	29
3	Petty Island	30
2–3	Palmyra	31
2	Burlington	32, 33

The spatial distribution of acoustic backscatter intensity exhibits a general along-estuary pattern that mirrors the predominant bed morphology and sediment type (Figure 17). For purposes of interpretation, backscatter intensity was divided into three categories: (1) *strong* (black to dark gray grayscale tones); (2) *moderate* (dark gray to light gray tones); and (3) *weak* (light grey to white tones). Backscatter intensity was

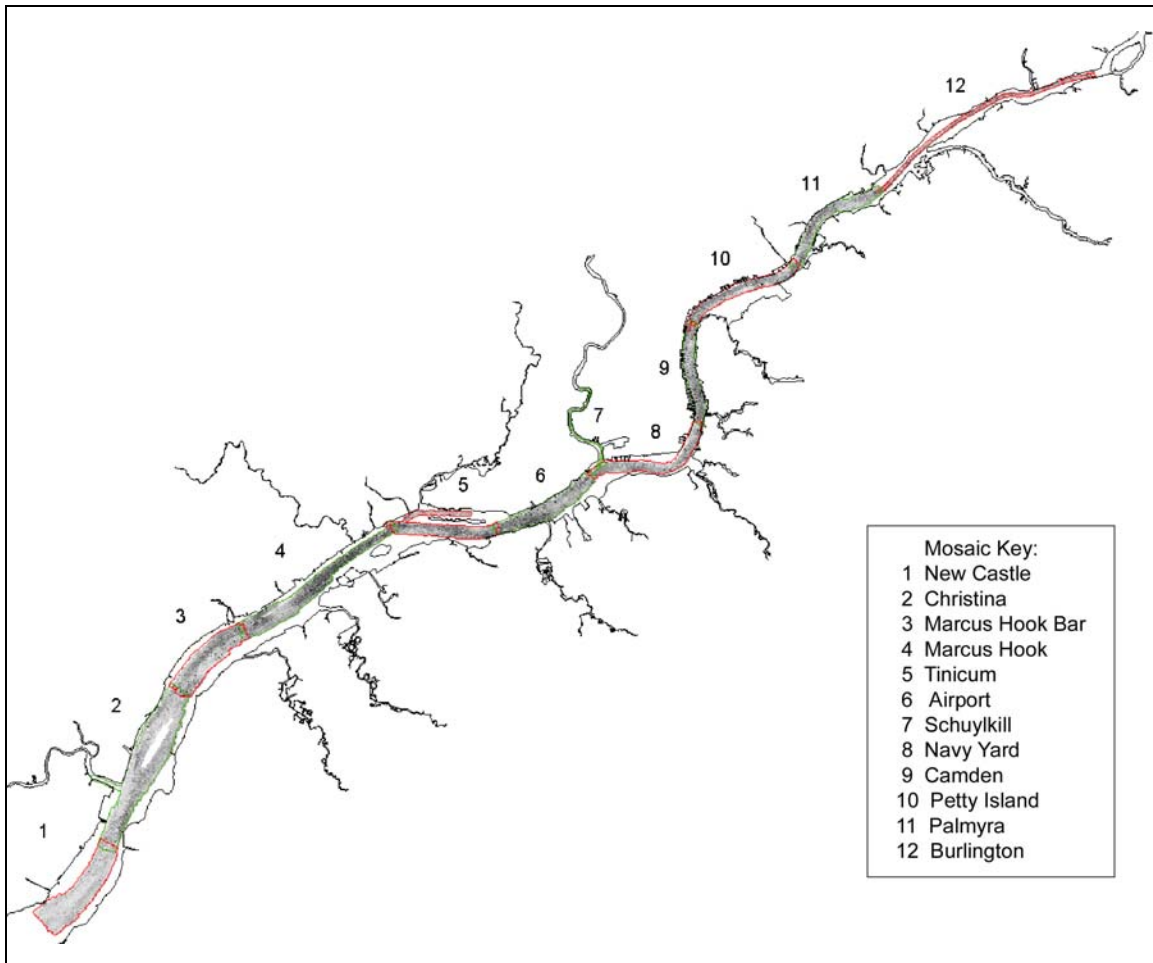


Figure 17. Sidescan sonar coverage map and acoustic backscatter distribution. See Table 2 for mosaic names and range. Interpreted versions of the 12 mosaics are presented in Figures 22–33.

moderate in Zones 2 and 3, moderate to strong in Zone 4, and weak in Zone 5, yet intra-zone variations spanning the full backscatter intensity spectrum were observed in places. Grain-size analysis confirmed that backscatter intensity generally increased with increasing grain size; however, sandy, rippled bottoms produced intensities that were equivalent to flat, gravelly bottoms. The strongest backscatter intensity was observed between Tinicum Island and Chester, most likely due an abundance of cobble and rock fragments present at the bed (Figure 17). In contrast, the lowest backscatter was observed just downriver off Marcus Hook, where a fluidized mud bottom was present. Backscatter intensity is uniformly weak downriver of the Marcus Hook Bar, consistent with the progressive increase in the mud content of the bed sediment. Further interpretation of the backscatter distribution is provided in Section 5.4.

5.3. Sediment Physical Properties

5.3.1. Porosity

Water content and porosity data are presented in Appendix D. As expected, the porosity of the subtidal estuary and marsh deposits varied with grain size among surficial (core top) samples, as well as with compaction, increasing with depth in the sediment column. Within 60 cm of the sediment-water interface, porosities ranged from 44 to 91 % with a mean of 73 ± 0.09 % (1σ , $n=310$). As expected, sandy deposits exhibited lower initial (uncompacted) porosities than those of mud. The porosity of uniform muds decreased downcore by as much as 20–30 %, whereas grain-size variation modulated the downcore porosities of interbedded silts and clays (Figure 18).

5.3.2. Grain Size

Grain-size data (samples 1G–184G) were plotted in ternary charts to classify bottom types based on weight percentages of gravel, sand, mud, silt, and clay (Figure 19). Grain-size results for the lower estuary south of New Castle (samples 185G–298G) are not described here, though the data are tabulated in Appendix E. Bottom sediments of the upper estuary span the full range of sizes observed for river-estuaries in general, with all but three (gM, gmS, Z) of the 24 size classes represented (see Figure 4). For the gravel-sand-mud classification, gravel, sandy gravel, gravelly sand, and gravelly muddy sand were the most common gravel classes, whereas sand, muddy sand, sandy mud and mud characterized the majority of samples without gravel.

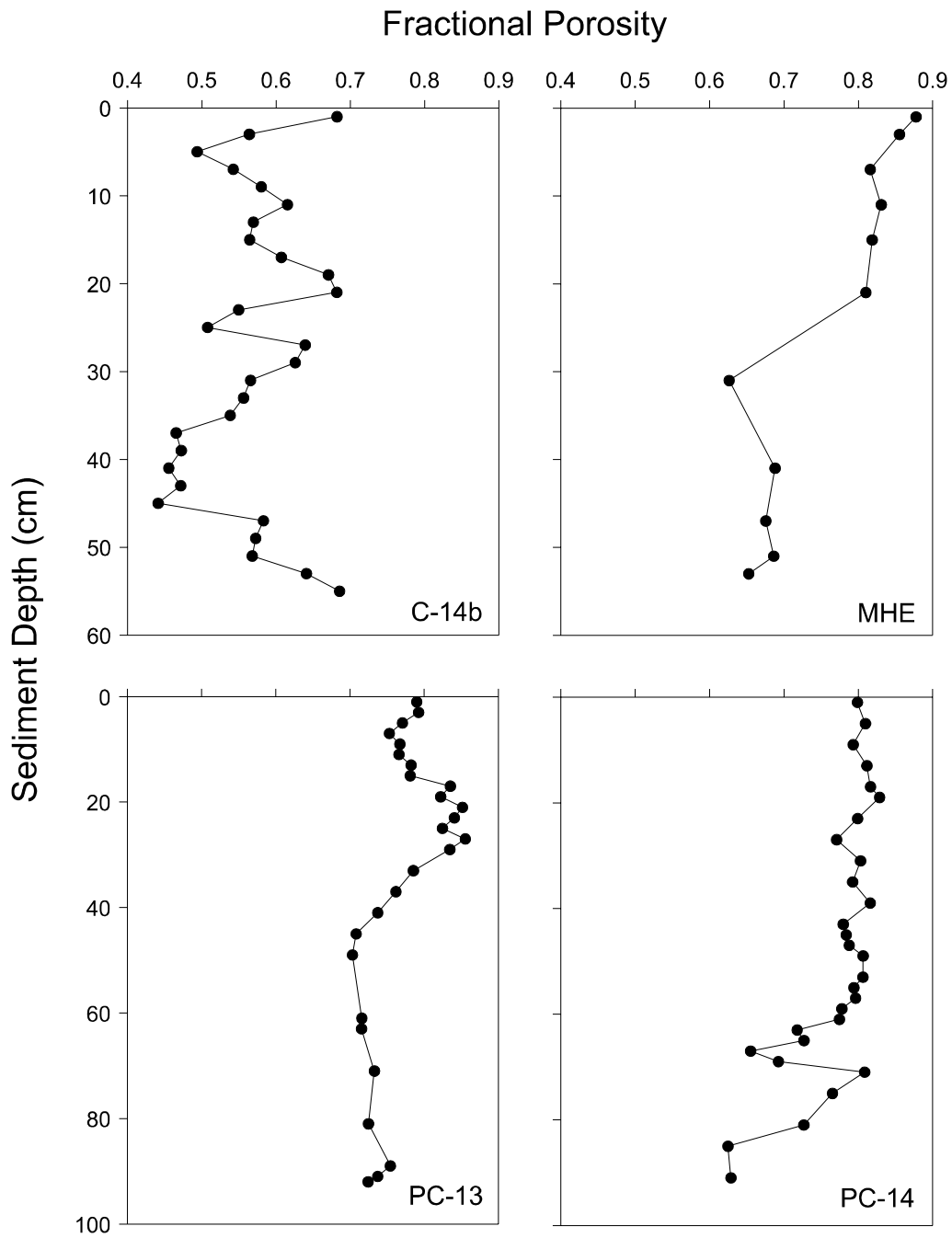


Figure 18. Downcore porosity profiles. Examples shown are from the estuary (C-14b, MHE) and tidal marsh sites (PC-13, PC-14). See Table 3 and Appendix C for locations.

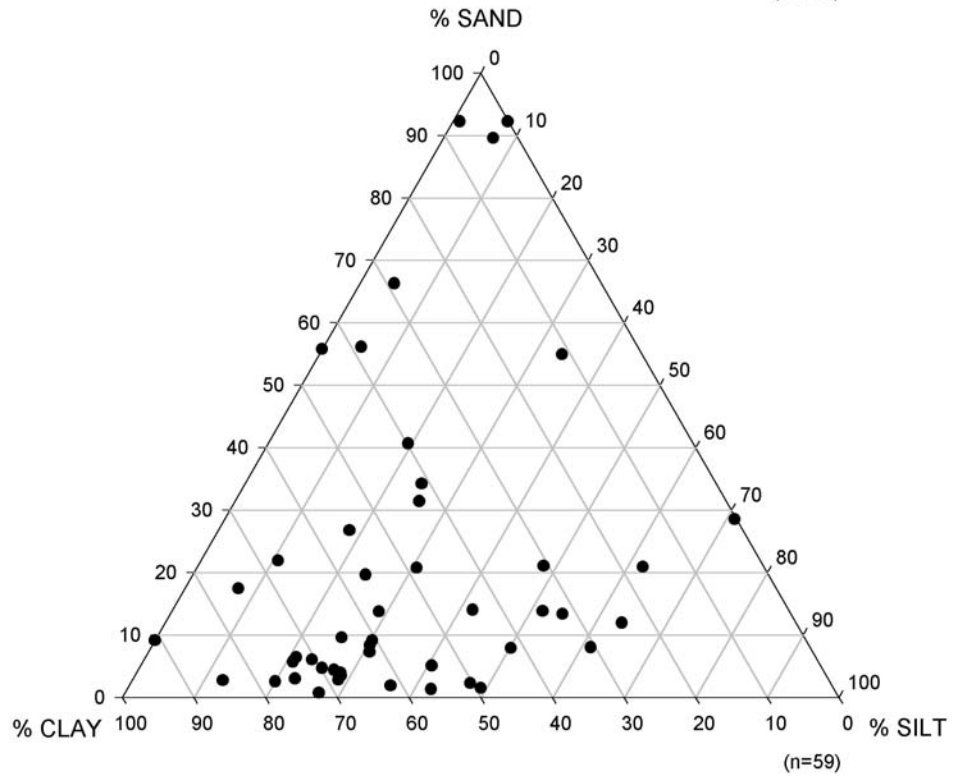
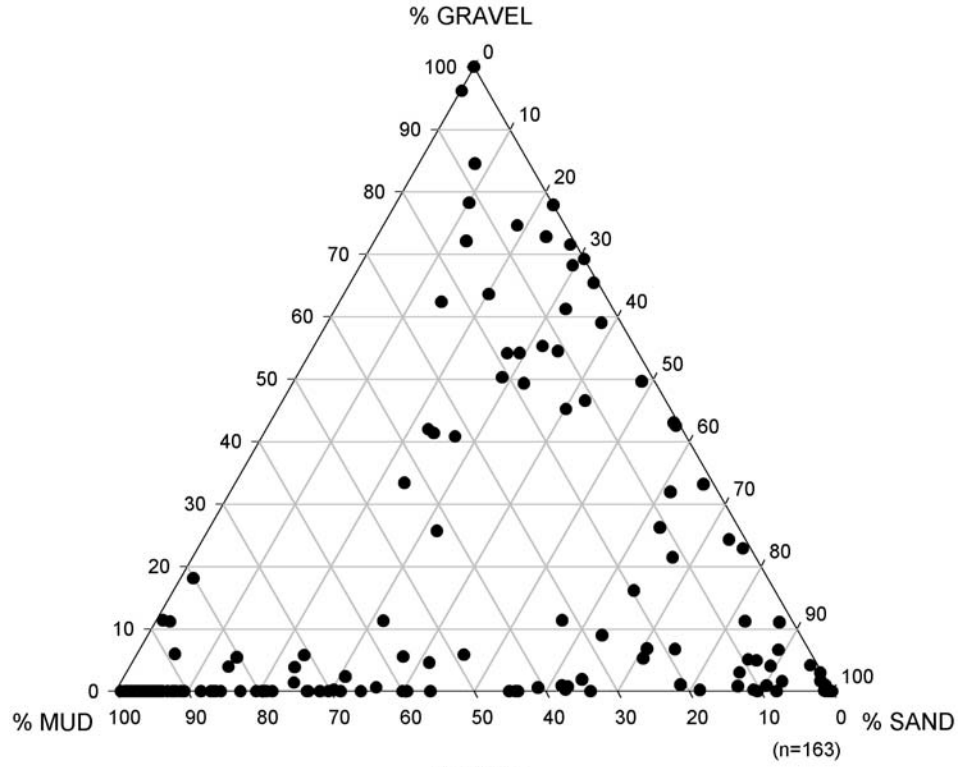


Figure 19. Results of grain-size analysis. Plotted are samples collected during cruise CH01-28. See Appendix E for tabulated data.

Silts and clays dominated the sand-silt-clay classification, with silty clay, clayey silt, sand clay, sandy silty clay, and clay being the most common classes. At grab-sampling sites 83G, 125G, and 131G, the bottom consisted of large cobbles and rock fragments that could not be recovered. Accordingly, a "rock" bottom type (R) not represented by the classification scheme is present in places. Lack of data clustering in the ternary plots indicates that distinct sedimentary provinces (i.e., facies) are not present within the natural channel (Figure 19), in other words, the sediment types are highly heterogeneous along the length surveyed and at the resolution of sampling.

In addition to spatial heterogeneity, temporal variability must be considered when interpreting the sediment-type distribution. For example, cores from the Rancocas River mouth and Marcus Hook shoal displayed a uniform layer of medium-grained sand atop interbedded, open-estuarine mud (Figure 20). This sedimentology implies a recent, abrupt increase in bottom energy manifested as a change from mud deposition in a shoal or mudflat setting (bottom of core) to bedload transport of sands derived from the estuarine channel or through shoreline erosion (core top). Another interpretation is that the supply of mud to these depositional sites has decreased through time such that sand has become predominant. Although the chronology and full nature of this change is unknown at present, it may be related to historical dredging disturbances and (or) shoreline stabilization works.

Along-estuary trends in sediment grain size were examined by plotting the weight percentages of gravel, sand, and mud as a function of axial position (Figure 21). Overall, the weight percentages of gravel varied by several orders of magnitude with no clear-cut trends, though a slight decrease around RM 75 in Zone 5 was indicated. The absolute weight percentages of sand generally decreased down-estuary from Zone 3 to Zone 5, but the cross-channel variability increased. In contrast, the across-channel variability in mud content decreased significantly along-estuary. The transition from a dominantly coarse-grained (sand and gravel) to fine-grained bottom (clayey silt to silty clay) occurs near the Zone 4–Zone 5 boundary, between RM 75 and RM 85. At least two factors may be

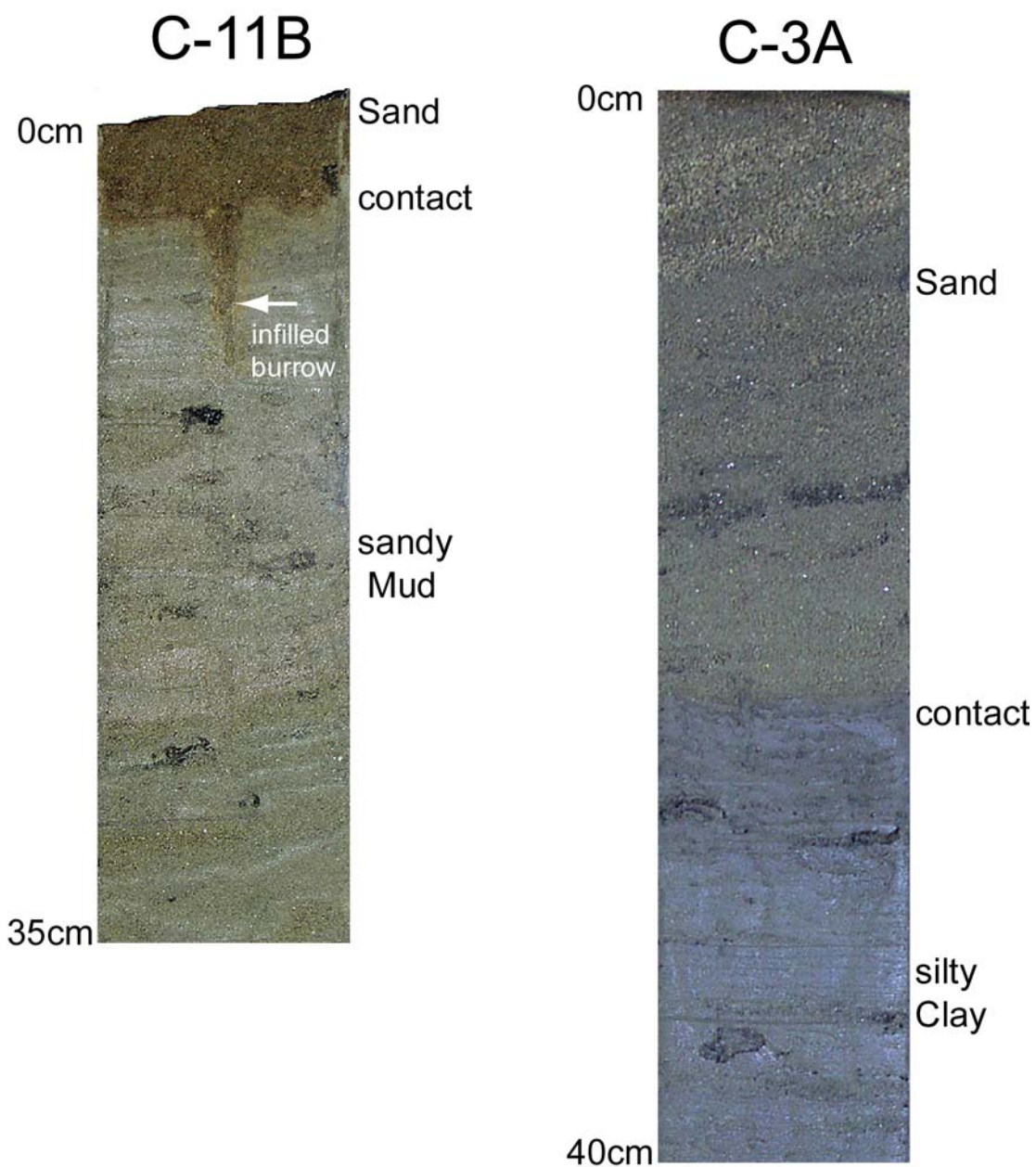


Figure 20. Photographs of cores C-3A and C-11B. See Figure 40 for location map and Appendix C for geographic coordinates. The sharp contact between sediment types marks a recent change from a fine-grained deposition to coarse-grained bed load environments.

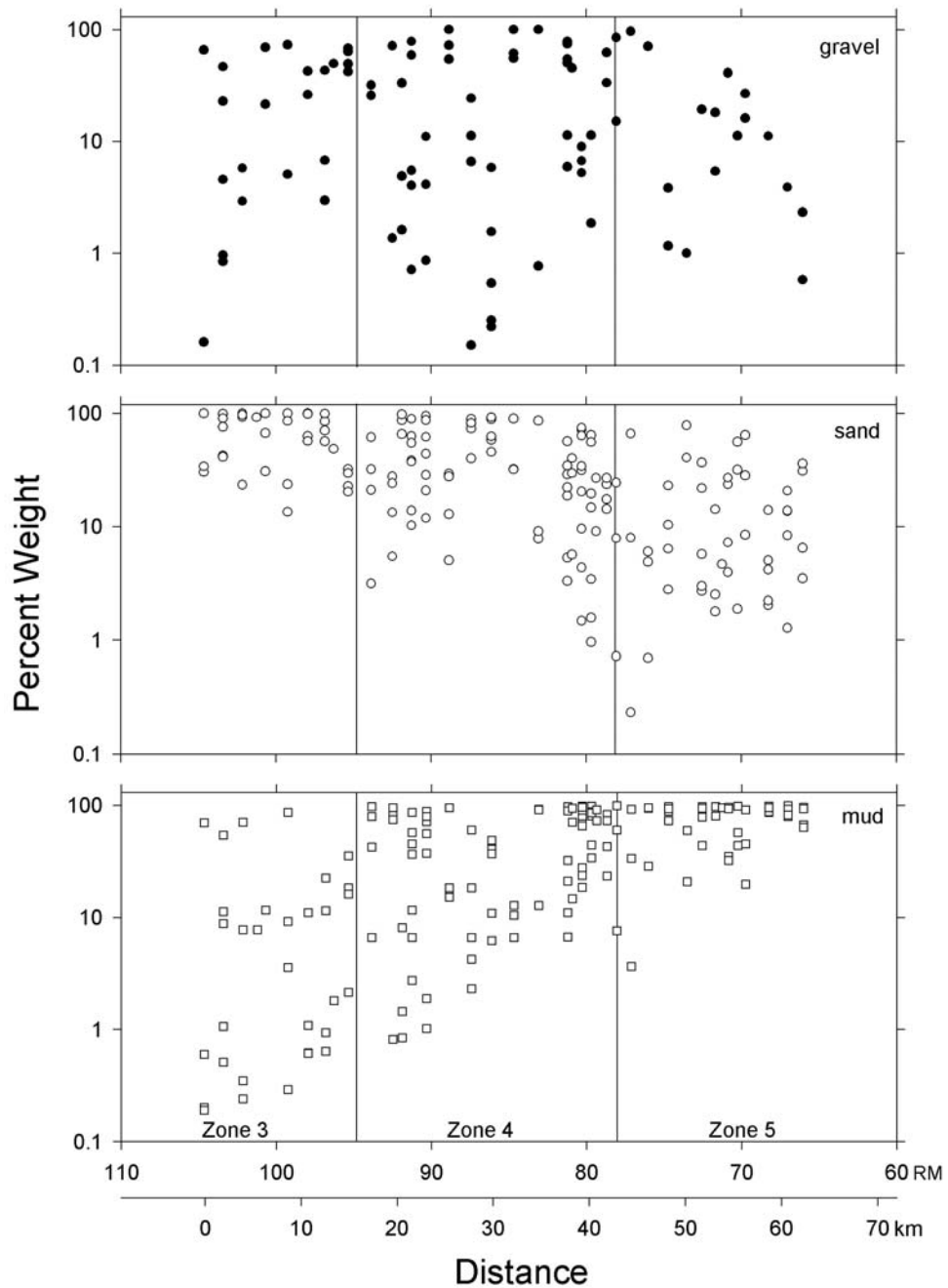


Figure 21. Plots of grain-size trends. Shown are grain-size analytical results for samples collected during cruise CH01-28 (see Appendix C for locations). Weight percentages are plotted versus distance in river miles from the bay mouth (0 RM) and kilometers relative to the first sampling transect. Corresponding DRBC Zones are noted for reference.

responsible for this transition. First, the estuarine channel widens rapidly from RM 100 to RM 80, perhaps reducing tidal-current velocities to below the level of competency for sand transport. Second, given that the head of the salinity intrusion typically falls within this region, flocculation and rapid deposition of particle aggregates locally may increase the mud content of the bed. Although general estuarine processes can be invoked to explain the Zone 4–5 sand-to-mud transition, the causal mechanisms cannot be ascertained from the grain-size data alone.

5.4. Sedimentary Environments

A map depicting the distribution of sedimentary environments in the study area was created from the sidescan sonar mosaic and grain-size data, using dominant sediment type and mode of transport (as suggested by bedforms) as the primary delimiters. The map was created by overlaying georeferenced bottom-type and backscatter-mosaic layers in GIS and tracing the backscatter patterns according to intensity (grayscale tone), surface relief (extent of acoustic shadowing), and local bottom type. In this report, the sedimentary environments map is subdivided into 12 smaller maps scaled at approximately four-by-four nautical miles (Figures 22–33) with geographic bounds identical to those of the sampling coverage maps (Figures 5–16). The full-scale map is presented as a layer in the GIS database.

Six types of sedimentary environments were identified following criteria modified from (Knebel et al., 1999): (1) fine-grained deposition; (2) coarse-grained bedload; (3) fine-grained reworking; (4) mixed-grain reworking; (5) coarse-grained reworking; (6) and non-deposition or erosion. Specific characteristics of these environments are elaborated below and summarized in Table 3.

Areas of fine-grained sediment deposition (mud) exhibit uniformly weak to very weak backscatter intensity generated by flat bottoms composed of high-porosity (>75%) or fluidized mud. The Marcus Hook anchorage and Christina River mouth region are examples of the fine-grained deposition environment (Figure 25). These bottoms are generally devoid of bedforms, with the exception of linear, sedimentary furrows observed in places. The radioisotope Be-7 was detected at one fine-grained site off Marcus Hook, suggesting that deposition within these environments is active on a seasonal basis (see Section 5.6.2.).

responsible for this transition. First, the estuarine channel widens rapidly from RM 100 to RM 80, perhaps reducing tidal-current velocities to below the level of competency for sand transport. Second, given that the head of the salinity intrusion typically falls within this region, flocculation and rapid deposition of particle aggregates locally may increase the mud content of the bed. Although general estuarine processes can be invoked to explain the Zone 4–5 sand-to-mud transition, the causal mechanisms cannot be ascertained from the grain-size data alone.

5.4. Sedimentary Environments

A map depicting the distribution of sedimentary environments in the study area was created from the sidescan sonar mosaic and grain-size data, using dominant sediment type and mode of transport (as suggested by bedforms) as the primary delimiters. The map was created by overlaying georeferenced bottom-type and backscatter-mosaic layers in GIS and tracing the backscatter patterns according to intensity (grayscale tone), surface relief (extent of acoustic shadowing), and local bottom type. In this report, the sedimentary environments map is subdivided into 12 smaller maps scaled at approximately four-by-four nautical miles (Figures 22–33) with geographic bounds identical to those of the sampling coverage maps (Figures 5–16). The full-scale map is presented as a layer in the GIS database.

Six types of sedimentary environments were identified following criteria modified from (Knebel et al., 1999): (1) fine-grained deposition; (2) coarse-grained bedload; (3) fine-grained reworking; (4) mixed-grain reworking; (5) coarse-grained reworking; (6) and non-deposition or erosion. Specific characteristics of these environments are elaborated below and summarized in Table 3.

Areas of fine-grained sediment deposition (mud) exhibit uniformly weak to very weak backscatter intensity generated by flat bottoms composed of high-porosity (>75%) or fluidized mud. The Marcus Hook anchorage and Christina River mouth region are examples of the fine-grained deposition environment (Figure 25). These bottoms are generally devoid of bedforms, with the exception of linear, sedimentary furrows observed in places. The radioisotope Be-7 was detected at one fine-grained site off Marcus Hook, suggesting that deposition within these environments is active on a seasonal basis (see Section 5.6.2.).

Table 3. Characteristics of sedimentary environments.

Category	Backscatter Intensity and Continuity	Dominant Sediment Type	Bottom Morphology and Bedforms
1) Fine-grained deposition	Very weak to weak, continuous	Mud and fluid mud	Flat, no bedforms
2) Coarse-grained bedload	Moderate to strong, continuous	Moderately well-sorted sand and gravel	Wavy, well-developed fields of ripple and sand waves
3) Fine-grained reworking	Weak to moderate, discontinuous	Mud	Flat to wavy, sediment furrows
4) Mixed-grained reworking	Moderate to strong, discontinuous	Mixed gravel, sand, and mud	Flat to wavy, sediment ribbons and trails
5) Coarse-grained reworking	Strong, discontinuous	Poorly sorted sand and gravel	Flat to wavy, sediment ribbons
6) Non-deposition	Strong to very weak, discontinuous	Cobble and bedrock	wavy

Areas of coarse-grained bedload are indicated by moderate backscatter intensity produced by continuous, well-developed trains of asymmetric ripples or waves composed of sand and gravel. These bedforms are created by the rolling, bouncing, and sliding actions of sediment grains under unidirectional tidal currents. Both up-river and down-river ripple asymmetries are observed, suggesting movement under flood- and ebb-tidal currents, respectively. Note that a copious supply of non-cohesive sediment is required to maintain continuous trains of these bedforms. The tidal river between Burlington and the Betsey Ross Bridge exemplifies the coarse-grained bedload environment (Figures 32 and 33).

Areas of bottom reworking (fine-grained, mixed grained, and coarse-grained) are represented by patchy and discontinuous patterns of both strong and weak backscatter intensity generated by a wide range of bottom morphologies and sediment types (Table 3). The estuarine floor adjacent to the Delaware Memorial Bridge is an example of mixed-grained reworking environment (Figures 22 and 23). Lack of continuous bedform trains and presence of sedimentary cover are characteristics that distinguish reworking environments from the coarse-grained bedload and non-deposition or erosion categories, respectively. Reworked bottoms are locally flat or wavy and composed of low-porosity muds (<75 %) capped by discontinuous, flow-transverse ribbons of sand and gravel. These bottoms are particularly common the vicinity of engineering works such as bridge abutments and bulkheads, places where the native strata have been disturbed.

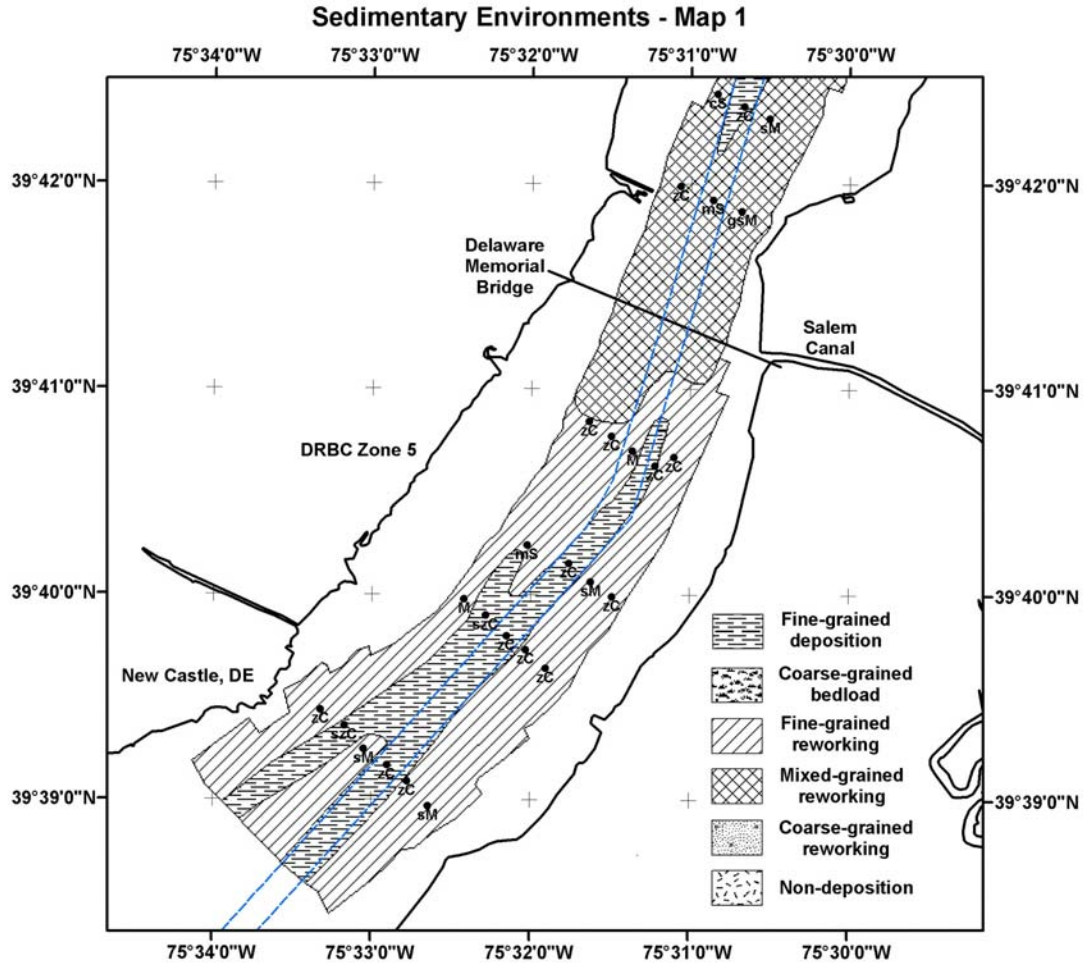


Figure 22. Sedimentary Environments Map 1. Shown is the distribution of environment types based on the New Castle sidescan mosaic and criteria described in the text. Grab-sampling locations and corresponding sediment type are also shown (see Fig. 4 for key). The dashed lines denote the shipping channel.

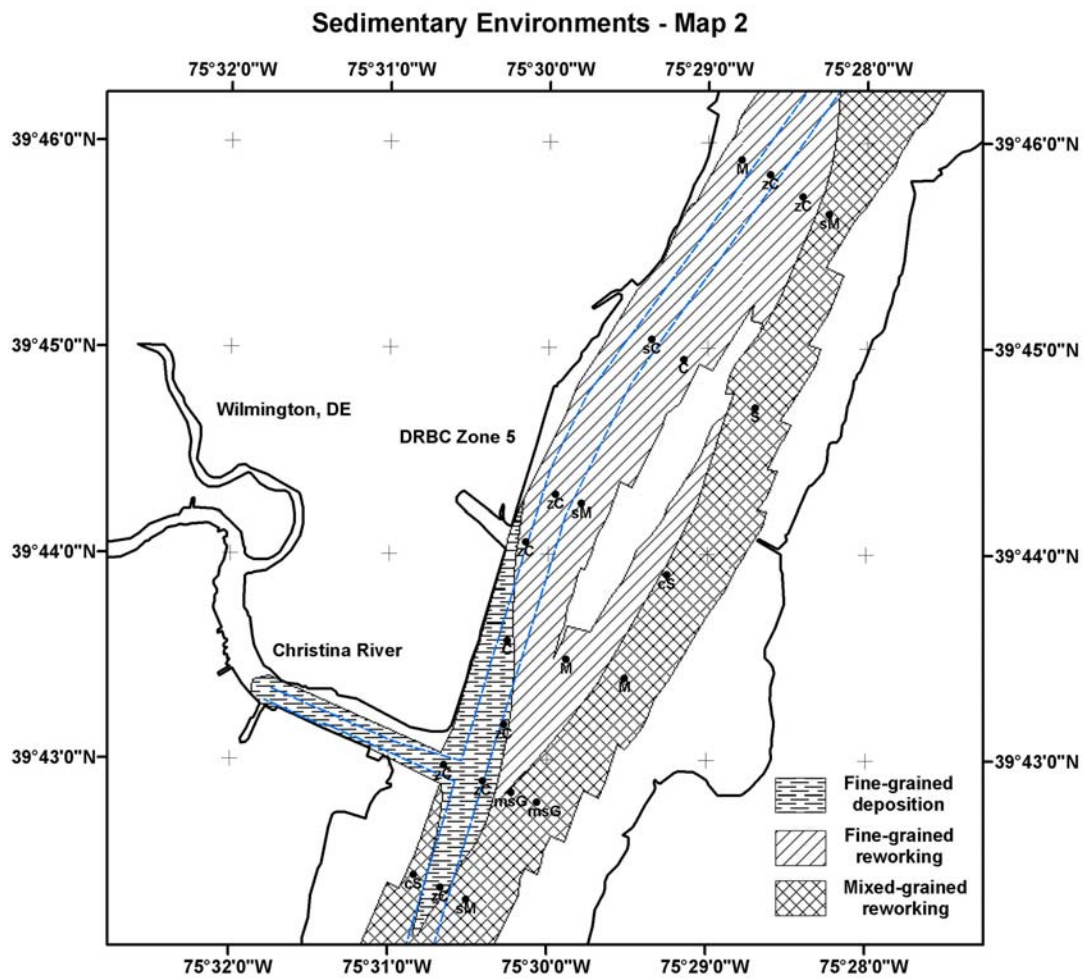


Figure 23. Sedimentary Environments Map 2 based on the New Castle and Christina sonar mosaics.

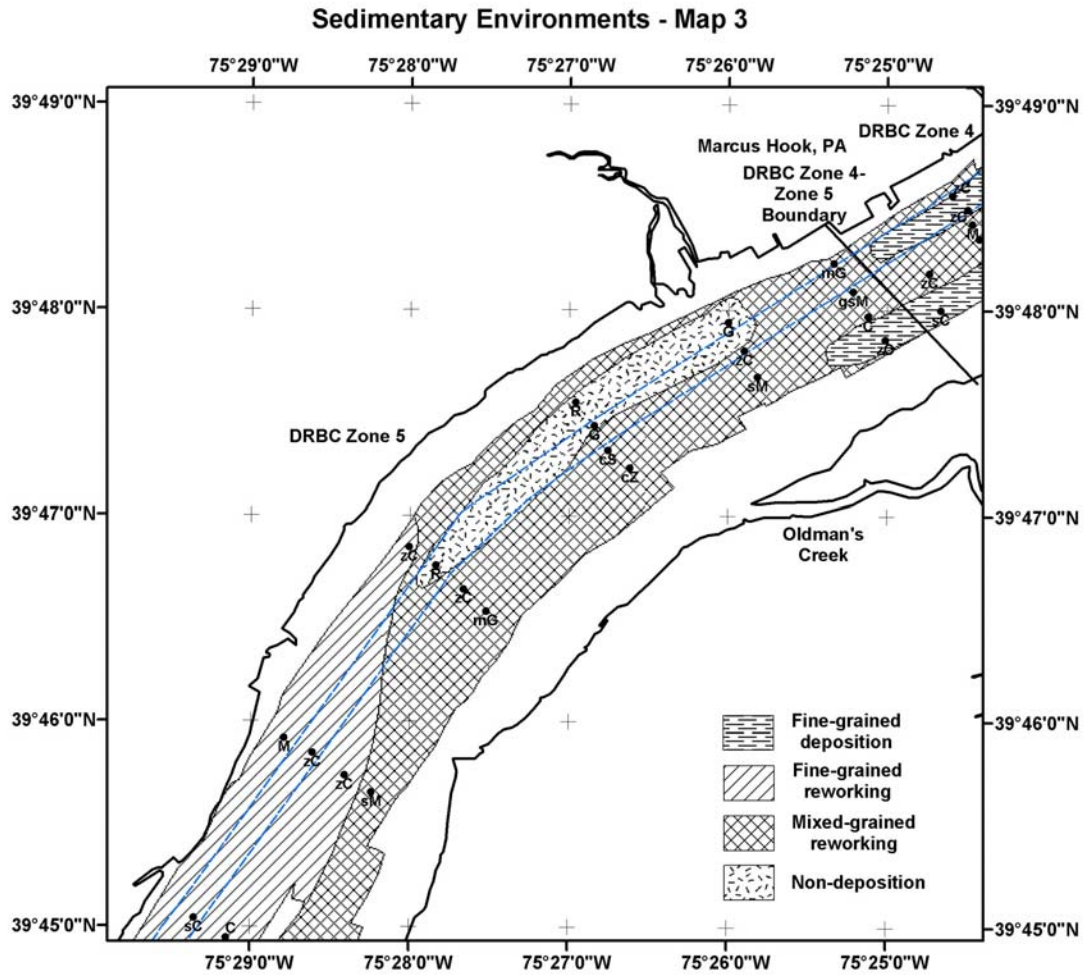


Figure 24. Sedimentary Environments Map 3 based on the Marcus Hook Bar mosaic.

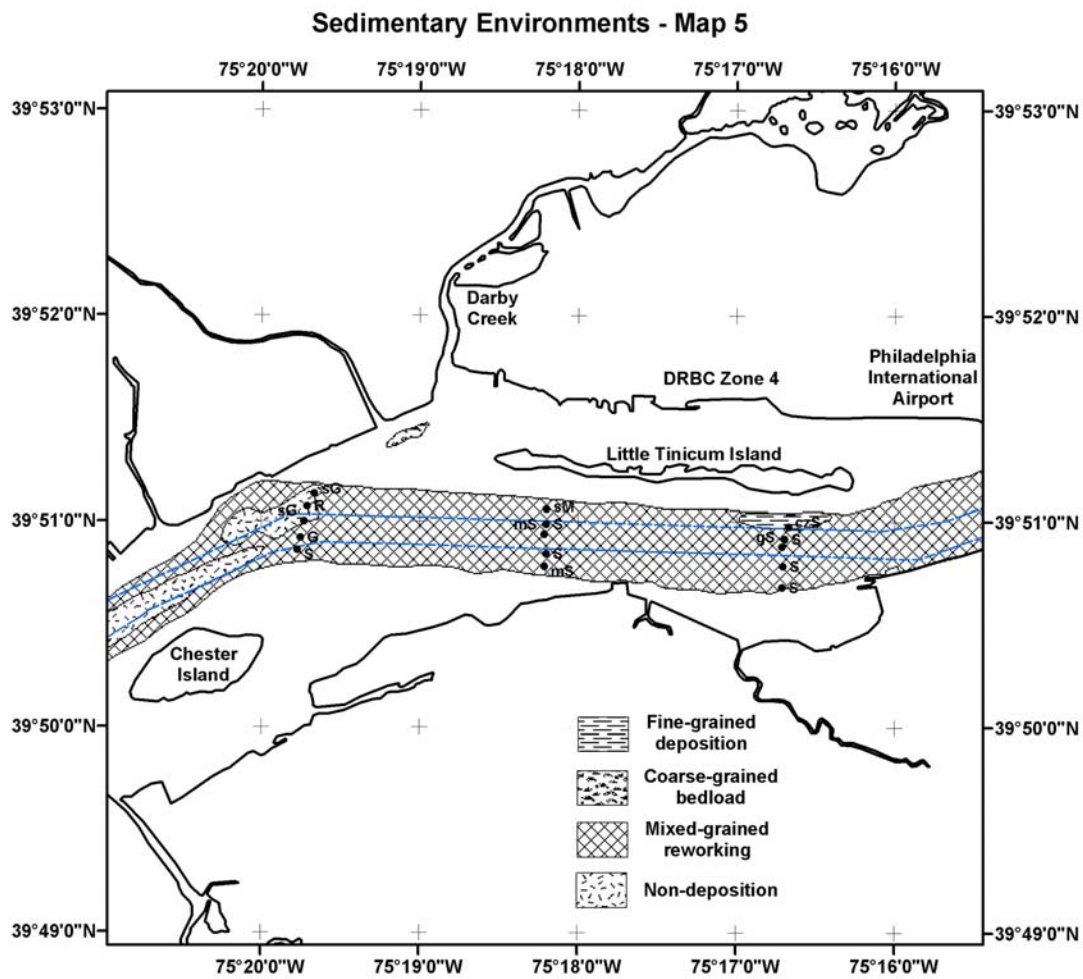


Figure 26. Sedimentary Environments Map 5 based on the Tinicum mosaic.

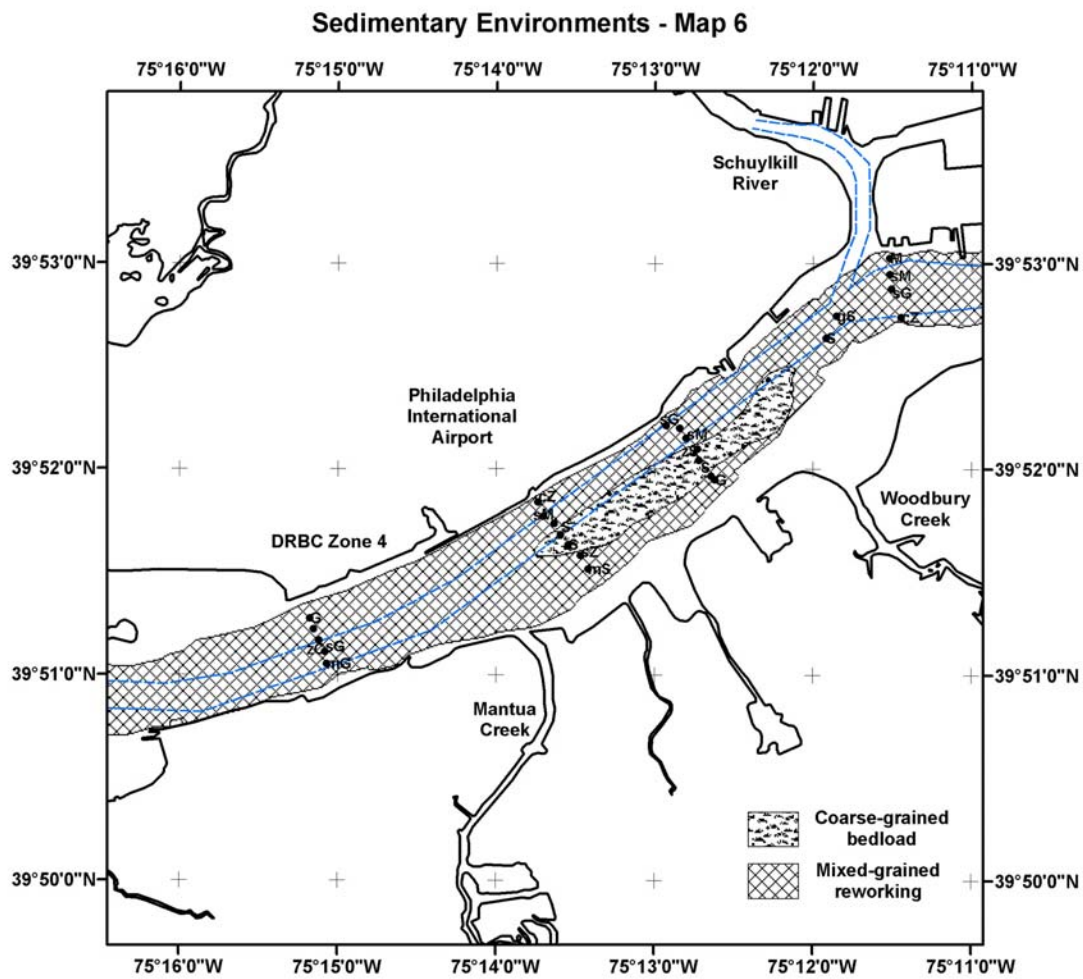


Figure 27. Sedimentary Environments Map 6 based on the Airport mosaic.

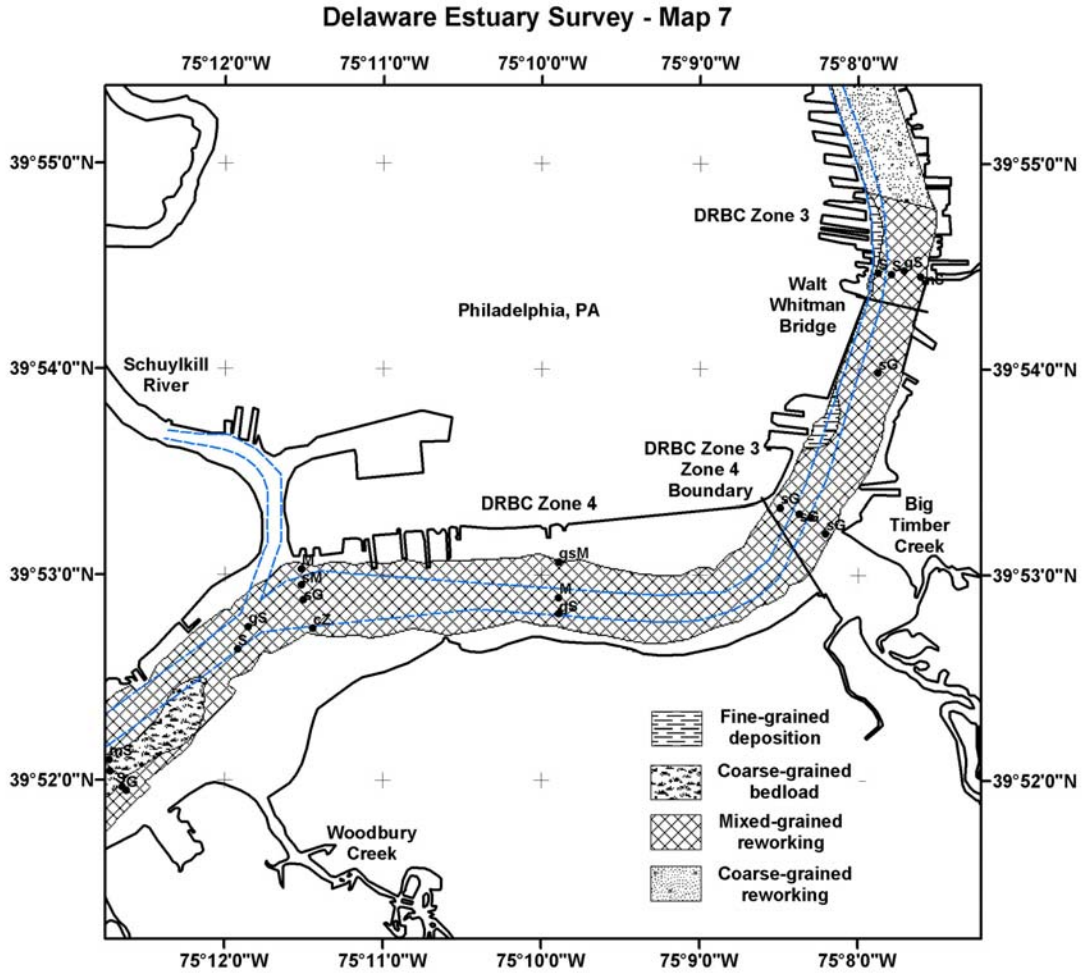


Figure 28. Sedimentary Environments Map 7 based on the Navy Yard mosaic. Note that the mixed- to coarse-grained reworking transition is more gradational than depicted.

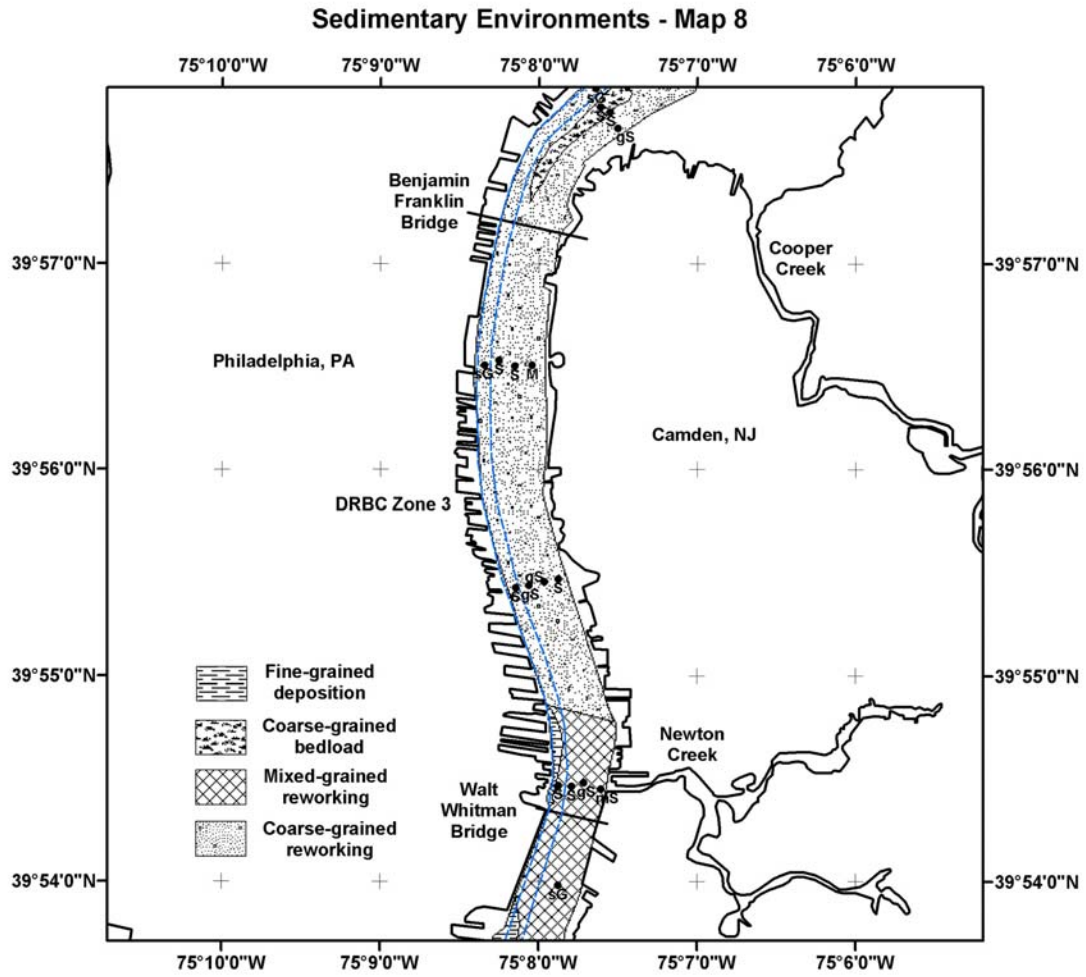


Figure 29. Sedimentary Environments Map 8 based on the Camden mosaic. Note that the mixed- to coarse-grained reworking transition is more gradational than depicted.

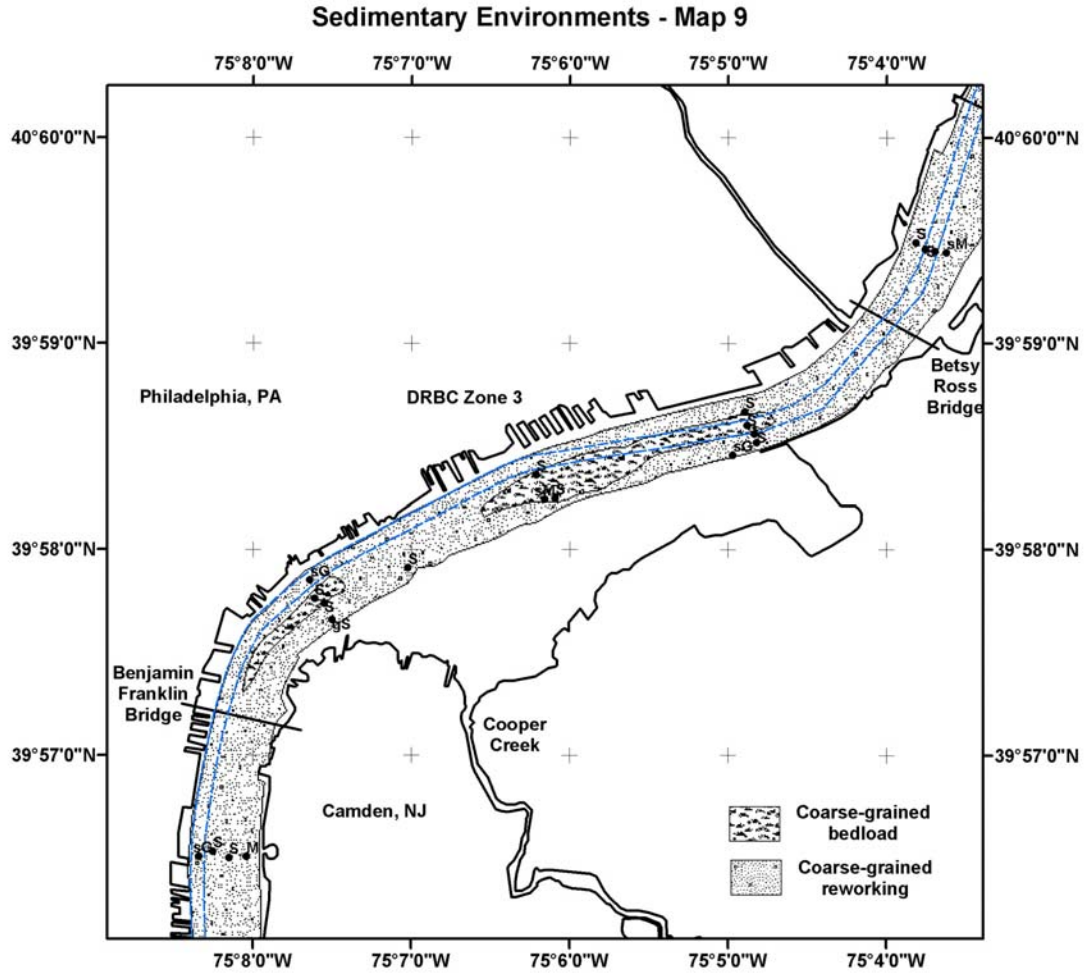


Figure 30. Sedimentary Environments Map 9 based on the Petty Island mosaic.

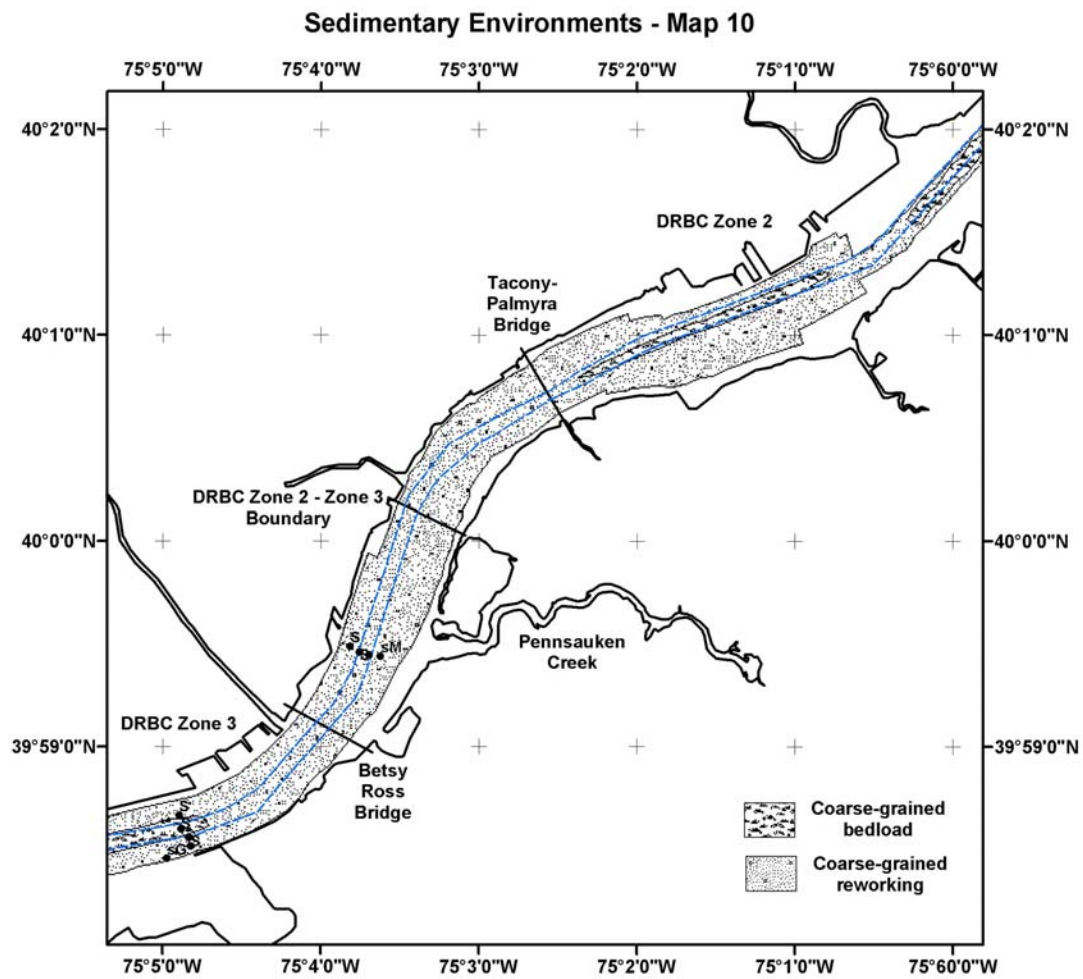


Figure 31. Sedimentary Environments Map 10 based on the Palmyra mosaic.

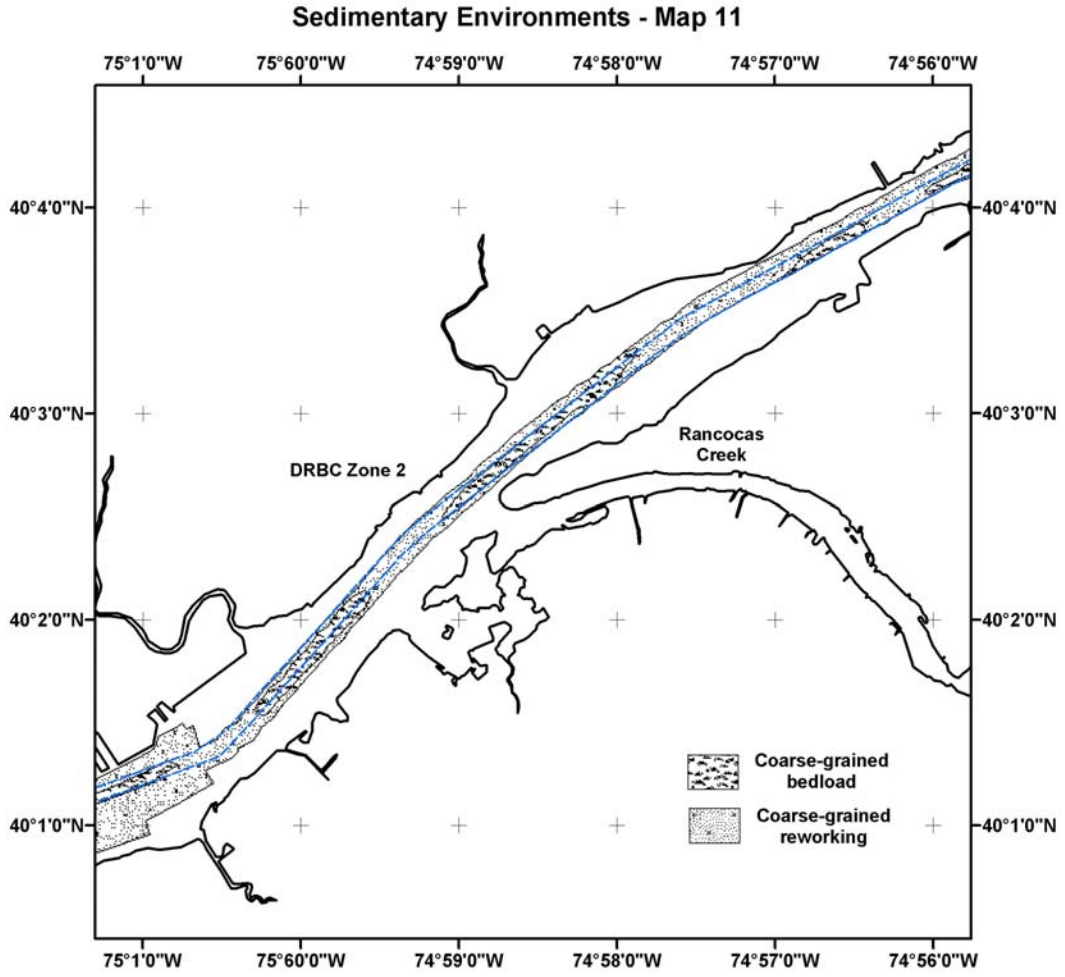


Figure 32. Sedimentary Environments Map 11 based on the Burlington mosaic.

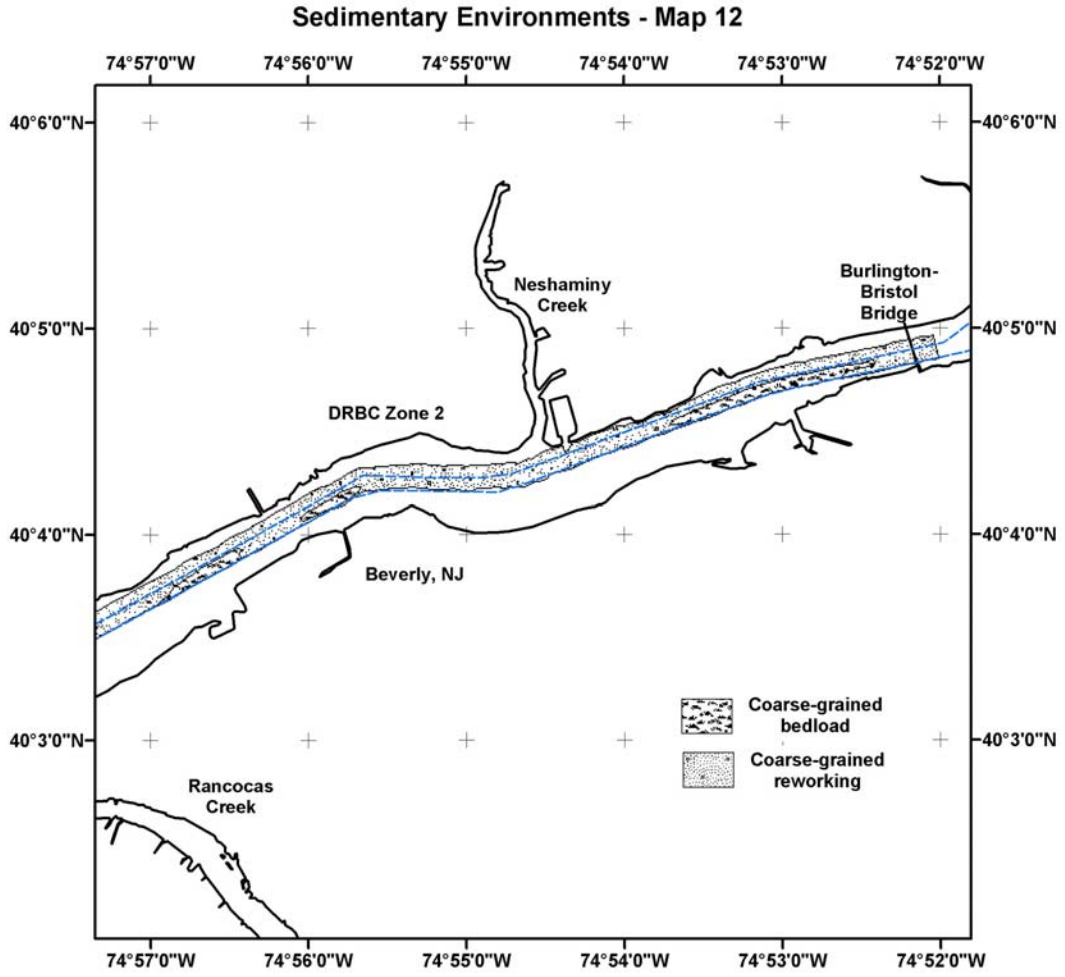


Figure 33. Sedimentary Environments Map 12 based on the Burlington mosaic.

Areas of non-deposition (or erosion), denoted by patterns of strong backscatter intensity continuous on scales of 10's of meters or more, are characterized by cobble bottoms or bedrock exposures. These bottoms lack evidence of sustained bedload transport and (or) net accumulation of sediment. The channel bottom adjacent to Chester Island is an example of the non-deposition sedimentary environment (Figures 26).

Note that the sedimentary environments maps presented herein are subject to refinement, perhaps reinterpretation, as new data become available. Moreover, the spatial distributions as mapped are representative for the survey period and reflect time-averaged sedimentation conditions. Temporal changes in hydrodynamics, not to mention human disturbances, are liable to modify the bottom to some extent, perhaps rendering these maps inaccurate in places. Also note that the boundaries drawn to set apart the various environment types are, in reality, more gradational than depicted in the maps.

5.5. Subbottom Observations

5.5.1. Features of Note

Because the chirp sonar dataset is extensive and difficult to generalize, only those results salient to the understanding of sediment transport and deposition in the upper estuary are elaborated. Details regarding the full dataset are available from the authors at request.

Sonar Line 103, collected in the northernmost part of the study area, illustrates the coarse-grained bedload environment (Figure 34). Though bedload transport occurs to some extent throughout the estuary, well-developed trains of ripples and waves are best developed in Zones 2–3, where copious sand and sandy gravel is available for transport. Line 103 reveals that coarse-grained material is derived locally from erosion of subbottom strata and packaged into asymmetric sand waves with an orientation (lee side upriver) indicative of transport during flood tides (Figure 34).

Sonar Line 39 depicts an example of a fine-grained deposition environment (Figure 35). Deposition of fine-grained suspended sediments generally increases down-estuary of Philadelphia and is initially apparent near Marcus Hook. There, a massive quantity of fluidized mud (soupy, silty clay) was present during the geophysical survey,

Areas of non-deposition (or erosion), denoted by patterns of strong backscatter intensity continuous on scales of 10's of meters or more, are characterized by cobble bottoms or bedrock exposures. These bottoms lack evidence of sustained bedload transport and (or) net accumulation of sediment. The channel bottom adjacent to Chester Island is an example of the non-deposition sedimentary environment (Figures 26).

Note that the sedimentary environments maps presented herein are subject to refinement, perhaps reinterpretation, as new data become available. Moreover, the spatial distributions as mapped are representative for the survey period and reflect time-averaged sedimentation conditions. Temporal changes in hydrodynamics, not to mention human disturbances, are liable to modify the bottom to some extent, perhaps rendering these maps inaccurate in places. Also note that the boundaries drawn to set apart the various environment types are, in reality, more gradational than depicted in the maps.

5.5. Subbottom Observations

5.5.1. Features of Note

Because the chirp sonar dataset is extensive and difficult to generalize, only those results salient to the understanding of sediment transport and deposition in the upper estuary are elaborated. Details regarding the full dataset are available from the authors at request.

Sonar Line 103, collected in the northernmost part of the study area, illustrates the coarse-grained bedload environment (Figure 34). Though bedload transport occurs to some extent throughout the estuary, well-developed trains of ripples and waves are best developed in Zones 2–3, where copious sand and sandy gravel is available for transport. Line 103 reveals that coarse-grained material is derived locally from erosion of subbottom strata and packaged into asymmetric sand waves with an orientation (lee side upriver) indicative of transport during flood tides (Figure 34).

Sonar Line 39 depicts an example of a fine-grained deposition environment (Figure 35). Deposition of fine-grained suspended sediments generally increases down-estuary of Philadelphia and is initially apparent near Marcus Hook. There, a massive quantity of fluidized mud (soupy, silty clay) was present during the geophysical survey,

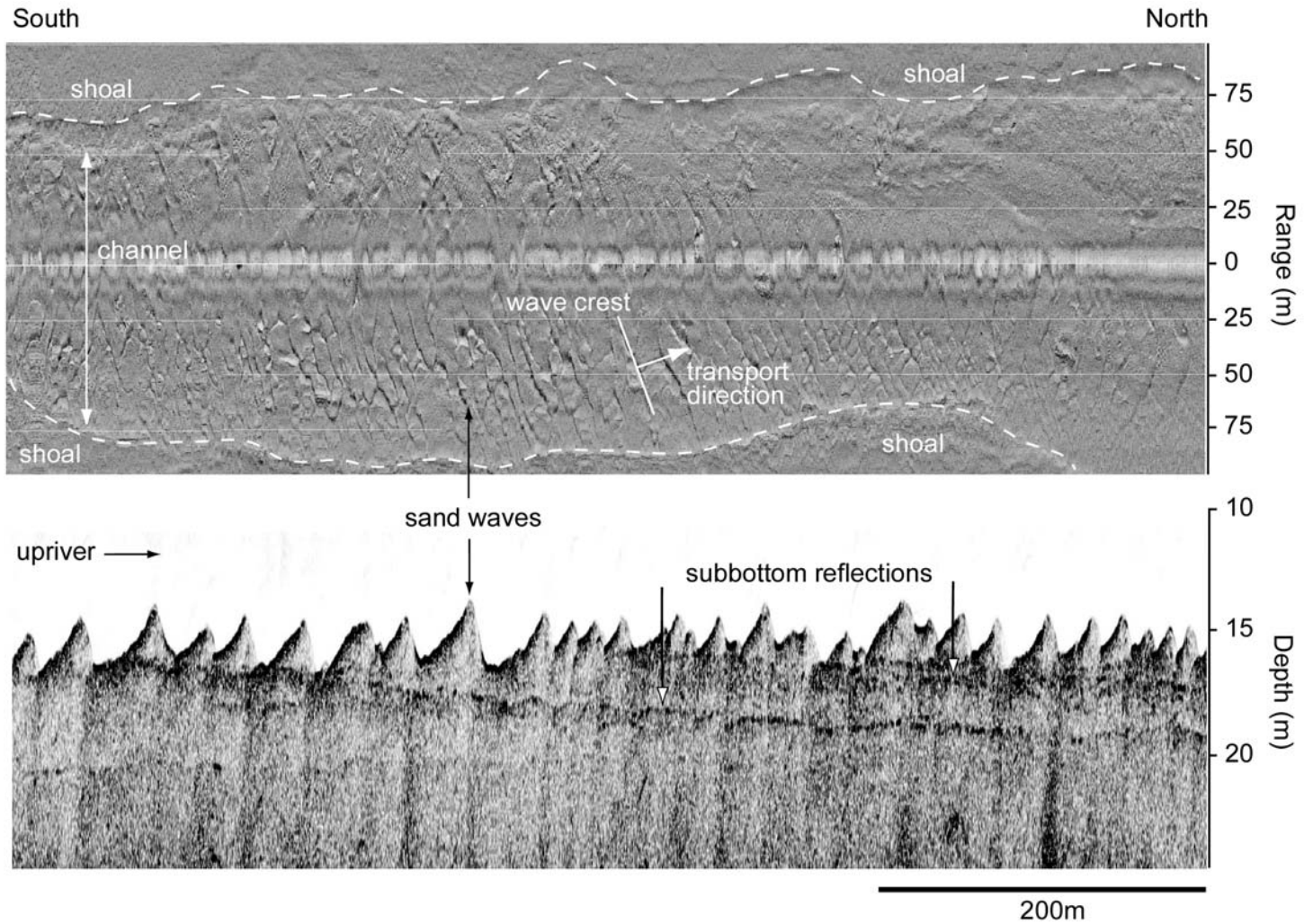


Figure 34. Sonar Line 103 (partial). Shown are the chirp profile (bottom) and corresponding sidescan image (see Figure 14 for location). Survey line trends along the channel of the tidal Delaware River, and the dashed line denotes the channel–shoal boundary. Bedload transport is indicated by a train of 2–3 meter amplitude sand waves oriented in the direction of flood-tidal currents. Note the truncation of subbottom strata, an indication of erosional reworking of the bottom.

particularly within the shipping channel, and later confirmed by coring in April and November of 2001. Though small patches of fluid mud were observed elsewhere down-estuary, the largest accumulations were present off Marcus Hook at the time of survey. Otherwise, normally consolidated silty clay and sandy, silty clay characterize the bottom in this area. In the shipping channel, fluid muds are underlain by gas-charged deposits (biogenic methane gas) that produce a "turbid" acoustic signature (Figure 35). Voids and bubbles observed in cores collected in channel confirm the presence of gas. Fortuitously, the fluid-mud layers were sufficiently thick to be resolved by the chirp sonar and therefore were mapped (Figure 36). Based on their spatial extent and porosity (see Core 15b in Appendix D), the fluid mud deposits had a cumulative dry mass estimated at $\sim 3.5 \times 10^5$ tons, a mass equivalent to $\sim 25\%$ of the annual fluvial sediment load delivered to the estuary. This observation suggests that material sequestered in isolated depocenters may collectively comprise a substantial fraction of the total sediment mass stored within the subtidal estuary.

Another example of a fine-grained depositional environment is illustrated by sonar Line 122. Most prominently south of the Delaware Memorial Bridge, mud deposition is relatively uniform across the natural channel as indicated by a ≤ 1 -m thick acoustically transparent layer atop more reflective strata (Figure 37). Bottom sediments in the channel are normally consolidated clays with variable amounts of sand and silt. Within the shipping channel, however, bottom sediments are far more variable across-channel with fine-grained, weakly reflective muds present on the western side, strongly reflective sandier muds on the eastern. On the eastern flank, coarse-grained sediments were commonly packaged into discontinuous ribbons and lineations plainly visible atop a muddy substrate (Figure 37). This pattern reveals a complex combination of suspended-load deposition and bedload transport within the shipping channel, a consequence of cross-channel variations in current velocity and sediment availability.

Previous work has shown that the sedimentary cover is thin to non-existent in places where bedrock is exposed at, or just below, the riverbed (Duran, 1986; USACE, 1973). This is exemplified by the Line 34 chirp profile, which shows a 1–2 m thick deposit of acoustically transparent strata resting on a strongly reflective surface with a distinct, undulating contact (Figure 38). From its acoustic properties the reflector is

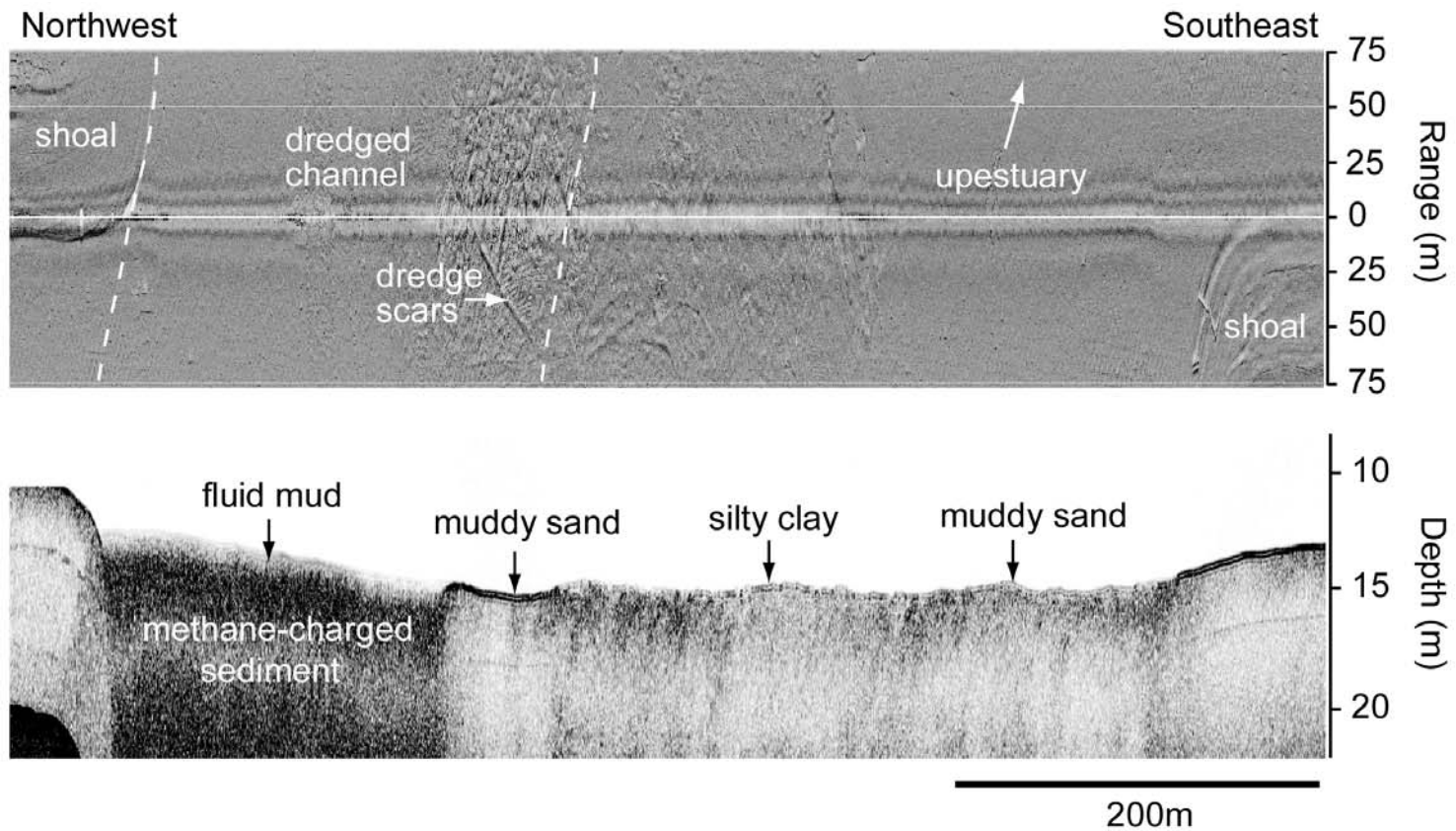


Figure 35. Sonar Line 39 (partial). Chirp profile (bottom) and sidescan image trend perpendicular to the estuarine channel. Bottom types noted are based on analysis of grab samples. The muddy bottom is morphologically smooth with a weak backscatter signature. Position of the dredged channel is depicted by dashed lines. Note the 2–3 m thick layer of fluid muds atop methane-charged sediment. Also note the dredge-cutter scars at the channel edge.

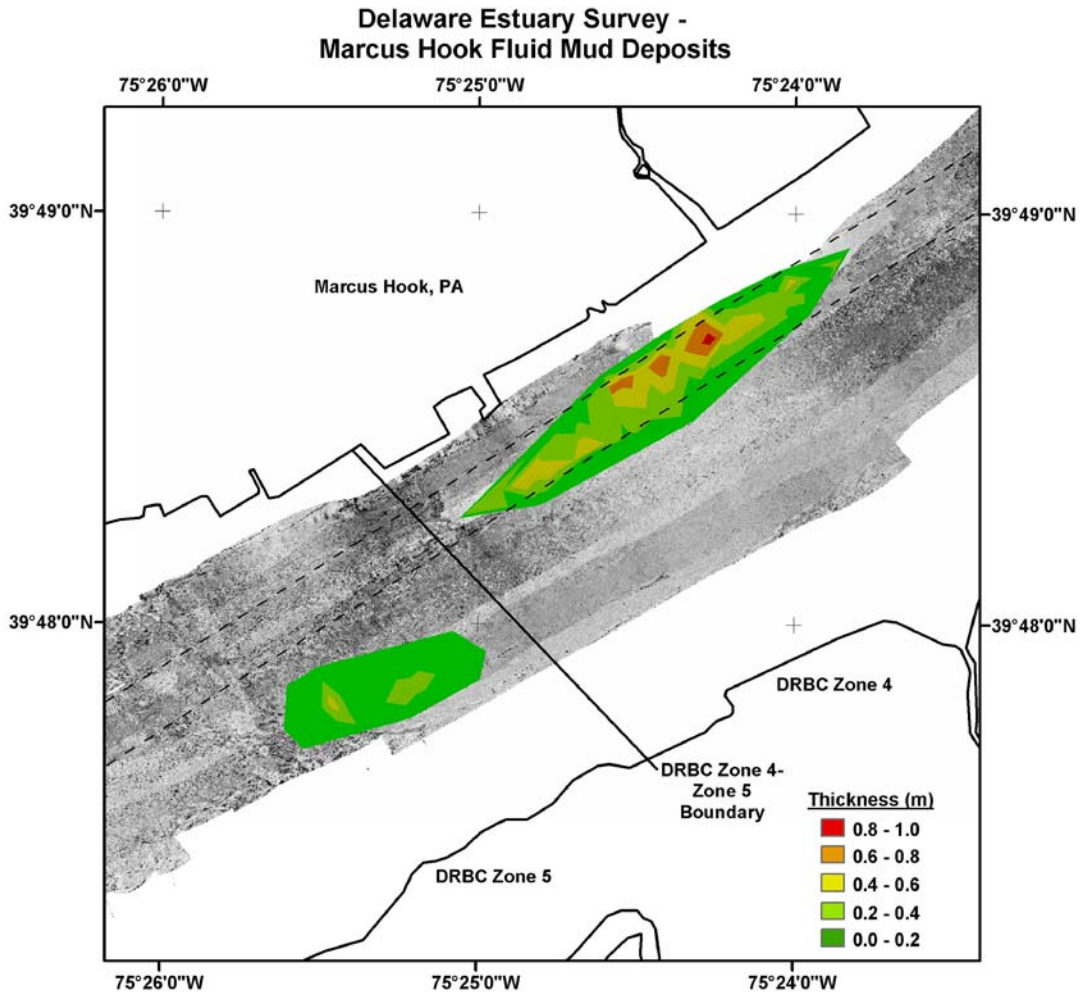


Figure 36. Fluid-mud distribution map. Shown is the contoured thickness of fluid mud deposits as mapped via chirp sonar in August 2001.

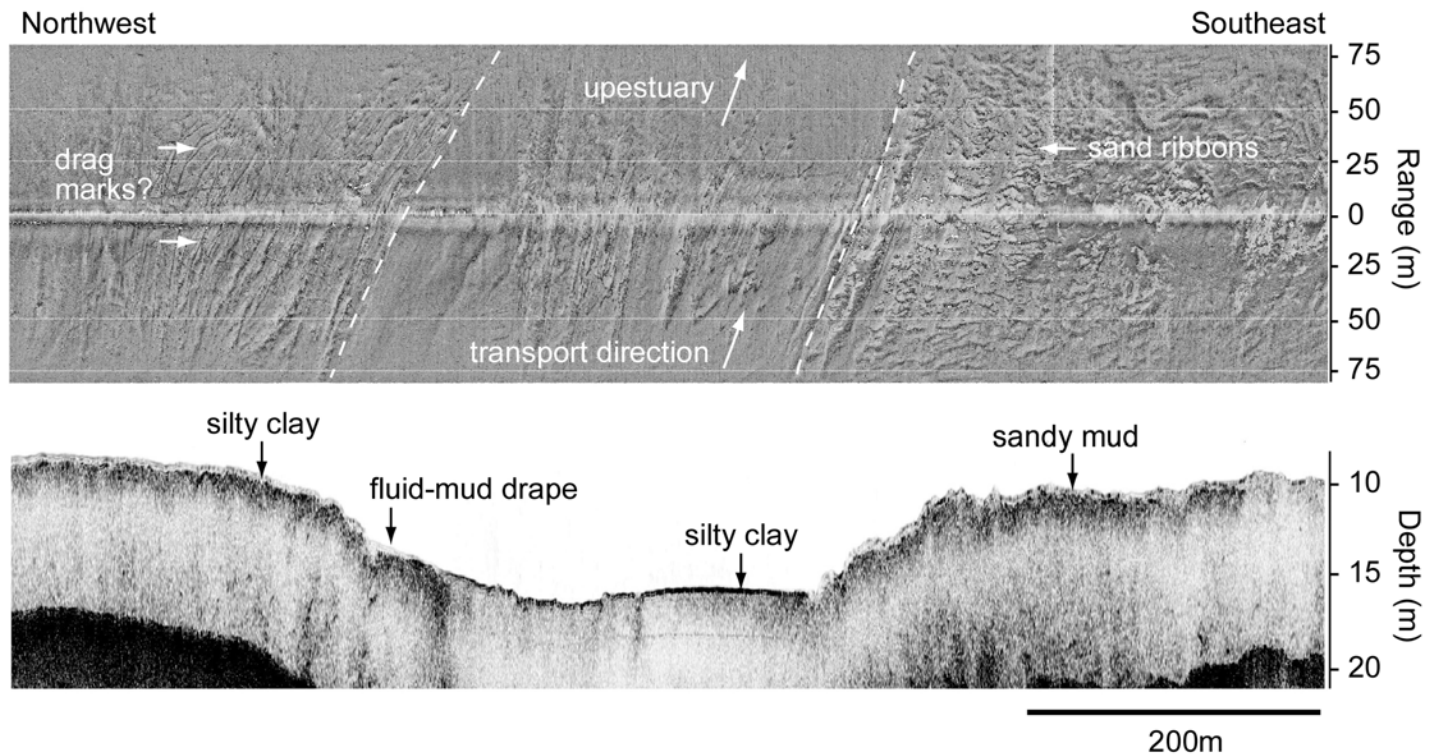


Figure 37. Sonar Line 122. The chirp profile (bottom) and sidescan sonograph trend perpendicular to the estuarine channel (see Figure 5 for location). Bottom types are based on analyses of grab samples. Moderate backscatter intensity is created by bedforms oriented both parallel and perpendicular to along-channel flow. Dredged channel bounds are denoted by dashed line on sonograph. Note that fluid mud preferentially accumulates on the western channel edge. Also note lineations that are interpreted to be drag marks.

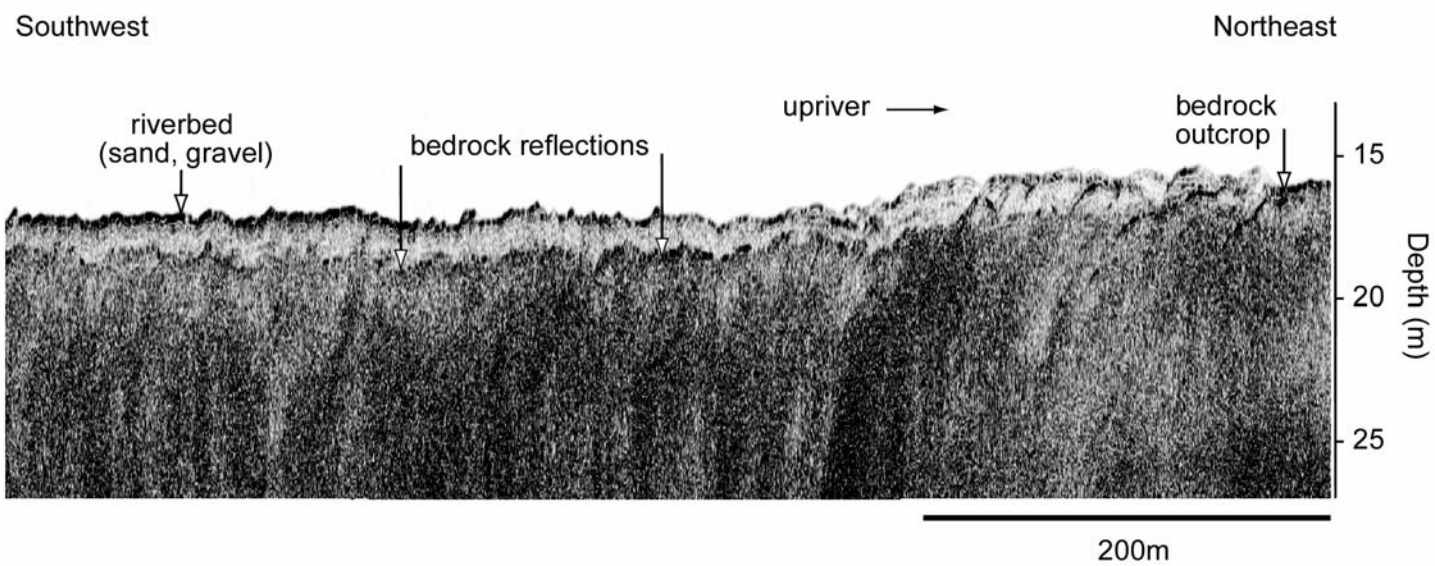


Figure 38. Sonar Line 34 (partial). Chirp profile trends along the dredged channel in the upper estuary (see Figure 8 for location). Note that bedrock is merely 1–2 m beneath the river bottom at this location and outcrops in places. See Figure 36 for contour map of bedrock occurrence.

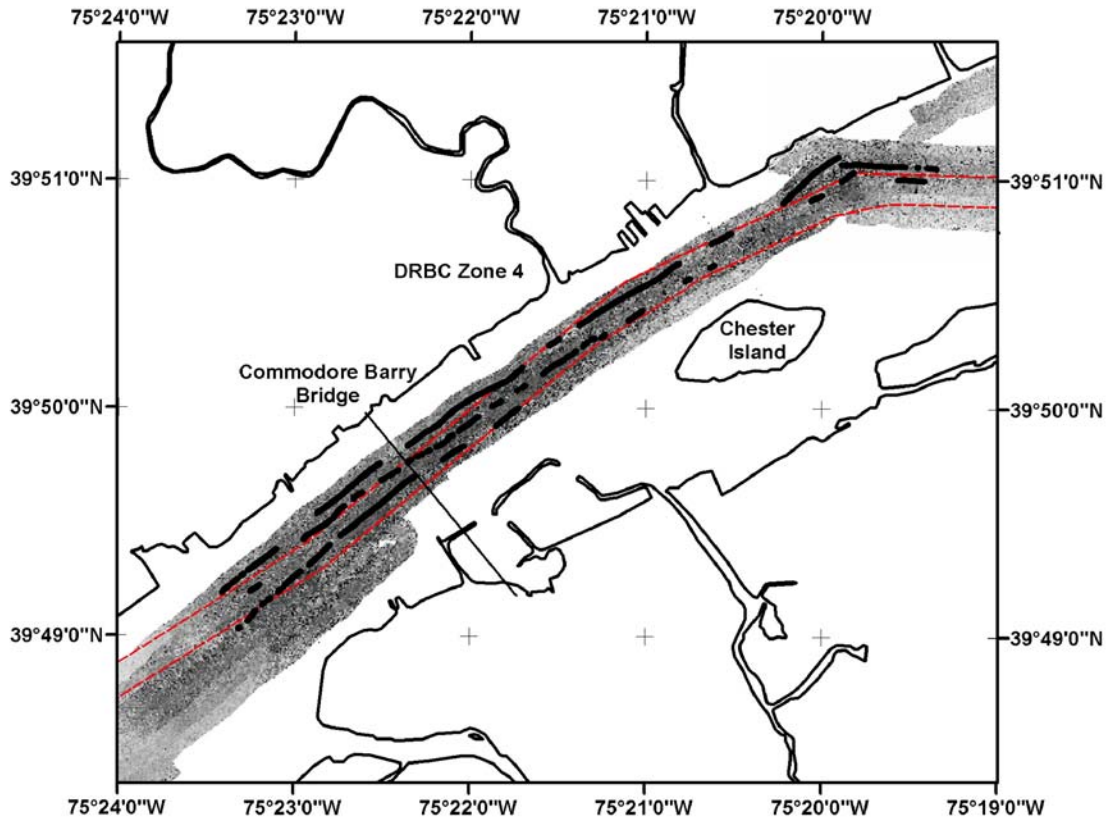


Figure 39. Bedrock occurrence map. Bold (black) lines denote areas surveyed where bedrock is exposed at, or within 50 cm of, the riverbed. The shipping channel is shown by the thin dotted line.

interpreted to be crystalline bedrock, perhaps the Wissahickon Schist mapped locally (Lyttle and Epstein, 1987; Schenck et al., 2000). Nearby grab samples confirmed the presence of a rocky bottom characterized by angular fragments and rounded cobbles, though the actual bedrock geology is unknown. Bedrock exposures at or within 50 cm of the bottom are particularly numerous between Tinicum Island and Chester. The mapped distribution of these exposures is shown in Figure 39.

The paucity of sedimentary cover in Zone 4 reveals that sediment accumulation is negligible on the long term, though there are clear exceptions. Where the bottom has been deepened through dredging, fine-grained sediments trapped within the channel can accumulate to form localized depocenters. Sediment accumulations within the shipping channel are not trivial; indeed, independent estimates (Biggs and Beasley, 1988; USACE, 1973) suggest that the mass of sediment dredged annually from the channel ($\sim 3 \times 10^6$ tons) exceeds that supplied to the estuary by rivers on an annual basis ($1\text{--}2 \times 10^6$ tons). Clearly, not only does channel maintenance create a bathymetric trap for sediments, it permanently removes material that would otherwise disperse throughout the open estuary and hydraulically contiguous environments. In this manner dredging constitutes a net sink for sediment in the river–estuary system.

5.6. Radioisotope Profiles and Sedimentation Rates

5.6.1. Reconnaissance Cs-137 Measurements

A total of 25 HDC samples from the subtidal estuary were collected early in this study to evaluate the potential of Cs-137 as a sediment chronometer. Of these, 13 cores from muddy depositional sites were selected for reconnaissance Cs-137 measurements (Figure 40; Table 4). Core subsamples were first counted at low resolution (top, middle, and bottom) as gross measure of sediment "age", because the mere presence/absence of Cs-137 in sediments is an indication of deposition after or before 1954, respectively. Only at three sites, Tinicum Island shoal (C-14b), Marcus Hook East (MHE), and Smyrna River mouth (C-16A), were Cs-137 activities high enough to warrant more detailed measurements. Elsewhere the activities were at or below detection limits (Appendix C), suggesting that net accumulation of mud was locally negligible and (or) the bottom erosional, since 1954. In sum, the reconnaissance measurements revealed that the rates of fine-sediment accumulation between Burlington and New Castle are by and large too

interpreted to be crystalline bedrock, perhaps the Wissahickon Schist mapped locally (Lyttle and Epstein, 1987; Schenck et al., 2000). Nearby grab samples confirmed the presence of a rocky bottom characterized by angular fragments and rounded cobbles, though the actual bedrock geology is unknown. Bedrock exposures at or within 50 cm of the bottom are particularly numerous between Tinicum Island and Chester. The mapped distribution of these exposures is shown in Figure 39.

The paucity of sedimentary cover in Zone 4 reveals that sediment accumulation is negligible on the long term, though there are clear exceptions. Where the bottom has been deepened through dredging, fine-grained sediments trapped within the channel can accumulate to form localized depocenters. Sediment accumulations within the shipping channel are not trivial; indeed, independent estimates (Biggs and Beasley, 1988; USACE, 1973) suggest that the mass of sediment dredged annually from the channel ($\sim 3 \times 10^6$ tons) exceeds that supplied to the estuary by rivers on an annual basis ($1\text{--}2 \times 10^6$ tons). Clearly, not only does channel maintenance create a bathymetric trap for sediments, it permanently removes material that would otherwise disperse throughout the open estuary and hydraulically contiguous environments. In this manner dredging constitutes a net sink for sediment in the river–estuary system.

5.6. Radioisotope Profiles and Sedimentation Rates

5.6.1. Reconnaissance Cs-137 Measurements

A total of 25 HDC samples from the subtidal estuary were collected early in this study to evaluate the potential of Cs-137 as a sediment chronometer. Of these, 13 cores from muddy depositional sites were selected for reconnaissance Cs-137 measurements (Figure 40; Table 4). Core subsamples were first counted at low resolution (top, middle, and bottom) as gross measure of sediment "age", because the mere presence/absence of Cs-137 in sediments is an indication of deposition after or before 1954, respectively. Only at three sites, Tinicum Island shoal (C-14b), Marcus Hook East (MHE), and Smyrna River mouth (C-16A), were Cs-137 activities high enough to warrant more detailed measurements. Elsewhere the activities were at or below detection limits (Appendix C), suggesting that net accumulation of mud was locally negligible and (or) the bottom erosional, since 1954. In sum, the reconnaissance measurements revealed that the rates of fine-sediment accumulation between Burlington and New Castle are by and large too

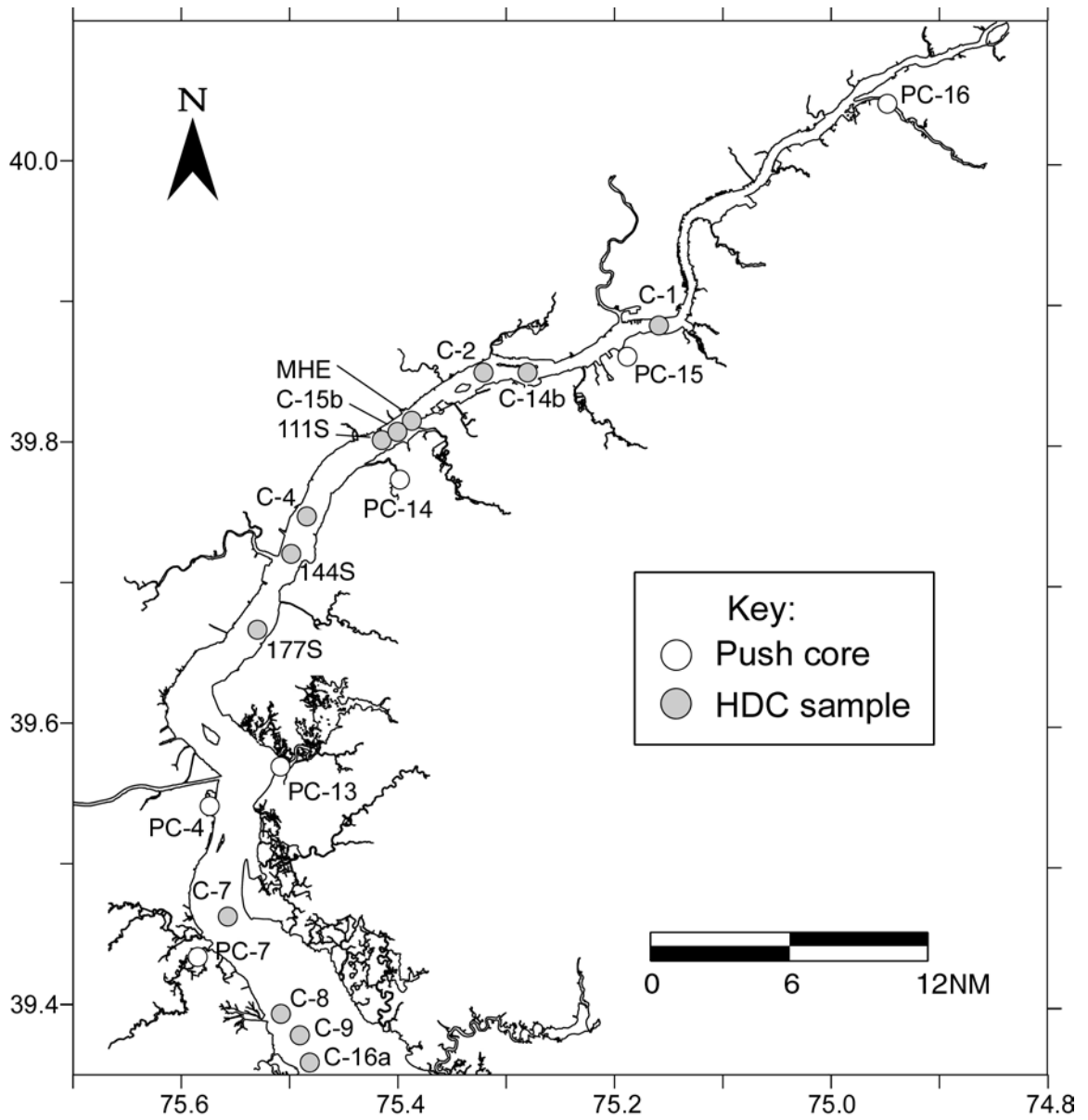


Figure 40. Locations of cores analyzed for radioisotopes.

low, or the bottom too disturbed, for the Cs-137 method to provide reliable chronologies. This result is consistent with sonar observations of a physically reworked bottom down-estuary of Philadelphia. As detailed later tidal marsh and floodplain sites of the upper estuary proved more amenable to Cs-137 dating.

Table 4. HDC sample and push-core locations

Location	Site	Collection Date	Latitude	Longitude
Rancocas Creek	PC-16	7/19/02	40° 02.053	74° 56.116
Woodbury Creek	PC-15	7/18/02	39° 51.040	75° 10.605
Tinicum Island shoal	C-14b	7/20/01	39° 51.023	75° 16.860
Marcus Hook ship channel	C-15b	7/20/01	39° 48.779	75° 23.975
Marcus Hook shoal	MHE	3/22/02	39° 48.627	75° 23.852
Oldmans Creek	PC-14	7/18/02	39° 46.546	75° 24.021
Salem River Marsh	PC-13	4/6/02	39° 34.645	75° 30.240
St. Georges Marsh	PC-4	2/23/02	39° 32.336	75° 34.157
Blackbird Creek	PC-7	4/5/02	39° 26.157	75° 34.924
Smyrna River mouth	C-16A	7/20/01	39° 21.165	75° 28.157

The idealized sediment-depth profile for an impulse tracer like Cs-137 generally mirrors the atmospheric source function and exhibits the following characteristics up-core: (1) a steep limb of increasing activity consistent with the 1954 onset; (2) a prominent peak representative of maximum atmospheric fallout around 1964; and (3) a limb of gradually decreasing activity to non-detectable values in post-1980 sediment intervals (Olsen et al., 1981). For the sedimentary record to faithfully archive the atmospheric source function, the following conditions must be met: (1) steady-steady sediment accumulation; (2) negligible post-deposition mixing of the solid phase (i.e., by burrowing organisms); and (3) chemical immobility of Cs-137 in the sediment column (no desorption). Because steady-state accumulation is atypical for dynamic sedimentary environments, a "1964" peak is not universally present in Cs-137 profiles, and instead the penetration depth of Cs-137 can be used to compute a sedimentation rate averaged since 1954 (Nittrouer et al., 1984). For this approach to be valid, sedimentation post-1954 must be more-or-less continuous, and deep biological mixing negligible. One effect of deep mixing is to increase Cs-137 penetration in the sediment column, thereby increasing the computed sedimentation rate over the true value. Numerical modeling has shown that

the influences of biological mixing (and chemical diffusion) are negligible when the true rate of sedimentation approaches 1 cm/yr (Olsen et al., 1981). Nonetheless, sedimentation rates based on radiotracer profiles should be conservatively viewed as *maximum* estimates when biological mixing is suspected.

None of the cores from the subtidal estuary displayed the ideal Cs-137 profile described above, and complementary Pb-210 profiles exhibited non-steady-state behavior, precluding use of these radiotracers to quantify sedimentation rates (Figure 41). Cesium-137 activity in cores C-14b, MHE, and C-16a was distributed near-uniformly with depth, an indication that deposition is rapid (and likely episodic) at these sites. This type of Cs-137 profile is typical for bottoms subject to intense erosion–deposition cycles or dredging disturbances (Schaffner et al., 1987; Olsen et al., 1993). Consequently, because these Cs-137 profiles might not be complete, the sedimentation rate can be only be constrained to >1 cm/yr.

5.6.2. Seasonal Deposition in the Estuary

Presence of Be-7 activity in two cores collected in spring 2001 shed light on the nature of seasonal deposition in the estuary. In general, occurrence of this radioisotope in bed sediments indicates that its depositional flux exceeds the rate of loss through radioactive decay or physical redistribution. In other words, Be-7 labels sediments that were suspended in the water column (in contact with the Be-7 source) on a timescale within about three half lives or five months of detection. Beryllium-7 was detected to depths of 32 cm and 4 cm in cores C-15b and C-9, respectively (Figure 42), consistent with short-term deposition rates on the order of centimeters per month. On the longer term net accumulation at Site C-15b is non-existent due to dredging, and ≥ 1 cm/yr at C-9 based Cs-137 occurrence (Figure 42). This observation reveals that although seasonal deposition rates are rapid, subsequent resuspension (or dredging) renders net accumulation rates considerably lower on the long term, a condition observed in other river-estuaries (Hirschberg et al., 1996; Woodruff et al., 2001). Although the actual mechanisms of short-term deposition in the estuary have yet to be elucidated, the Be-7 distributions reveal areas where fine-grained sediments are sequestered on a seasonal basis.

5.6.3. Marsh and Floodplain Sediment Accumulation

Five of the six marsh cores displayed Cs-137 activities that increased upcore and decrease subsequently toward the top (Figure 41). The lone exception was PC-7 (Blackbird Creek), in which Cs-137 activity was highest at the top. Only at Woodbury Creek (PC-15) did Cs-137 display the ideal profile with a prominent "1964" peak. At St. Georges Marsh, presence of Cs-137 to the core bottom suggests that the full inventory was not recovered. Likewise, some fraction of surficial Cs-137 inventory at the Salem Marsh site (PC-13) was lost when dense reed roots were removed to enable coring.

Sediment accumulation rates computed from the Cs-137 profiles following Equation 3 are presented in Table 5. Overall, accumulation rates ranged from 0.3 to 1.5 cm/yr, typical for subtidal–intertidal environments of New Jersey and Delaware. Because biological mixing intensity cannot be quantified from the Cs-137 profiles alone, potential mixing effects on the computed accumulation rates can only be surmised. Following the numerical modeling results of Olsen et al. (1981), at true sedimentation rates of 0.3–5.0 cm/yr and mixing intensities of 0.1–1.0 cm²/yr, the penetration of Cs-137 is increased by mixing to ≤ 6 cm below the "1954" datum. Mixing on this scale would cause the computed rates (Table 5) to be overestimated by 10–25 %, but the actual margin of error is apt to be much lower in the present case. Well-preserved bedding surfaces were observed in cores, suggesting that macrofaunal bioturbation is minimal, if present at all. Note that marsh sedimentation rates in general vary with various factors including sediment supply, elevation with respect to tidal inundation, and vegetation type and density. Because only one site at each marsh was sampled in this study, the spatial variability of intra-marsh sedimentation rate is unknown. *Accordingly, the reported sedimentation rate should not be assumed representative for the marsh as a whole.*

A noteworthy observation is that Cs-137 activity is present at significant levels in surficial deposits (core tops), despite the fact that atmospheric fallout has been insignificant since about 1980. Considering that significant post-depositional biological mixing is unlikely, there must be an additional source for Cs-137 in the estuary, perhaps wash-in from the watershed and (or) erosional redistribution of previously buried sediments. As discussed later, radioisotope inventories provide additional insight to the nature of Cs-137 in the estuary.

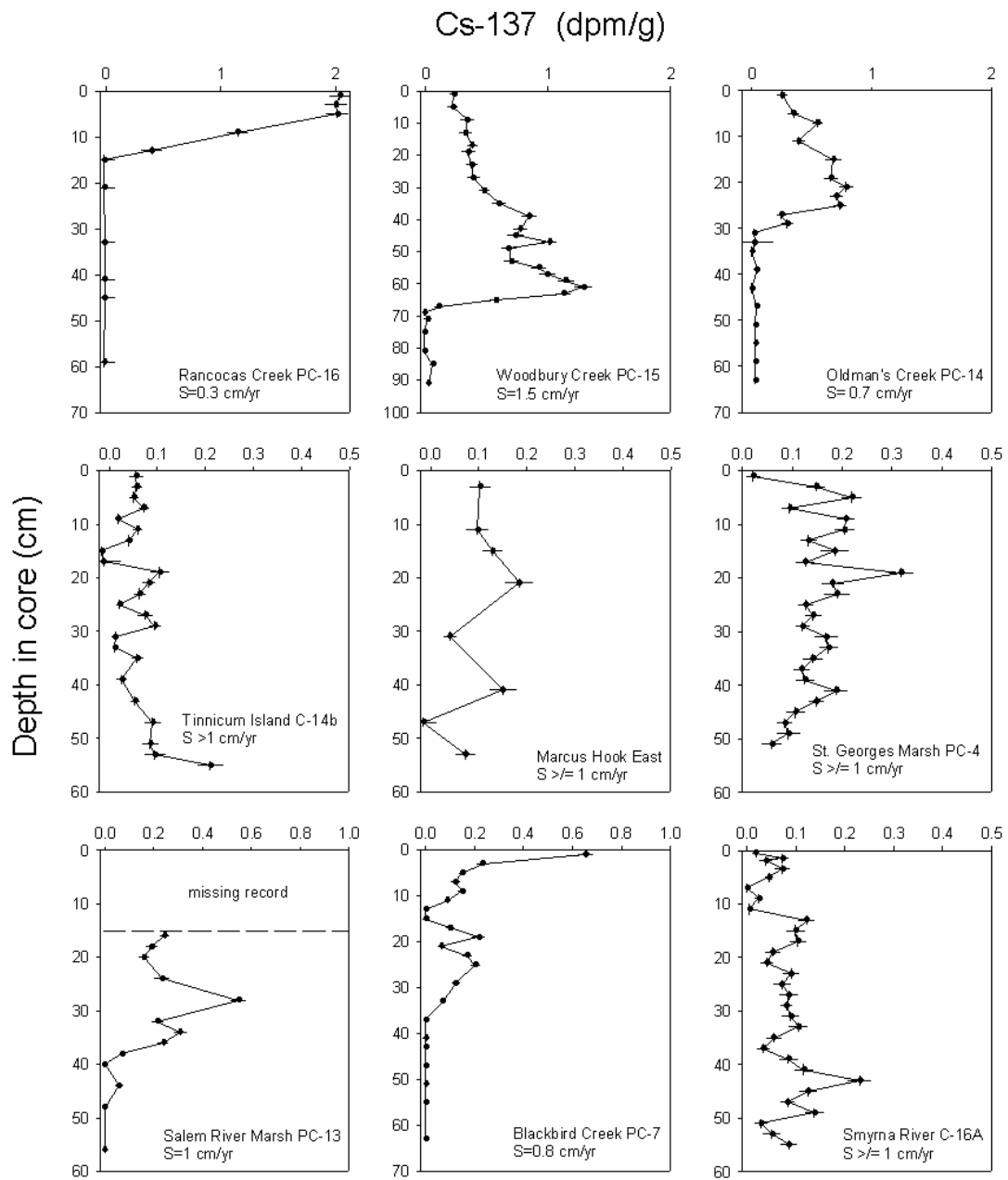


Figure 41. Cs-137 activity profiles for estuary and marsh cores. Note the different depth scales.

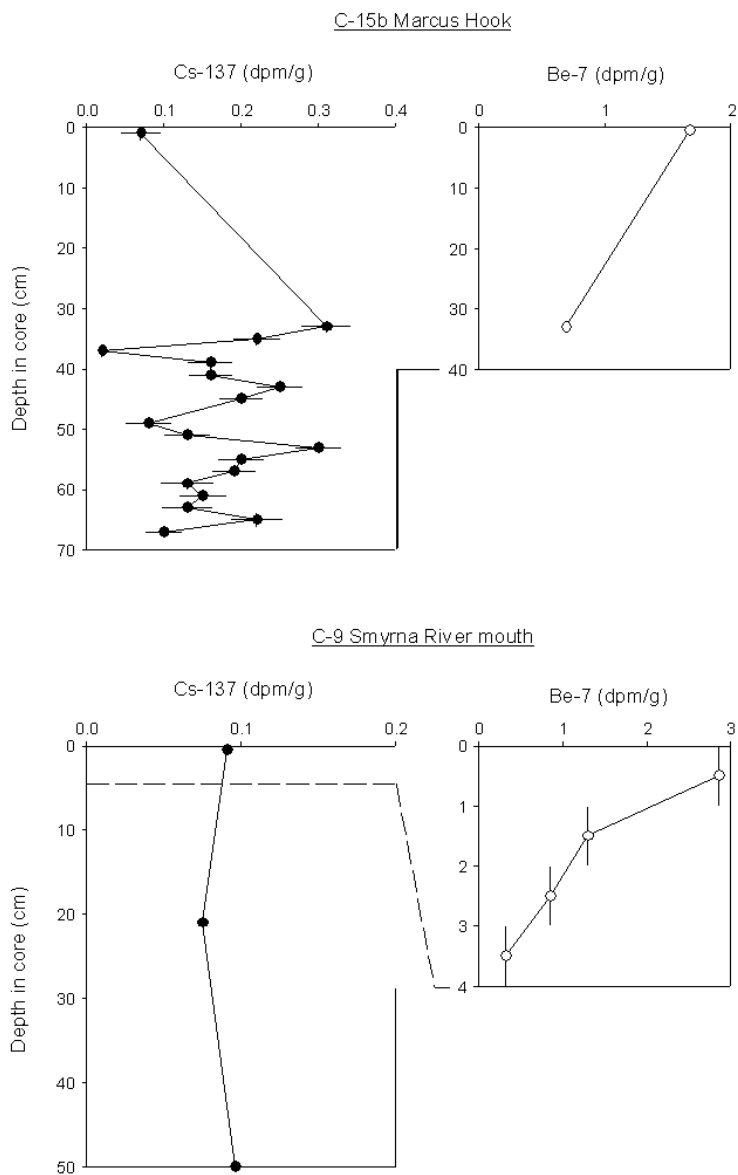


Figure 42. Cs-137 and Be-7 activity profiles from HDC cores. Note difference in depth scales.

Excess Pb-210 profiles for four of the marsh sites exhibited steady-state behavior, shown by a monotonic decrease in activity with depth (Figure 43). Sedimentation rates computed by least-squares linear regression of the activity profile ranged from 0.7 to 1.4 cm/yr. Lead-210 and Cs-137 based rates agreed well for sites PC-13 and PC-14 but differed by nearly a factor of two for PC-15 (Table 5). In part this difference may be attributed to the dissimilar timespans over which these radiotracers average sedimentation rate, in the case of PC-15, 47 years for Cs-137 and 90 years for Pb-210. Because the Pb-210 geochronology averages rates over a wider range of sedimentary conditions, including periods of non-deposition or minor erosion, it is intuitive that they should be somewhat lower than those based on Cs-137 chronology. An alternative explanation is that the rate of sedimentation at site PC-15 has increased during the past several decades, perhaps due to increasing sediment delivery to the marsh. Although this scenario cannot be ruled out completely, a recent increase in sedimentation rate is not immediately apparent from the radioisotope profiles.

Lead-210 profiles for sites MHE and C14b exhibited variable activities downcore with no net decrease (Figure 43). These non-steady-state profiles cannot be used to compute reliable sedimentation rates, but they support the inference that the bed is physically reworked and that short-term deposition is episodic; similar Pb-210 profiles have been observed in other river-estuaries where bed sediments are known to be continually resuspended and redeposited (Hirschberg et al., 1996). Again, presence of well-preserved bedding structures in these deposits supports the contention that physical processes, rather than bioturbation, are responsible for the shape of the activity profiles.

5.6.4. Radioisotope Inventories

Sediment inventories of radioisotopes (the depth-integrated activity) are useful for establishing how the supply of a radiotracer is partitioned by physical and physiochemical processes within river-estuarine systems. Specifically, the spatial distributions of inventories can elucidate material depocenters that result from sediment "focusing", a process by which suspended sediments (and adsorbed constituents) are preferentially sequestered in some areas over others (Olsen et al., 1993). For example, a

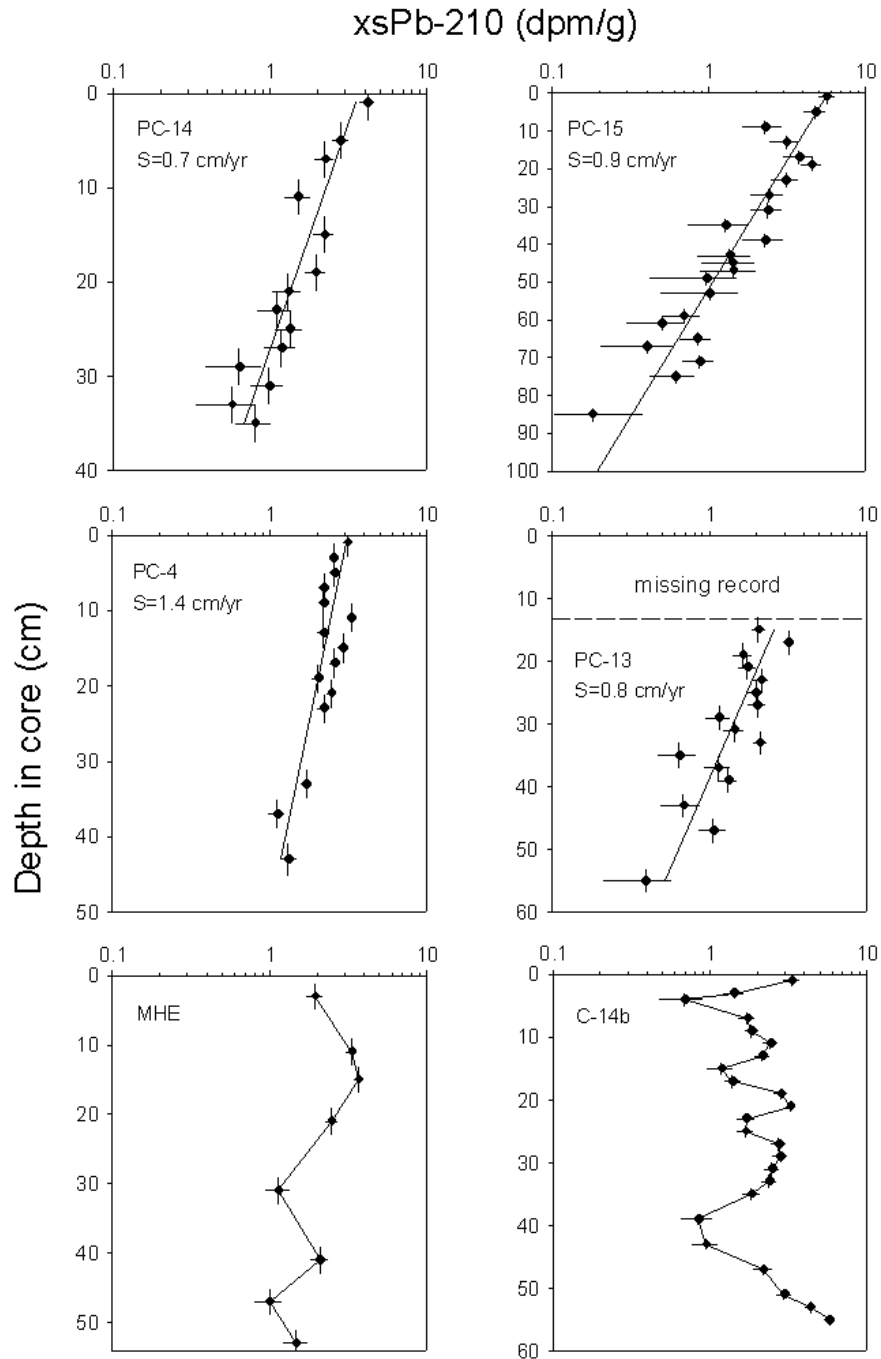


Figure 43. Profiles of excess Pb-210 activity. Note the different depth scales. Steady-state-type profiles are observed for marsh sites PC-4, PC-13, PC-14, and PC-15 (see text), non-steady-state for MHE and C-14b in the open estuary.

Table 5. Sediment accumulation rates and radioisotope inventories

Site	Cs-137 penetration (cm)	Cs-137 maximum (cm)	Cs-137 sed. rate (cm/yr)	Cs-137 inventory (dpm/cm ²)	Pb-210 sed. rate (cm/yr)	xsPb-210 inventory (dpm/cm ²)
C-1	nd ^a	nm ^b	-	-	-	-
C-2	nd	nm	-	-	-	-
C-4	nd	nm	-	-	-	-
C-7	nd	nm	-	-	-	-
C-14b	55	nm	>1.0	3.0	-	-
C-15b	68	nm	-	-	-	-
C-16A	55	43	≥1.0	3.5	-	-
MHE	54	nm	≥1.0	2.0	-	-
PC-4	19	51	>1.0	4.4	1.4	60
PC-7	37	nm	0.8	2.4	-	27
PC-13	40	29	1.0	4.0 ^c	0.8	28
PC-14	32	nm	0.7	11.5	0.7	52
PC-15	70	61	1.5	22.0	0.9	78
PC-16	14	nm	0.3	12.0	-	33

^and, non-detectable; ^bnm, no Cs-137 maximum; ^cincomplete inventory (see text)

measured Cs-137 inventory in excess of the expected depositional flux could result from extended scavenging during lateral transport of particles prior to burial, and (or) sources of inventory in addition to the local atmospheric flux. Conversely, inventories less than the expected value could be related to loss through erosion or chemical desorption (Olsen et al., 1982). In the case of tidal marsh deposits the two most important sources of Cs-137 and Pb-210 are (1) atmospheric deposition on exposed marsh surfaces and (2) tidal advection, i.e., inventory derived from open-estuary waters.

Cesium-137 and Pb-210 inventories were computed according to the following:

$$I = \sum \rho_s X_i (1 - \phi_i) A_i \quad (4)$$

where I is the radioisotope inventory (dpm/cm²), ρ_s the mineral density (2.65 g/cm³), X is the thickness of the sediment interval i (cm), ϕ is the porosity, and A is the activity at interval i (dpm/g). For cores in which radioisotope measurements were continuous with sediment depth, inventories were summed over the 2-cm intervals. Otherwise, activity and porosity values for omitted intervals were interpolated from adjacent values prior to computing the inventory.

Cesium-137 inventories ranged from 1.8 to 21.8 dpm/cm² and generally increased with distance up-estuary from Zone 5 to Zone 2 (Table 5). Inventories for PC-14, PC-15, and PC-16 were respectively 105 %, 52 %, and 57 % of the 1954–1980 atmospheric supply of 21 dpm/cm², and are high compared to the Delaware salt marsh (Kim et al., 1997) and US lowlands in general (Graustein and Turekian, 1986). These high inventories likely arise from a combination of high specific activity (due to fine-sediment size or clay mineralogy) and rapid sedimentation rate. Clearly, the freshwater marshes sampled in this study are efficient traps for Cs-137 derived from the local atmospheric flux or through tidal advection. By comparison, sites in the open estuary had Cs-137 inventories merely 10–14 % of the predicted value, where Cs-137 was measurable at all. These low inventories may reflect the coarser grain size of the estuarine sediments (i.e., lower specific activity) and (or) an incomplete post-1954 sedimentary record.

Lead-210 inventories provide further insight into the behavior of particle-reactive substances in the Delaware Estuary. The overall spatial distribution of Pb-210 inventories paralleled that of Cs-137, though the spread between high (78 dpm/cm²) and low (26 dpm/cm²) values was somewhat smaller (Table 5). The excess Pb-210 inventory range for the Delaware salt marsh and US lowlands is 25.6–27.7 dpm/cm² (Graustein and Turekian, 1986; Kim et al., 1997), 32 dpm/cm² being the theoretical steady-state inventory supported by a mean atmospheric flux of 1 dpm/cm²/yr (Graustein and Turekian, 1986). By comparison, inventories for Oldman's Creek, St. Georges Marsh, and Woodbury Creek are respectively 1.6, 1.9, and 2.4 times the theoretical value. This suggests that Pb-210 inventory in addition to that derived from the atmospheric is sequestered, tidal waters being a probable source. Inventories for Salem Marsh and Blackbird Creek at 27–28 dpm/cm² approximate the theoretical value, implying that Pb-210 is supplied by atmospheric deposition alone.

It should be noted that Cs-137 is not an ideal proxy for particle-associated chemical species in general. Although this radioisotope is strongly adsorbed to clay minerals in freshwater environments, in marine waters a larger fraction of dissolved-phase Cs-137 stays in solution as it must compete with cations for sorption sites on suspended particles (Olsen et al., 1982 and references therein). This is relevant to the study area as the sampling locations fall within both oligohaline and mesohaline waters.

On the other hand, Pb-210 is considerably more particle reactive than Cs-137, and the observation that Pb-210 and Cs-137 inventories exhibit similar spatial patterns suggests that the Cs-137 distributions are not solely a product of the physicochemical environment.

Another relevant influence on radioisotope distributions in river-estuarine systems is suspended-sediment concentration. The loading of metals (Fe, Mn, Co, and radioisotopes by relation) tends to be lower in the presence of high suspended-sediment concentrations (Benoit and Rozan, 1999). This is observed in the Delaware estuarine turbidity maximum, where water-column metals concentrations exhibit a regional low (Biggs et al., 1983). Because the tidal marshes down-estuary of Marcus Hook are hydraulically contiguous with waters of the turbidity maximum zone, low radioisotope inventories may reflect low specific activities due to high suspended-sediment concentrations.

In summary, it is clear from the radioisotope geochronologies and inventories that Woodbury Creek, Oldman's Creek, Rancocas Creek, St. George's marsh, and Salem marsh are important material sinks in the upper Delaware Estuary. Because they are situated within a particularly sediment-rich reach, there is great potential for these and adjacent tidal marshes to trap material supplied by tidal waters. Indeed, it is probable that the greater tidal-marsh system constitutes a significant terminal sink for fine-grained sediment derived from the Delaware watershed, as well as down-estuary erosional sources. Given their proximity to industrial centers it is therefore likely that these marshes sequester particle-associated pollutants transported in the tidal Delaware River (e.g., Orson et al., 1992). Detailed studies of sediment transport and deposition within the tidal marshes are needed to elucidate their role as fine-sediment sources and (or) sinks in the greater Delaware River-Estuary system.

6. CONCLUSIONS

The major conclusions of this study are summarized below.

(1) Bottom sediment types in the tidal Delaware River and upper estuary range from mud to gravel and are extremely variable both along- and across-channel. Gravel, sand, and mud weight percentages vary by orders of magnitude, though the across-channel variability of sand and mud increases and decreases, respectively, from DRBC Zone 3 to

On the other hand, Pb-210 is considerably more particle reactive than Cs-137, and the observation that Pb-210 and Cs-137 inventories exhibit similar spatial patterns suggests that the Cs-137 distributions are not solely a product of the physicochemical environment.

Another relevant influence on radioisotope distributions in river-estuarine systems is suspended-sediment concentration. The loading of metals (Fe, Mn, Co, and radioisotopes by relation) tends to be lower in the presence of high suspended-sediment concentrations (Benoit and Rozan, 1999). This is observed in the Delaware estuarine turbidity maximum, where water-column metals concentrations exhibit a regional low (Biggs et al., 1983). Because the tidal marshes down-estuary of Marcus Hook are hydraulically contiguous with waters of the turbidity maximum zone, low radioisotope inventories may reflect low specific activities due to high suspended-sediment concentrations.

In summary, it is clear from the radioisotope geochronologies and inventories that Woodbury Creek, Oldman's Creek, Rancocas Creek, St. George's marsh, and Salem marsh are important material sinks in the upper Delaware Estuary. Because they are situated within a particularly sediment-rich reach, there is great potential for these and adjacent tidal marshes to trap material supplied by tidal waters. Indeed, it is probable that the greater tidal-marsh system constitutes a significant terminal sink for fine-grained sediment derived from the Delaware watershed, as well as down-estuary erosional sources. Given their proximity to industrial centers it is therefore likely that these marshes sequester particle-associated pollutants transported in the tidal Delaware River (e.g., Orson et al., 1992). Detailed studies of sediment transport and deposition within the tidal marshes are needed to elucidate their role as fine-sediment sources and (or) sinks in the greater Delaware River-Estuary system.

6. CONCLUSIONS

The major conclusions of this study are summarized below.

(1) Bottom sediment types in the tidal Delaware River and upper estuary range from mud to gravel and are extremely variable both along- and across-channel. Gravel, sand, and mud weight percentages vary by orders of magnitude, though the across-channel variability of sand and mud increases and decreases, respectively, from DRBC Zone 3 to

Zone 5. The transition from a dominantly coarse-grained (sand and gravel) to fine-grain (clayey silt to silty clay) bottom type falls near the Zone 4–Zone 5 boundary between River Miles 75 and 85. Evidence of a recent and localized change in sediment-transport mode, perhaps due to waterway engineering practices, is provided by an abrupt downcore change from medium-grained sand to mud at sites near the Rancocas River mouth and Marcus Hook shoal. It is clear that the present bottom-sediment types differ from the native sedimentology in places.

(2) Six major types of sedimentary environment were observed in the study area: (1) reworked bottom (three subclasses); (2) fine-grained deposition; (3) coarse-grained bedload; (4) non-deposition or erosion. The vast majority of the area surveyed was characterized by a reworked bottom composed of various sediment types with grain sizes that generally decrease down-estuary of Philadelphia. Reworking is signified by characteristic bedforms created by bottom currents and sediment transport, and is independently confirmed by non-steady-state profiles of Cs-137 and excess Pb-210. These radioisotopes reveal that fine-sediment deposition in much of the subtidal estuary is episodic and discontinuous on decadal timescales. The most significant finding of this study is that fine-sediment accumulation occurs as discrete depocenters concentrated between Marcus Hook and New Castle; at the time of surveying, extensive deposits of fluidized mud were observed in the Marcus Hook shipping channel with an estimated mass 3.5×10^5 tons dry weight. Areas of non-deposition or erosion are characterized by patchy bedrock exposures and (or) a coble bottom and are confined to the Tinicum Island–Chester reach. Areas of coarse-grained bedload transport, characterized by continuous trains of sand ripples and waves, are best developed in the tidal river north of Philadelphia.

(3) Fine-grained sediment deposition in the subtidal water of the upper estuary is intense (centimeters per month) on a seasonal basis as revealed by sediment distributions of the short-lived radioisotope Be-7. In contrast, sedimentation rates averaged over the past several decades from Cs-137 profiles are on the order ~ 1 cm/yr, where net accumulation is apparent at all. From this relationship it is clear that a large proportion of

sediments deposits rapidly emplaced on a seasonal basis are subsequently resuspended and redistributed such that net accumulation is low on the long term. This redistribution effect is suggested by sediment inventories of Cs-137, merely 9–14 % of the predicted inventory and considerably lower than inventories for adjacent tidal marshes.

(4) Sediment accumulation in tidal marshes of the upper Delaware Estuary is considerably more continuous (steady-state) than within adjacent open-water environments. Based on Cs-137 and Pb-210 chronologies, sedimentation rates ranged from 0.3 cm/yr (in Rancocas Creek) to 1.5 cm/yr (in Woodbury Creek). Sediment inventories of Cs-137 and excess Pb-210 suggest that Woodbury Creek, Oldman's Creek, and Rancocas Creek (all freshwater marshes) are particularly important repositories for fine-grained sediment and particle-associated substances in the upper estuary. Additional studies of sediment transport and deposition within these and other marshes are needed to identify their role as material sources and (or) sinks.

7. REFERENCES

- Benoit, G. and Rozan, T.F., 1999. The influence of size distribution on the particle concentration effect and trace metal partitioning in rivers. *Geochimica et Cosmochimica Acta*, 63: 113–127.
- Biggs, R.B. and Beasley, E.L., 1988. Bottom and suspended sediments in the Delaware River and Estuary. In: S.K. Majumdar, Miller, E.W., Sage, L.E. (Editor), *Ecology and Restoration of the Delaware River Basin*. The Pennsylvania Academy of Science, pp. 116–131.
- Biggs, R.B., Sharp, J.H., Church, T.M. and Tramontano, J.M., 1983. Optical properties, suspended sediments, and chemistry associated with the turbidity maxima of the Delaware estuary. *Canadian Journal of Fisheries and Aquatic Sciences*, 40 (Suppl. 1): 172–179.
- Church, T.M. and Lord, C.J., 1981. Uranium, Thorium and Lead nuclides in a Delaware salt marsh. *Estuarine, Coastal and Shelf Science*, 13: 267–275.
- Cutshall, N.H., Larsen, I.L. and Olsen, C.R., 1983. Direct analysis of Pb-210 in sediment samples: self-absorption corrections. *Nuclear Instruments and Methods*, 206: 309–312.
- DiLorenzo, J.L., Huang, P., Thatcher, M.L. and Najarian, T.O., 1993. Dredging impacts of Delaware estuary tides, *Proceedings of the 3rd International Conference Sponsored by the Waterway, Port, Coastal and Ocean Division, ASCE, September 8-10, 1993. Estuarine and Coastal Modeling III, Oak Brook, Illinois*, pp. 86–104.
- DRBC, 1998. *Study of the Loading of Polychlorinated Biphenyls from Tributaries and Point Sources Discharging to the Tidal Delaware River*, 85 pp.
- Duran, P.P., 1986. *Distribution of bottom sediments and effects of proposed dredging in the ship channel of the Delaware River between northeast Philadelphia, Pennsylvania and Wilmington, Delaware, 1984*. U.S. Geological Survey Hydrologic Investigations Atlas, HA697.
- Fletcher, C.A., Knebel, H.J. and Kraft, J.C., 1990. Holocene evolution of an estuarine coast and tidal wetlands. *Geological Society of America Bulletin*, 102: 283–297.
- Folk, R.L., 1974. *Petrology of Sedimentary Rocks*. University of Texas, Austin, Texas, 182 pp.
- Graustein, W.C. and Turekian, K.K., 1986. Pb-210 and Cs-137 in air and soils measure the rate and vertical profile of aerosol scavenging. *Journal of Geophysical Research*, 91: 14355–14366.

- Hirschberg, D.J., Chin, P., Feng, H. and Cochran, J.K., 1996. Dynamics of sediment and contaminant transport in the Hudson River Estuary: evidence from sediment distributions of naturally occurring radionuclides. *Estuaries*, 19: 931–949.
- Johnson, H.P. and Helferty, M., 1990. The geological interpretation of sidescan sonar. *Reviews of Geophysics*, 28(4): 357–380.
- Kim, G., Hussain, N., Church, T.M. and Carey, W.L., 1997. The fallout isotope Bi-207 in a Delaware salt marsh: a comparison with Pb-210 and Cs-137 as a geochronological tool. *The Science of the Total Environment*, 196: 31–41.
- Knebel, H.J., Signell, R.P., Rendig, R.R., Poppe, L.J. and List, J.H., 1999. Seafloor environments in the Long Island Sound estuarine system. *Marine Geology*, 155: 277–318.
- Kraft, J.C., Yi, H. and Khalequzzaman, M., 1992. Geologic and human factors in the decline of the tidal marsh lithosome: the Delaware Estuary and Atlantic coastal zone. *Sedimentary Geology*, 80: 233–246.
- Larsen, I.L. and Cutshall, N.H., 1981. Direct determination of Be-7 in sediments. *Earth and Planetary Science Letters*, 54: 379–384.
- Lyttle, P.T. and Epstein, J.B., 1987. Geologic Map of the Newark 1°x2° Quadrangle, New Jersey, Pennsylvania, and New York. U.S. Geological Survey Miscellaneous Investigations Series, I-1715 (2 sheets), scale 1:250,000.
- Mansue, L.J. and Commings, A.B., 1974. Sediment Transport by Streams Draining into the Delaware Estuary. U.S. Geological Survey Water-Supply Paper 1532-H.
- Monetti, M.A., 1996. Worldwide Deposition of Strontium-90 Through 1990. Environmental Monitoring Laboratory Report-579. U.S. Department of Energy, New York, 31 pp.
- Newell, W.L., Powars, D.S., Owens, J.P., Stanford, S.D. and Stone, B.D., 1998. Surficial Geologic Map of Central and Southern New Jersey, U.S. Geological Survey Miscellaneous Investigations Series, Map I-2540-D, scale 1:100,000.
- Nichols, M.M., 1988. Consequences of Dredging. In: B. Kjerfve (Editor), *Hydrodynamics of Estuaries, Volume II, Estuarine Case Studies*. CRC Press, Boca Raton, pp. 89–99.
- Nikitina, D.L., Pizzuto, J.E., Schwimmer, R.A. and Ramsey, K.W., 2000. An updated Holocene sea-level curve for the Delaware coast. *Marine Geology*, 171: 7–20.

- Nittrouer, C.A., Larsen, I.L., Demaster, D.J., McKee, B.A., and Cutshall, N.H., 1984. The effect of sediment mixing on Pb-210 accumulation rates for the Washington continental shelf: *Marine Geology*, 54: 201–221.
- NOS, 1998. National Ocean Service Hydrographic Survey Data, ver. 4.0. Digital Data on Compact Disk. National Geophysical Data Center.
- Olsen, C.R., Cutshall, N.H. and Larsen, I.L., 1982. Pollutant-particle associations and dynamics in coastal marine environments: a review. *Marine Chemistry*, 11: 501–533.
- Olsen, C.R., Larsen, I.L., Lowry, P.D. and Cutshall, N.H., 1986. Geochemistry and Deposition of Be-7 in River-Estuarine and Coastal Waters. *Journal of Geophysical Research*, 91(C1): 896–908.
- Olsen, C.R. et al., 1993. The concept of an equilibrium surface applied to particle sources and contaminant distributions in estuarine sediments. *Estuaries*, 16: 683–696.
- Olsen, C.R., Simpson, H.J., Peng, T.H., Bopp, R.F. and Trier, R.M., 1981. Sediment mixing and accumulation effects on radionuclide depth profiles in Hudson estuary sediments. *Journal of Geophysical Research*: 11020–11028.
- Oostdam, B.L., 1971. Suspended Sediment Transport in the Delaware Bay. Ph.D dissertation Thesis, University of Delaware, Newark, 316 pp.
- Orson, R.A., Simpson, R.L. and Good, R.E., 1992. A mechanism for the accumulation and retention of heavy metals in tidal freshwater marshes of the upper Delaware River estuary. *Estuarine, Coastal and Shelf Science*, 34: 171–186.
- Owens, J.P. and Denny, C.S., 1979. Upper Cenozoic Deposits of the Central Delmarva Peninsula, Maryland and Delaware. Geological Survey Professional Paper 1067-A, 28 pp.
- Parker, G.G., Hely, A.G., Keighton, W.B. and Olmsted, F.D., 1964. Water Resources of the Delaware River Basin. Geological Survey Professional Paper 381, 200 pp.
- Ritchie, J.C. and McHenry, R.J., 1990. Application of Radioactive Fallout Cesium-137 for Measuring Soil Erosion and Sediment Accumulation Rates and Patterns: A Review. *Journal of Environmental Quality*, 19: 215–233.
- Schaffner, L.C., Diaz, R.J., Olsen, C.R. and Larsen, I.L., 1987. Faunal characteristics and sediment accumulation processes in the James River estuary, Virginia. *Estuarine, Coastal and Shelf Science*, 25: 211–226.
- Schenck, W.S., Plank, M.O. and Srogi, L.A., 2000. Bedrock Geologic Map of the Piedmont of Delaware and Adjacent Pennsylvania. Delaware Geological Survey, Geologic Map Series, No.10, scale 1:36,000.

- Sommerfield, C.K. and Madsen, J.A., 2002. Sediment trapping and transport in the lower Delaware River and Estuary: initial results of a regional sonar study, 37th Annual Meeting of the Northeastern Section, Geological Society of America, Springfield, Massachusetts, pp. P-54.
- Trefethen, J.M., 1950. Classification of sediments. *American Journal of Science*, 248: 55–62.
- USACE, 1973. Long-Range Spoil Study. Part III, Sub-study 2 (Nature and Cause of the Shoal). USACE, North Atlantic Division, Philadelphia.
- Woodruff, J.D., Geyer, W.R., Sommerfield, C.K. and Driscoll, N.W., 2001. Seasonal variation of sediment deposition in the Hudson River estuary. *Marine Geology*, 179: 105–119.

APPENDIX A. SONAR TRACKLINE DATA

Line	Date	Start Time†	End Time	XTF File Size (KBytes)
1	08/13/2001	17:47:57	18:25:06	138637
2	08/13/2001	19:11:55	19:55:16	147689
3A	08/13/2001	19:56:50	20:21:29	87347
3B	08/13/2001	20:22:00	20:35:59	48247
4	08/13/2001	20:36:40	21:20:05	148675
5	08/14/2001	13:55:55	14:38:19	149482
6	08/14/2001	14:38:43	15:27:44	166912
7A	08/14/2001	16:40:05	17:04:53	118287
7_REP	08/15/2001	14:50:54	15:42:03	168199
8	08/14/2001	17:05:17	17:50:06	152381
9	08/14/2001	17:54:17	18:47:13	179948
10	08/14/2001	18:50:49	19:41:29	172262
11	08/15/2001	15:57:42	16:41:55	153588
12	08/15/2001	16:49:42	17:33:45	149805
13	08/15/2001	17:41:13	18:17:16	122313
14	08/15/2001	18:37:42	19:22:15	151477
15	08/15/2001	19:31:36	20:14:37	146278
16	08/15/2001	20:27:24	20:57:53	103633
17	08/16/2001	14:17:27	14:45:38	95799
18	08/16/2001	14:54:06	15:38:54	152279
19	08/16/2001	15:41:21	16:25:35	150428
20	08/16/2001	17:54:01	18:33:36	148522
21	08/16/2001	18:44:02	19:20:36	124319
22	08/16/2001	19:27:41	20:04:02	123566
23	08/16/2001	20:48:50	21:25:06	123444
24	08/17/2001	14:07:58	14:51:36	148370
25	08/17/2001	14:54:27	15:29:41	119826
26	08/17/2001	15:32:54	16:14:08	140209
27	08/17/2001	16:15:14	16:52:45	127856
28	08/17/2001	16:53:09	17:31:10	129295
29	08/17/2001	17:34:50	18:16:18	141025
30	08/17/2001	18:21:23	19:05:17	149287
31	08/17/2001	19:07:26	19:51:27	149663
32	08/20/2001	13:46:07	14:40:28	192713
32A	08/20/2001	15:18:23	15:36:20	61210
33	08/20/2001	15:38:59	16:43:50	220687
34	08/20/2001	16:48:34	17:50:25	210393
34A	08/20/2001	17:59:29	18:19:47	69106
35	08/20/2001	18:23:04	19:27:31	219267
36	08/20/2001	19:56:06	20:42:00	156206
37	08/21/2001	13:49:20	14:33:36	129550
38	08/21/2001	14:36:21	15:13:46	127246
39	08/21/2001	15:22:38	16:29:38	227801
40	08/21/2001	16:30:07	16:45:42	52982
41	08/21/2001	17:09:10	17:45:21	123047
42	08/21/2001	17:46:32	18:17:37	105665
43	08/21/2001	18:21:55	19:03:09	140141
44	08/21/2001	19:05:40	19:36:02	103217

Line	Date	Start Time†	End Time	XTF File Size (KBytes)
45	08/22/2001	14:04:49	14:41:49	125827
46	08/22/2001	14:44:43	15:20:13	120650
47	08/22/2001	15:23:50	15:56:59	112711
48	08/22/2001	16:09:13	16:41:25	109477
49	08/22/2001	16:42:24	17:01:32	65077
50	08/22/2001	17:04:57	17:27:21	76187
51	08/22/2001	17:27:39	17:42:28	50364
52	08/22/2001	17:46:57	17:54:04	24209
53	08/22/2001	17:58:32	18:05:40	24286
54	08/22/2001	18:09:55	19:09:05	201137
55	08/22/2001	19:11:50	19:57:06	153936
56	08/23/2001	14:11:14	14:41:38	103387
57	08/23/2001	14:45:15	15:12:26	92450
58	08/23/2001	15:16:57	15:34:30	59671
59	08/23/2001	15:41:10	15:54:57	46913
60	08/23/2001	16:13:14	16:26:49	46428
61	08/23/2001	16:42:22	17:03:34	72081
62	08/23/2001	17:21:43	17:56:36	118593
63	08/23/2001	18:00:51	18:11:40	36815
64	08/23/2001	18:16:44	18:51:16	117412
65	08/23/2001	19:00:10	19:34:54	118075
66	08/23/2001	19:36:26	19:57:09	70500
67	08/23/2001	20:03:53	20:14:10	34987
68	08/23/2001	20:22:05	20:29:42	25907
69	08/24/2001	14:33:16	14:53:20	68282
69A	08/24/2001	15:01:45	15:29:05	92906
70	08/24/2001	15:30:56	16:06:42	121577
70A	08/24/2001	16:07:17	16:20:15	44166
71	08/24/2001	16:22:58	16:52:20	99885
72	08/24/2001	16:53:07	16:53:39	1837
72A	08/24/2001	16:54:49	17:17:03	75634
73	08/24/2001	17:19:03	17:40:13	72005
74	08/24/2001	17:48:02	18:20:59	117140
75	08/24/2001	18:34:50	18:39:01	14264
76	08/24/2001	18:46:57	18:59:04	41235
77	08/24/2001	19:22:03	19:26:46	16032
78	08/24/2001	19:29:44	19:36:32	23138
79	08/24/2001	19:49:20	19:55:47	21948
80	10/22/2001	16:08:33	16:42:23	124518
81	10/22/2001	16:45:07	16:52:55	26538
82	10/22/2001	16:56:31	17:08:24	40359
83	10/22/2001	17:11:32	17:44:37	112431
84	10/22/2001	17:47:53	18:27:56	136120
85	10/22/2001	18:30:04	19:02:41	110875
86	10/22/2001	19:06:42	19:43:06	123744
87	10/22/2001	19:48:41	20:23:24	117990
88	10/23/2001	14:19:52	14:55:50	122274
89	10/23/2001	14:59:51	15:44:19	151131
90	10/23/2001	15:47:08	16:30:26	147162
91	10/23/2001	16:32:34	17:16:16	148530

Line	Date	Start Time†	End Time	XTF File Size (KBytes)
92	10/23/2001	17:31:42	17:45:32	47049
93	10/23/2001	17:48:07	18:03:41	52931
94	10/23/2001	19:17:57	19:31:06	122687
95	10/23/2001	19:32:58	20:03:51	139988
96	10/24/2001	19:36:16	20:20:57	284930
97	10/24/2001	20:21:21	21:07:39	295052
98	10/25/2001	13:26:39	14:13:25	159065
99	10/25/2001	14:16:15	15:06:05	169326
100	10/25/2001	15:12:19	15:53:27	139869
101	10/25/2001	15:55:02	16:11:57	57555
102	10/25/2001	16:15:35	16:25:59	35336
103	10/25/2001	16:34:36	17:17:25	145470
104	10/25/2001	18:33:22	19:15:27	143048
105	10/25/2001	19:35:08	19:49:16	48077
106	10/25/2001	19:54:24	20:15:30	71758
107	10/26/2001	14:02:25	15:08:52	225846
108	11/28/2001	17:04:15	18:58:57	391749
109	11/28/2001	19:35:31	20:41:13	313246
110	11/28/2001	20:44:23	21:10:07	87500
111	11/28/2001	21:12:12	21:33:08	71180
112	12/05/2001	16:40:36	16:56:53	69208
113	12/05/2001	16:59:06	17:16:03	76865
114	12/05/2001	17:20:15	17:43:38	105962
115	12/05/2001	17:52:54	18:02:55	45408
116	12/05/2001	18:13:27	18:21:57	38505
117	12/05/2001	18:29:14	18:36:01	30712
118	12/05/2001	18:41:58	18:47:08	23444
119	12/05/2001	18:59:22	19:06:39	32998
120	12/05/2001	19:13:35	19:25:42	54928
121	12/05/2001	19:30:09	19:38:45	39016
122	12/05/2001	19:46:27	19:57:09	48400

† All times are Greenwich Mean Time (+5 hours Eastern Standard Time)

APPENDIX B. GIS DATABASE ON CD-ROM

Two CD-ROMs are included with this report. CD-ROM #1 contains three folders: (1) Data, (2) Figures_Tables_Plots, and (3) GIS_ArcMap_Documents. The Data folder contains GIS-based files that were used in the generation of all maps in the report text. Details on these GIS-based files are provided below. The Figures_Tables_Plots folder contains *.jpg format files of figures presented in the report, tables in Excel format summarizing the sidescan and chirp tracklines, as well as grab and HDC sampling station details, and various plots in *.jpg format of the surveyed area. The GIS_ArcMap_Documents folder contains *.mxd format files that can be opened in ArcGIS 8.2 and that were used to generate figures in the report.

CD-ROM #2 contains one folder, SSS_Mosaics, containing all of the sidescan sonar mosaics georeferenced to the other datasets. To display files used in the *.mxd format files in ArcGIS 8.2, copy all data from the CD-ROMs onto the “hard” disk of a computer and then copy the SSS_Mosaics folder into the Data folder contained on CD-ROM #1. This GIS database may be viewed (but not modified) using Arc Explorer 2, free GIS software available for download from ESRI's website (www.esri.com/software/arcexplorer).

Note: All GIS-shapefiles therein are defined by UTM, WGS-84 Zone 18N, northing and easting meters coordinates.

The Data folder on CD-ROM #1 contains four folders: (1) Background_Data, (2) Grabs_and_Cores, and (3) Survey_Tracklines, and (4) Bathymetric soundings. The data within each of these folders is described in detail below.

Background Data Folder

The background data folder contains general files that were used in the generation of the figures/maps that were supplied in the report. These files include:

- 1) Within a subfolder, NOAA Charts within the survey area. These charts are included in a *.tif format with accompanying *.tfw files.
- 2) NOAA Medium-Resolution Digital Vector Coastline for the survey area. The coastline is included as GIS-shapefile coastline_med_utm.shp, *.shx, and *.dbf.

- 3) General start and end positions for all the major bridges crossing the river in the survey area. These files are included as GIS-shapefiles in a format of `bridge_name.shp`, `*.shx`, and `*.dbf`. For example, for the Commodore Barry Bridge the accompanying files are `commodore_barry_bridge.shp`, `*.shx`, and `*.dbf`. The bridges included are the: Ben Franklin Bridge, Betsy Ross Bridge, Burlington-Bristol Bridge, Commodore Barry Bridge, Delaware Memorial Bridge, Tacony_Palmyra Bridge, and Walt Whitman Bridge.
- 4) DRBC Zone boundaries within the survey area. These files are included as GIS-shapefiles in a format of `boundary_name.shp`, `*.shx`, and `*.dbf`. For example, for the DRBC Zone 2–Zone 3 boundary the accompanying files are `drbc_zone2_zone3.shp`, `*.shx`, and `*.dbf`. The boundaries included are the: DRBC Zone 2–Zone 3, DRBC Zone 3–Zone 4, and DRBC Zone 4–Zone 5 boundaries.
- 5) The position of the shipping (dredged) channel within the survey area. The channel is included as GIS-shapefile `dredged_channel.shp`, `*.shx`, and `*.dbf`.
- 6) The position of the 18’ depth contour within the survey area. The 18’ contour is included as GIS-shapefile `contour_18.shp`, `*.shx`, and `*.dbf`.

Grabs_and_Cores Folder

The `grabs_and_cores` folder contains files that were used to show the locations of the grab samples and slow cores that were collected in the survey area. These files include:

- 1) The locations of the grab samples. This file is included as GIS-shapefile `dr_grab_cores.shp`, `*.shx`, and `*.dbf`.
- 2) The locations of the HDC samples (a.k.a. slow cores). This file is included as GIS-shapefile `dr_slow_cores.shp`, `*.shx`, and `*.dbf`.
- 3) The sediment classifications for the grab samples. See the report for definitions of the abbreviations for the sediment classifications. This file is included as GIS-shapefile `grab_cores_class.shp`, `*.shx`, and `*.dbf`.
- 4) Tables of the sediment grain-size data. See the report text for a description of the sediment classifications scheme and sediment-type abbreviations. Percentage gravel, sand, mud, silt, clay, and sediment type are tabulated. This information

can be accessed also in an ArcGIS 8.2 session by loading this shapefile and, using the “information” button from the tools menu, “clicking” on a grab sample location. This file is included as GIS-shapefile dr_grab_cores_info.shp, *.shx, and *.dbf.

Survey_Tracklines Folder

The Survey_Tracklines folder contains files that provide the geographic position of the sidescan sonar and Chirp tracklines. These files also can be used to annotate at 1 minute, and/or 10 minute time-intervals along the tracklines:

- 1) Sidescan sonar and Chirp trackline positions. Files are included as GIS-shapefiles in a format of line_number.shp, *.shx, and *.dbf. For example, for trackline 122, the accompanying files are 1122.shp, *.shx, and *.dbf.
- 2) One-minute time-interval waypoints along the sidescan sonar and Chirp tracklines. These files are included as GIS-shapefiles in a format of line_number_m.shp, *.shx, and *.dbf. For example, for Trackline 122, the accompanying one minute waypoint files are 1122m.shp, *.shx, and *.dbf.
- 3) Ten-minute time interval waypoints along the sidescan sonar and Chirp tracklines. These files are included as GIS-shapefiles in a format of line_number_t.shp, *.shx, and *.dbf. For example, for Trackline 122, the accompanying ten minute waypoint files are 1122t.shp, *.shx, and *.dbf.

Bathymetric Soundings Folder

The Bathymetry Folder contains a complete set of bathymetric soundings for the survey area collected during 1979–1982 by the National Ocean Service of NOAA. These data are in ASCII xyz format, where x=decimal degrees longitude, y=decimal degrees latitude, and z=depth in meters. The original source for these soundings is: NOS Hydrographic Survey Data, Version 4.1, 1998, CD-ROMs prepared by the National Geophysical Data Center. For more information see www.ngdc.noaa.gov/mgg/fliers/98mgg03.html.

SSS_Mosaics Folder on CD-ROM #2

The SSS_Mosaics folder contains the complete set of sidescan sonar mosaics processed at 1-m resolution. From south to north, the 12 sidescan mosaics are: 1) new_castle, 2) christina, 3) marcus_hook_bar, 4) marcus_hook, 5) tinicum, 6) airport, 7) schuykill, 8) navy, 9) camden, 10) petty_island, 11) palmyra, and 12) burlington. For proper operation of the ArcGIS 8.2 *.mxd files included on CD-ROM, copy the SSS_Mosaics folder as a subfolder in the Data folder on CD-ROM #1. Files within the folder include:

- 1) Within a subfolder, outlines of the outer boundary of the sidescan mosaics. These files are included as GIS-shapefiles in a format of mosaic_name.shp, *.shx, and *.dbf. For example, for the sidescan mosaic near the Philadelphia International Airport the accompanying files are airport.shp, *.shx, and *.dbf.
- 2) The sidescan mosaics. These mosaics are included in a *.tif format with accompanying *.tfw files.

Questions concerning the information contained on these CD-ROMs should be addressed to Dr. John Madsen, Department of Geology, University of Delaware, Newark, DE 19716. Phone: 302-831-1608. E-mail: jmadsen@udel.edu.

APPENDIX C. SEDIMENT SAMPLING STATIONS

Sample [†] No.	Sampling Date	Time [‡] (hr.min.)		Water Depth (m)	N Latitude (deg.min.)		W Longitude (deg.min.)	
Cruise CH0401								
C-1	04/11/2001	8	32	6.7	39°	53.1357	75°	9.5848
C-2	04/11/2001	9	43	6.1	39°	51.3448	75°	19.0823
C-3a	04/11/2001	10	20	5.5	39°	46.7921	75°	27.2000
C-3b	04/11/2001	10	45	6.7	39°	46.8605	75°	27.1974
C-4	04/11/2001	11	16	4.8	39°	44.6583	75°	29.3288
C-5	04/11/2001	12	2	6.1	39°	42.6700	75°	29.9190
C-6,7	04/11/2001	13	45	11.2	39°	27.5760	75°	33.9735
C-8	04/11/2001	14	50	5.2	39°	22.1459	75°	30.1677
C-9	04/11/2001	15	30	5.2	39°	22.1459	75°	28.1918
Cruise CH0701								
C-10	07/19/2001	22	45	4.2	40°	2.9780	74°	58.6671
C-11a	07/19/2001	23	10	4.5	40°	2.4470	74°	59.1740
C-11b	07/19/2001	23	35	4.5	40°	2.4470	74°	59.1740
C-12	07/20/2001	0	0	4.5	40°	1.4540	75°	0.4630
C-13	07/20/2001	0	23	5.5	40°	1.0400	75°	1.7020
C-14a	07/20/2001	3	0	4.5	39°	51.0230	75°	16.8600
C-14b	07/20/2001	3	0	4.5	39°	51.0230	75°	16.8600
C-15a	07/20/2001	3	50	9.1	39°	48.7790	75°	23.9750
C-15b	07/20/2001	3	50	9.1	39°	48.7790	75°	23.9750
C-16a	07/20/2001	11	0	6.1	39°	21.1650	75°	28.1570
C-16b	07/20/2001	11	30	6.1	39°	21.1650	75°	28.1570
Cruise CH01-28								
1G	11/17/2001	7	14	8.2	39°	59.4400	75°	3.6200
2G	11/17/2001	7	44	15.4	39°	59.4500	75°	3.6900
3G	11/17/2001	7	29	14.3	39°	59.4600	75°	3.7500
4G	11/17/2001	7	54	9.1	39°	59.4900	75°	3.8100
5S2	11/17/2001	8	23	8.9	39°	59.4500	75°	3.6000
5S1	11/17/2001	8	6	8.8	39°	59.4500	75°	3.6300
6S	11/17/2001	8	42	8.2	39°	59.4600	75°	3.6100
7S	11/17/2001	8	59	8.1	39°	59.5200	75°	3.5900
8S	11/17/2001	9	21	8.9	39°	59.7100	75°	3.5200
9G	11/17/2001	9	43	9.2	39°	58.5200	75°	4.8200
10G	11/17/2001	10	0	14.1	39°	58.5600	75°	4.8300
11G	11/17/2001	10	19	15.6	39°	58.6000	75°	4.8800
12G	11/17/2001	10	38	13.7	39°	58.6700	75°	4.8900
9G2	11/17/2001	10	58	8.0	39°	58.4600	75°	4.9700
13G	11/17/2001	11	17	11.3	39°	58.2500	75°	6.0900
14G	11/17/2001	11	31	12.3	39°	50.3200	75°	6.1300
15G	11/17/2001	11	51	13.7	39°	58.3600	75°	6.2100
16G	11/17/2001	12	2	15.6	39°	58.2400	75°	6.1570
17G	11/17/2001	12	18	7.3	39°	57.9100	75°	7.0200
18G	11/17/2001	12	31	7.7	39°	57.6600	75°	7.5000

Sample	Date	Time	Depth (m)	Lat N	Lon W
19G	11/17/2001	12 41	12.4	39° 57.7400	75° 7.5500
20G	11/17/2001	12 50	14.0	39° 57.7600	75° 7.6100
21G	11/17/2001	13 6	17.1	39° 57.8500	75° 7.6400
22G	11/17/2001	13 24	14.5	39° 56.5100	75° 8.0400
23G	11/17/2001	13 35	14.1	39° 56.5000	75° 8.1500
24G	11/17/2001	13 44	15.4	39° 56.5300	75° 8.2500
25G	11/17/2001	13 56	17.4	39° 56.5100	75° 8.3400
22S	11/17/2001	14 39	13.7	39° 56.4900	75° 8.0300
26G	11/17/2001	15 2	12.4	39° 55.4700	75° 7.8700
27G	11/17/2001	15 13	14.1	39° 55.4600	75° 7.9600
28G	11/17/2001	15 26	15.9	39° 55.4400	75° 8.0600
29G	11/17/2001	15 37	16.4	39° 55.4300	75° 8.1400
30G	11/17/2001	15 49	16.3	39° 54.4500	75° 7.6000
31G	11/17/2001	15 59	17.5	39° 54.4800	75° 7.7100
32G	11/17/2001	16 13	17.8	39° 54.4600	75° 7.7900
33G	11/17/2001	16 21	17.2	39° 54.4700	75° 7.8700
34G	11/17/2001	16 31	19.3	39° 53.9800	75° 7.8700
35G	11/17/2001	16 52	12.0	39° 53.2000	75° 8.2000
36G	11/17/2001	17 3	16.4	39° 53.2800	75° 8.3000
37G	11/17/2001	17 13	17.3	39° 53.3000	75° 8.3700
38G	11/17/2001	17 25	8.0	39° 53.3300	75° 8.4900
39G	11/17/2001	17 41	17.8	39° 52.8100	75° 9.8900
40G	11/17/2001	17 53	16.0	39° 52.8900	75° 9.8900
41G	11/17/2001	18 9	11.7	39° 52.5890	75° 9.5450
42G	11/17/2001	18 22	9.5	39° 53.0650	75° 9.8890
40S	11/17/2001	18 36	16.5	39° 52.8990	75° 9.8990
41S	11/17/2001	18 51	12.2	39° 52.9650	75° 9.9010
43G	11/17/2001	19 20	16.3	39° 52.7400	75° 11.4400
44G	11/17/2001	19 47	16.5	39° 52.8100	75° 11.4600
45G	11/17/2001	19 57	15.1	39° 52.8800	75° 11.5000
46G	11/17/2001	20 6	15.6	39° 52.9480	75° 11.5120
47G	11/17/2001	20 15	14.9	39° 53.0270	75° 11.5120
46S	11/17/2001	20 24	15.6	39° 52.9510	75° 11.5120
48G	11/17/2001	20 35	14.6	39° 52.8996	75° 11.7966
49G	11/17/2001	20 59	16.5	39° 52.7450	75° 11.8510
50G	11/17/2001	21 13	14.8	39° 52.6378	75° 11.9183
46S2	11/17/2001	21 44	14.9	39° 52.9426	75° 11.4995
51G	11/17/2001	22 10	14.4	39° 52.2098	75° 12.9231
52G	11/17/2001	22 21	15.3	39° 52.2013	75° 12.8421
53G	11/17/2001	22 35	15.6	39° 52.1548	75° 12.7995
54G	11/17/2001	22 46	14.5	39° 52.1006	75° 12.7234
55G	11/17/2001	23 6	15.4	39° 52.0432	75° 12.7199
56G	11/17/2001	23 17	15.1	39° 51.9637	75° 12.6402
57G	11/17/2001	23 30	16.3	39° 51.9461	75° 12.6169
55S	11/17/2001	23 44	15.8	39° 52.0557	75° 12.6938
58G	11/18/2001	0 10	13.4	39° 51.8374	75° 13.7329

Sample	Date	Time	Depth (m)	Lat N	Lon W
59G	11/18/2001	0 19	14.2	39° 51.7761	75° 13.6954
60G	11/18/2001	0 33	15.3	39° 51.7353	75° 13.6322
61G	11/18/2001	0 42	14.9	39° 51.6847	75° 13.5878
62G	11/18/2001	0 52	15.1	39° 51.6330	75° 13.5397
63G	11/18/2001	1 1	16.1	39° 51.5854	75° 13.4616
64G	11/18/2001	1 12	16.7	39° 51.5174	75° 13.4134
59S	11/18/2001	1 22	14.4	39° 51.7870	75° 13.6839
59S2	11/18/2001	1 31	14.6	39° 51.7790	75° 13.6899
65G	11/18/2001	1 55	10.7	39° 51.2769	75° 15.1740
66G	11/18/2001	2 8	14.3	39° 51.2242	75° 15.1515
67G	11/18/2001	2 20	16.2	39° 51.1693	75° 15.1163
68G	11/18/2001	2 36	16.3	39° 51.1153	75° 15.0792
69G	11/18/2001	3 29	16.9	39° 51.0576	75° 15.0650
67S	11/18/2001	3 37	16.1	39° 51.1677	75° 15.1250
70G	11/18/2001	3 59	11.7	39° 50.9798	75° 16.6653
71G	11/18/2001	4 7	17.4	39° 50.9177	75° 16.6905
72G	11/18/2001	4 23	18.6	39° 50.8802	75° 16.7084
73G	11/18/2001	4 33	17.7	39° 50.7845	75° 16.7033
74G	11/18/2001	4 39	18.2	39° 50.6838	75° 16.7098
70S	11/18/2001	4 51	9.8	39° 50.9903	75° 16.7029
75G	11/18/2001	5 20	11.8	39° 50.7893	75° 18.2094
76G	11/18/2001	5 43	15.2	39° 50.8468	75° 18.2002
77G	11/18/2001	5 55	16.7	39° 50.9409	75° 18.2103
78G	11/18/2001	6 30	15.7	39° 50.9900	75° 18.2000
79G	11/18/2001	6 38	11.0	39° 51.0600	75° 18.2000
80G	11/18/2001	6 53	14.8	39° 50.8600	75° 19.7700
81G	11/18/2001	7 3	14.9	39° 50.9200	75° 19.7500
82G	11/18/2001	7 13	15.1	39° 51.0000	75° 19.7300
83G	11/18/2001	7 24	10.5	39° 51.0700	75° 19.7100
84G	11/18/2001	7 33	11.1	39° 51.1300	75° 19.6600
85G	11/18/2001	7 52	13.7	39° 50.1900	75° 21.3400
86G	11/18/2001	8 6	14.8	39° 50.2500	75° 21.3800
87G	11/18/2001	8 25	16.5	39° 50.3100	75° 21.4500
88G	11/18/2001	8 38	10.8	39° 50.3800	75° 21.5000
87S	11/18/2001	8 52	16.2	39° 50.3000	75° 21.4500
89G	11/18/2001	9 10	9.9	39° 49.5800	75° 22.9300
90G	11/18/2001	9 22	11.6	39° 49.5400	75° 22.8800
91G	11/18/2001	9 29	10.8	39° 49.4700	75° 22.8300
92G	11/18/2001	9 47	14.2	39° 49.4300	75° 22.7700
93G	11/18/2001	9 55	14.7	39° 49.3700	75° 22.7100
94G	11/18/2001	10 4	10.3	39° 49.3000	75° 22.6300
95G	11/18/2001	10 13	10.3	39° 49.2500	75° 22.5900
96G	11/18/2001	10 45	15.8	39° 49.1100	75° 23.3500
97G	11/18/2001	10 52	15.6	39° 49.0200	75° 23.2300
98G	11/18/2001	11 0	15.6	39° 48.9000	75° 23.1100
99G	11/18/2001	11 16	14.4	39° 48.4800	75° 23.7000

Sample	Date	Time	Depth (m)	Lat N	Lon W
101G	11/18/2001	11 28	15.7	39° 48.6200	75° 23.8100
102G	11/18/2001	11 44	16.1	39° 48.6700	75° 23.8600
103G	11/18/2001	11 52	16.4	39° 48.7500	75° 23.9100
104G	11/18/2001	12 1	16.0	39° 48.7800	75° 23.9300
105G	11/18/2001	12 10	15.0	39° 48.8214	75° 23.9575
106G	11/18/2001	12 21	9.9	39° 48.8859	75° 24.0255
105S	11/18/2001	12 51	15.3	39° 48.8190	75° 23.9700
99S	11/18/2001	13 10	14.8	39° 48.4900	75° 23.7100
107G	11/18/2001	14 25	15.5	39° 48.3600	75° 23.9980
108G	11/18/2001	14 38	15.2	39° 48.5600	75° 24.1200
109G	11/18/2001	14 54	15.4	39° 48.5590	75° 24.5870
110G	11/18/2001	15 3	15.4	39° 48.4900	75° 24.4900
111G	11/18/2001	15 14	15.8	39° 48.4200	75° 24.4600
112G	11/18/2001	15 28	16.1	39° 48.3500	75° 24.4200
113G	11/18/2001	15 38	16.4	39° 48.2870	75° 24.3750
114G	11/18/2001	15 46	15.1	39° 48.2300	75° 24.3300
115G	11/18/2001	15 55	14.1	39° 48.1600	75° 24.2800
111S	11/18/2001	16 6	16.3	39° 48.4200	75° 24.4900
111S2	11/18/2001	17 7	15.3	39° 48.4000	75° 24.4600
116G	11/18/2001	17 21	13.7	39° 48.0000	75° 24.6600
117G	11/18/2001	17 34	16.4	39° 48.1800	75° 24.7300
118G	11/18/2001	17 44	15.0	39° 48.2300	75° 25.3300
119G	11/18/2001	17 53	16.6	39° 48.0900	75° 25.2100
120G	11/18/2001	18 5	14.5	39° 47.9695	75° 25.1161
121G	11/18/2001	18 15	12.4	39° 47.8587	75° 25.0099
121S	11/18/2001	18 20	12.2	39° 47.8851	75° 25.0099
122G	11/18/2001	18 34	11.0	39° 47.6756	75° 25.8096
123G	11/18/2001	18 47	16.6	39° 47.7992	75° 25.8980
124G	11/18/2001	19 13	11.7	39° 47.9423	75° 25.9996
125G	11/18/2001	19 34	8.8	39° 47.5525	75° 26.9600
126G	11/18/2001	19 47	14.3	39° 47.4376	75° 26.8405
127G	11/18/2001	20 1	12.6	39° 47.3188	75° 26.7549
128G	11/18/2001	20 10	8.7	39° 47.2298	75° 26.6153
128S	11/18/2001	20 25	8.6	39° 47.2311	75° 26.6144
129G	11/18/2001	20 48	8.4	39° 46.5379	75° 27.5139
130G	11/18/2001	21 1	8.3	39° 46.6459	75° 27.6617
131G	11/18/2001	21 18	14.5	39° 46.7571	75° 27.8334
132G	11/18/2001	21 29	10.1	39° 46.8507	75° 28.0023
130S	11/18/2001	21 41	8.5	39° 46.6459	75° 27.6755
133G	11/18/2001	22 0	10.0	39° 45.9181	75° 28.7878
134G	11/18/2001	22 16	16.0	39° 45.8432	75° 28.6084
135G	11/18/2001	22 22	9.2	39° 45.7361	75° 28.4015
136G	11/18/2001	22 33	10.2	39° 45.6541	75° 28.2372
135S	11/18/2001	22 41	9.5	39° 45.7450	75° 28.4029
137G	11/18/2001	22 58	8.1	39° 44.7132	75° 28.6986
138G	11/18/2001	23 12	8.9	39° 43.9025	75° 29.2493

Sample	Date	Time	Depth (m)	Lat N	Lon W
139G	11/18/2001	23 46	15.6	39° 45.0403	75° 29.3504
140G	11/18/2001	23 57	9.8	39° 44.9467	75° 29.1458
141G	11/19/2001	0 37	10.4	39° 44.2415	75° 29.7913
142G	11/19/2001	0 57	16.0	39° 44.2870	75° 29.9492
142S	11/19/2001	1 7	16.1	39° 44.2886	75° 29.9464
143G	11/19/2001	1 21	13.5	39° 44.0598	75° 30.1401
143S	11/19/2001	1 26	13.4	39° 44.0591	75° 30.1433
145G	11/19/2001	1 46	7.6	39° 43.4898	75° 29.8824
146G	11/19/2001	1 57	9.9	39° 43.4001	75° 29.5134
144G	11/19/2001	2 8	16.9	39° 43.5782	75° 30.2550
144S	11/19/2001	2 12	16.9	39° 43.5752	75° 30.2618
144S2	11/19/2001	2 18	16.9	39° 43.5784	75° 30.2541
147G	11/19/2001	2 33	15.4	39° 43.1722	75° 30.2719
147S	11/19/2001	2 36	13.8	39° 43.1804	75° 30.2637
148G	11/19/2001	3 11	12.6	39° 42.7922	75° 30.0604
149G	11/19/2001	3 22	14.3	39° 42.8373	75° 30.2234
150G	11/19/2001	3 49	16.6	39° 42.8925	75° 30.4005
150S	11/19/2001	4 7	16.4	39° 42.8863	75° 30.3960
151G	11/19/2001	2 49	14.7	39° 42.9701	75° 30.6491
151S	11/19/2001	2 51	15.4	39° 42.9774	75° 30.6546
151S2	11/19/2001	3 0	15.3	39° 42.9714	75° 30.6386
152G	11/19/2001	4 27	11.9	39° 42.4384	75° 30.8363
152S	11/19/2001	4 30	12.2	39° 42.4342	75° 30.8368
152S2	11/19/2001	4 39	12.2	39° 42.4404	75° 30.8318
153G	11/19/2001	4 50	18.4	39° 42.3752	75° 30.6661
154G	11/19/2001	5 5	19.7	39° 42.3175	75° 30.5058
155G	11/19/2001	5 15	17.9	39° 41.8671	75° 30.6784
156G	11/19/2001	5 22	19.2	39° 41.9193	75° 30.8565
157G	11/19/2001	5 39	13.3	39° 41.9891	75° 31.0606
157S	11/19/2001	5 52	13.3	39° 41.9817	75° 31.0629
158G	11/19/2001	8 6	10.7	39° 40.8400	75° 31.6300
158S	11/19/2001	9 3	10.7	39° 40.8500	75° 31.6300
159G	11/19/2001	8 15	12.7	39° 40.7670	75° 31.4930
160G	11/19/2001	8 24	15.8	39° 40.6950	75° 31.3640
161G	11/19/2001	8 34	13.6	39° 40.6270	75° 31.2150
161S	11/19/2001	8 51	13.6	39° 40.6300	75° 31.2080
162G	11/19/2001	8 42	8.9	39° 40.6700	75° 31.0990
163G	11/19/2001	10 12	9.8	39° 39.6400	75° 31.9000
163S	11/19/2001	11 22	10.3	39° 39.6400	75° 31.8800
164G	11/19/2001	10 23	10.8	39° 39.7300	75° 32.0280
165G	11/19/2001	10 36	15.5	39° 39.8000	75° 32.1500
166G	11/19/2001	10 43	9.4	39° 39.9000	75° 32.2800
166S	11/19/2001	11 9	8.4	39° 39.8000	75° 32.2800
167G	11/19/2001	10 52	8.5	39° 39.9800	75° 32.4200
168G	11/19/2001	11 44	9.5	39° 38.9674	75° 32.6395
169G	11/19/2001	11 54	13.0	39° 39.0878	75° 32.7690

Sample	Date	Time	Depth (m)	Lat N	Lon W
169S	11/19/2001	13 9	13.9	39° 39.0700	75° 32.7900
170G	11/19/2001	12 4	16.1	39° 39.1700	75° 32.9000
170S	11/19/2001	12 57	16.5	39° 39.1690	75° 32.9100
171G	11/19/2001	12 14	9.0	39° 39.2500	75° 33.0490
172G	11/19/2001	12 23	9.9	39° 39.3600	75° 33.1700
173G	11/19/2001	12 34	10.2	39° 39.4400	75° 33.3170
173S	11/19/2001	12 43	10.1	39° 39.4400	75° 33.3000
174G	11/19/2001	9 16	8.1	39° 40.2400	75° 32.0200
174S	11/19/2001	10 2	9.4	39° 40.2600	75° 31.9700
175G	11/19/2001	9 26	15.5	39° 40.1500	75° 31.7600
176G	11/19/2001	9 33	10.6	39° 40.0600	75° 31.6200
177G	11/19/2001	9 39	9.9	39° 39.9900	75° 31.4900
177S	11/19/2001	9 45	9.9	39° 39.9970	75° 31.4850
178G	11/19/2001	14 19	8.0	39° 31.1200	75° 32.3500
179G	11/19/2001	14 28	14.0	39° 31.2000	75° 32.6780
180G	11/19/2001	14 59	16.0	39° 31.2800	75° 33.0000
181G	11/19/2001	15 7	14.2	39° 31.3700	75° 33.1600
182G	11/19/2001	15 59	9.0	39° 31.3370	75° 33.3100
183S	11/19/2001	15 42	12.0	39° 27.9130	75° 34.0440
184S1	11/19/2001	16 18	9.4	39° 25.6300	75° 32.2280
184S2	11/19/2001	16 26	9.2	39° 25.6310	75° 32.2200
Cruise CH02-02					
MHW	3/22/2002	9 27	12.1	39° 48.7790	75° 23.9750
MHE	3/22/2002	10 02	12.6	39° 48.4900	75° 23.7100
Cruise CH02-09					
184G	06/12/2002	5 14	9.55	39° 38.6923	75° 33.9533
185G	06/12/2002	5 28	11.02	39° 38.6350	75° 33.8054
186G	06/12/2002	5 36	16.71	39° 38.5723	75° 33.6456
187G	06/12/2002	5 48	15.75	39° 38.5352	75° 33.5312
188G	06/12/2002	6 6	10.86	39° 38.5050	75° 33.4213
189S	06/12/2002	6 21	9.62	39° 38.4400	75° 34.2636
190G	06/12/2002	6 41	11.43	39° 37.7003	75° 34.8477
191G	06/12/2002	6 57	19.3	39° 37.6703	75° 34.6463
192G	06/12/2002	7 7	16.9	39° 37.6756	75° 34.5094
193G	06/12/2002	7 15	12.15	39° 37.6449	75° 34.4074
193G2	06/12/2002	7 22	13.47	39° 37.6623	75° 34.4179
194G	06/12/2002	7 33	16.24	39° 37.2446	75° 34.8930
195G	06/12/2002	7 44	16.51	39° 37.1960	75° 34.6271
196G	06/12/2002	7 58	11.08	39° 36.6870	75° 34.7882
197G	06/12/2002	8 19	17.07	39° 36.7326	75° 34.6376
198G	06/12/2002	8 40	16.09	39° 36.7722	75° 34.6502
199G	06/12/2002	8 54	13.05	39° 36.7804	75° 34.4774
200G	06/12/2002	9 12	13.25	39° 35.6628	75° 34.0842
201G	06/12/2002	9 30	14.77	39° 35.7001	75° 34.0109
202G	06/12/2002	9 47	14.71	39° 35.7291	75° 33.8947
203G	06/12/2002	10 0	13.36	39° 35.7832	75° 33.7720

Sample	Date	Time	Depth (m)	Lat N	Lon W
204G	06/12/2002	10 13	11.73	39° 34.6726	75° 33.4383
205G	06/12/2002	10 23	16.29	39° 34.6836	75° 33.2711
206G	06/12/2002	10 34	15.5	39° 34.7248	75° 33.2936
207G	06/12/2002	10 49	9.85	39° 34.7891	75° 33.1507
208G	06/12/2002	10 57	8.53	39° 34.8582	75° 32.9686
209S	06/12/2002	11 12	14.77	39° 34.4595	75° 33.1622
210G	06/12/2002	11 27	12.97	39° 33.9711	75° 33.3055
211G	06/12/2002	11 37	15.5	39° 34.0581	75° 33.0052
212G	06/12/2002	11 57	15.5	39° 34.0810	75° 32.8812
213G	06/12/2002	11 48	10.61	39° 34.1402	75° 32.6834
212S	06/12/2002	12 9	15	39° 34.0801	75° 32.8816
214G	06/12/2002	12 22	7.67	39° 33.2261	75° 33.2195
215G	06/12/2002	12 33	12.32	39° 33.2913	75° 32.9063
216G	06/12/2002	12 44	13.95	39° 33.3428	75° 32.7416
217G	06/12/2002	12 57	16	39° 33.3721	75° 32.6092
218G	06/12/2002	13 7	17.16	39° 33.4140	75° 32.4688
219G	06/12/2002	13 19	11.9	39° 33.4449	75° 32.3227
220G	06/12/2002	13 43	13.19	39° 32.4186	75° 32.9375
221G	06/12/2002	13 54	19.79	39° 32.4488	75° 32.6537
222G	06/12/2002	14 5	19.24	39° 32.4360	75° 32.5566
223G	06/12/2002	14 16	15.96	39° 32.4243	75° 32.3923
224G	06/12/2002	14 51	12.99	39° 30.1190	75° 33.6566
225G	06/12/2002	15 3	17.72	39° 30.0888	75° 33.4625
226G	06/12/2002	15 11	14.7	39° 30.0588	75° 33.3101
227G	06/12/2002	15 22	11.96	39° 29.9927	75° 32.9640
228G	06/12/2002	15 56	12.9	39° 28.6439	75° 34.0416
229G	06/12/2002	16 7	17.06	39° 28.6061	75° 33.8164
230G	06/12/2002	16 25	16.59	39° 28.5883	75° 33.7038
231G	06/12/2002	16 38	10.51	39° 28.5503	75° 33.2584
232G	06/12/2002	17 02	7.3	39° 27.4780	75° 33.9267
236G	06/12/2002	17 28	11.92	39° 27.6991	75° 33.0350
233G	06/12/2002	17 42	19.33	39° 27.5290	75° 33.6340
234G	06/12/2002	18 02		39° 27.5576	75° 33.6751
232S	06/12/2002	18 16	12.4	39° 27.4695	75° 33.8873
235G	06/12/2002	18 28	12.04	39° 27.5967	75° 33.3737
236S1	06/12/2002	18 35	12.38	39° 27.5988	75° 33.0396
236S2	06/12/2002	18 51	11.41	39° 27.6826	75° 33.0400
235S	06/12/2002	19 02	10.66	39° 27.6038	75° 33.2243
237S	06/12/2002	19 18	11.13	39° 26.8572	75° 32.3277
238G	06/12/2002	19 33	15.35	39° 26.6542	75° 32.7635
239G	06/12/2002	19 50	15.53	39° 26.6011	75° 32.8542
240S	06/12/2002	20 12	13.47	39° 26.4619	75° 33.1307
241S	06/12/2002	20 32	7.74	39° 24.8841	75° 31.2410
242S	06/12/2002	20 46	14.93	39° 25.0154	75° 31.0149
243S	06/12/2002	21 00	14.38	39° 25.0937	75° 30.8963
244S	06/12/2002	21 16	10.76	39° 25.3004	75° 30.5635

Sample	Date	Time	Depth (m)	Lat N	Lon W
245G	06/12/2002	21 35	7.51	39° 24.5391	75° 29.6837
246S	06/12/2002	21 58	16.4	39° 24.3043	75° 30.0283
248G	06/12/2002	22 42	6.92	39° 24.1198	75° 30.3575
248S	06/12/2002	22 49	6.83	39° 24.1143	75° 30.3658
247G	06/12/2002	22 58	14.85	39° 24.2251	75° 30.0975
245S	06/12/2002	23 10	7.7	39° 24.5338	75° 29.6878
249G	06/13/2002	23 35	7.42	39° 21.8820	75° 28.2742
249S	06/13/2002	23 46	8.98	39° 22.0404	75° 28.0138
250G	06/13/2002	00 02	14.83	39° 22.1889	75° 27.6901
251S	06/13/2002	00 12	14.78	39° 22.2691	75° 27.5913
252S	06/13/2002	00 25	9.15	39° 22.3947	75° 27.3317
253S	06/13/2002	00 50	11.65	39° 21.0635	75° 25.8632
254G	06/13/2002	01 04	18.09	39° 20.9113	75° 26.0765
257S	06/13/2002	01 24	9.44	39° 20.4151	75° 26.8451
256G	06/13/2002	01 35	12.55	39° 20.7040	75° 26.3068
255G	06/13/2002	01 47	18.26	39° 20.8431	75° 26.1932
258G	06/13/2002	02 13	6.85	39° 19.2133	75° 24.9381
259G	06/13/2002	02 30	19.6	39° 19.4536	75° 24.5984
260G	06/13/2002	02 39	22.2	39° 19.5522	75° 24.4675
261S	06/13/2002	02 52	14.68	39° 19.6630	75° 24.2711
262S	06/13/2002	03 19	14	39° 18.4486	75° 22.9280
263G	06/13/2002	03 39	19.07	39° 18.3236	75° 23.0667
264G	06/13/2002	04 00	18.3	39° 18.2330	75° 23.1665
265G	06/13/2002	04 15	15.88	39° 18.0647	75° 23.3652
264S	06/13/2002	04 31	18.3	39° 18.2263	75° 23.1555
265S	06/13/2002	04 51	10.99	39° 17.8567	75° 23.6289
266S	06/13/2002	05 14	10.6	39° 17.0295	75° 22.8259
267S	06/13/2002	05 32	12.33	39° 17.1469	75° 22.4437
268S	06/13/2002	05 43	17.17	39° 17.2451	75° 22.2253
269S	06/13/2002	06 07	16.02	39° 17.3280	75° 21.9799
270S	06/13/2002	06 33	8.68	39° 17.5340	75° 21.5387
271S	06/13/2002	06 55	10.1	39° 16.1561	75° 21.9896
272G1	06/13/2002	07 15	15.67	39° 16.4568	75° 21.2929
272G2	06/13/2002	07 23	16	39° 16.4710	75° 21.2723
274S	06/13/2002	07 45	10.13	39° 16.7775	75° 20.7248
273G	06/13/2002	08 16	16.06	39° 16.6319	75° 20.9825
275G	06/13/2002	08 48	7.17	39° 16.3273	75° 19.1835
276G	06/13/2002	09 05	8.15	39° 16.0444	75° 19.7667
277G	06/13/2002	09 20	16.33	39° 15.8155	75° 20.2524
278G	06/13/2002	09 43	11.68	39° 15.6541	75° 20.5779
279G	06/13/2002	10 01		39° 15.4668	75° 20.9568
280G	06/13/2002	10 10	7.14	39° 15.4305	75° 21.0855
281G	06/13/2002	10 22	7	39° 15.1467	75° 21.6664
282G	06/13/2002	10 30	6.54	39° 15.1474	75° 21.6628
283G	06/13/2002	10 42	7.04	39° 14.5564	75° 20.3673
284S	06/13/2002	10 53	11.67	39° 14.8579	75° 19.8271

Sample	Date	Time		Depth (m)		Lat N		Lon W
286G1	06/13/2002	11	05	12.54	39°	15.1769	75°	19.3323
286G2	06/13/2002	11	11	12.9	39°	15.1543	75°	19.3332
285G	06/13/2002	11	20	16.54	39°	15.0224	75°	19.5786
287G	06/13/2002	11	30	6.9	39°	15.5454	75°	18.6635
288G	06/13/2002	12	02	7.69	39°	13.5688	75°	20.1789
289G	06/13/2002	12	09	6.91	39°	13.7933	75°	19.7118
290G	06/13/2002	12	18	8.94	39°	13.9839	75°	19.2984
291G	06/13/2002	12	29	16.27	39°	14.3216	75°	18.5568
292G	06/13/2002	12	37	6.54	39°	14.6681	75°	17.8734
293G	06/13/2002	12	48	6.98	39°	14.9739	75°	17.2321
294S	06/13/2002	13	52	8.32	39°	13.0124	75°	18.3275
295G	06/13/2002	13	35	16.11	39°	13.3489	75°	17.7988
296G	06/13/2002	13	21	11.96	39°	13.5052	75°	17.4637
297G	06/13/2002	13	09	6.79	39°	13.8318	75°	16.8910
298G	06/13/2002	13	02	9.07	39°	14.1641	75°	16.3248

† "C" and "S" denote core samples, "G" grab samples

‡ Eastern Standard Time for CH0104, CH0107, CH02-02, and CH01-28; Greenwich Mean

Time for CH02-09

APPENDIX D. WATER CONTENT AND POROSITY DATA

Cruise	Sample ID	Interval (cm)	Water Content (%)	Porosity (%)
CH0103	C1	14-15	47.2	70.1
CH0103	C1	22-23	41.8	65.3
CH0103	C1	53-55	40.6	64.2
CH0103	C2	0-1	58.0	78.4
CH0103	C2	1-2	52.9	74.7
CH0103	C2	22-23	48.5	71.2
CH0103	C2	55-57	48.0	70.8
CH0103	C4	1-2	55.8	76.8
CH0103	C4	20-21	52.9	74.7
CH0103	C4	56-58	50.7	73.0
CH0103	C5	0-1	39.5	63.1
CH0103	C5	1-2	31.5	54.7
CH0103	C7	10-11	53.1	74.8
CH0103	C7	25-26	54.3	75.7
CH0103	C7	61-63	54.1	75.6
CH0103	C8	0-1	61.1	80.5
CH0103	C8	1-2	59.2	79.2
CH0103	C8	2-3	57.5	78.0
CH0103	C8	3-4	48.2	71.0
CH0103	C8	19-20	57.0	77.7
CH0103	C8	47-49	58.6	78.8
CH0103	C8	57-59	52.9	74.6
CH0103	C9	0-1	63.8	82.2
CH0103	C9	1-2	53.6	75.2
CH0103	C9	2-3	47.8	70.6
CH0103	C9	3-4	33.7	57.1
CH0103	C9	20-22	49.0	71.6
CH0103	C9	57-59	43.3	66.7
CH0701	C14B	0-2	45.0	68.2
CH0701	C14B	2-4	33.0	56.4
CH0701	C14B	4-6	27.1	49.4
CH0701	C14B	6-8	31.1	54.2
CH0701	C14B	8-10	34.5	58.0
CH0701	C14B	10-12	37.9	61.5
CH0701	C14B	14-16	33.0	56.4
CH0701	C14B	18-20	43.7	67.0
CH0701	C14B	22-24	31.7	54.9
CH0701	C14B	26-28	40.3	63.9
CH0701	C14B	30-32	33.2	56.6

Cruise	Sample ID	Interval (cm)	Water Content (%)	Porosity (%)
CH0701	C14B	34-36	30.7	53.8
CH0701	C14B	38-40	25.4	47.2
CH0701	C14B	42-44	25.4	47.1
CH0701	C14B	46-48	34.7	58.3
CH0701	C14B	50-52	33.4	56.8
CH0701	C14B	52-54	40.5	64.1
CH0701	C14B	12-14	33.5	56.9
CH0701	C14B	16-18	37.1	60.7
CH0701	C14B	20-22	44.9	68.2
CH0701	C14B	24-26	28.2	50.8
CH0701	C14B	28-30	38.9	62.6
CH0701	C14B	32-34	32.3	55.6
CH0701	C14B	36-38	24.9	46.5
CH0701	C14B	40-42	24.2	45.5
CH0701	C14B	44-46	23.1	44.1
CH0701	C14B	48-50	33.8	57.2
CH0701	C14B	54-56	45.4	68.5
CH0701	C15A	0-2	73.5	87.9
CH0701	C15A	32-34	61.6	80.8
CH0701	C15A	34-36	55.2	76.4
CH0701	C15A	36-38	38.3	62.0
CH0701	C15A	38-40	51.0	73.2
CH0701	C15A	40-42	54.7	76.0
CH0701	C15A	42-44	55.7	76.8
CH0701	C15A	44-46	56.4	77.2
CH0701	C15A	46-48	53.7	75.2
CH0701	C15A	48-50	55.7	76.7
CH0701	C15A	50-52	56.0	76.9
CH0701	C15A	52-54	57.4	77.9
CH0701	C15A	54-56	57.8	78.2
CH0701	C15A	56-58	57.3	77.9
CH0701	C15A	58-60	55.2	76.4
CH0701	C15A	60-62	55.1	76.3
CH0701	C15A	62-64	56.7	77.4
CH0701	C15A	64-66	55.1	76.3
CH0701	C15A	66-68	53.3	75.0
CH0701	C16B	0-1	46.2	69.2
CH0701	C16B	1-2	52.1	74.1
CH0701	C16B	2-3	54.0	75.5
CH0701	C16B	3-4	54.8	76.1
CH0701	C16B	4-6	37.7	61.4
CH0701	C16B	6-8	31.5	54.7
CH0701	C16B	8-10	35.7	59.3
CH0701	C16B	10-12	31.6	54.8
CH0701	C16B	12-14	55.1	76.3
CH0701	C16B	14-16	50.6	72.9

Cruise	Sample ID	Interval (cm)	Water Content (%)	Porosity (%)
CH0701	C16B	18-20	39.9	63.5
CH0701	C16B	22-24	45.9	69.0
CH0701	C16B	24-26	45.3	68.5
CH0701	C16B	26-28	45.1	68.3
CH0701	C16B	28-30	43.1	66.6
CH0701	C16B	30-32	43.4	66.8
CH0701	C16B	32-34	38.4	62.1
CH0701	C16B	34-36	42.8	66.2
CH0701	C16B	36-38	42.3	65.8
CH0701	C16B	38-40	44.2	67.5
CH0701	C16B	40-42	45.3	68.5
CH0701	C16B	42-44	56.5	77.3
CH0701	C16B	44-46	49.5	72.0
CH0701	C16B	46-48	35.9	59.5
CH0701	C16B	48-50	42.7	66.2
CH0701	C16B	50-52	40.3	63.9
CH0701	C16B	52-54	46.9	69.9
CH0701	C16B	54-56	53.2	74.9
CH01-28	111S	8-10	46.8	69.8
CH01-28	111S	22-24	57.1	77.8
CH01-28	111S	34-36	41.0	64.5
CH01-28	144S1	0-2	62.0	81.1
CH01-28	144S1	28-30	59.4	79.3
CH01-28	144S1	58-60	55.7	76.7
CH01-28	174S	0-1	59.5	79.4
CH01-28	174S	1-2	61.8	80.9
CH01-28	174S	2-3	66.0	83.6
CH01-28	174S	3-4	61.0	80.4
CH01-28	174S	4-6	63.1	81.8
CH01-28	174S	6-8	66.8	84.1
CH01-28	177S	6-8	52.5	74.4
CH01-28	177S	24-26	48.8	71.4
CH01-28	177S	40-42	44.1	67.4
MARSH	PC1	0-2	78.9	90.7
MARSH	PC1	28-30	49.9	72.3
MARSH	PC1	56-58	46.1	69.2
MARSH	PC3	0-2	58.0	78.4
MARSH	PC3	34-36	57.2	77.8
MARSH	PC3	58-60	48.5	71.2
MARSH	PC4	0-2	60.0	79.8
MARSH	PC4	2-4	63.5	82.1

Cruise	Sample ID	Interval (cm)	Water Content (%)	Porosity (%)
MARSH	PC4	4-6	62.9	81.6
MARSH	PC4	6-8	61.1	80.5
MARSH	PC4	8-10	60.8	80.3
MARSH	PC4	10-12	61.9	81.0
MARSH	PC4	12-14	60.5	80.1
MARSH	PC4	14-16	63.8	82.2
MARSH	PC4	16-18	61.0	80.4
MARSH	PC4	18-20	59.2	79.2
MARSH	PC4	20-22	60.9	80.3
MARSH	PC4	22-24	55.1	76.3
MARSH	PC4	24-26	56.7	77.4
MARSH	PC4	26-28	54.8	76.1
MARSH	PC4	28-30	51.0	73.2
MARSH	PC4	30-32	53.9	75.4
MARSH	PC4	32-34	57.0	77.6
MARSH	PC4	34-36	56.3	77.2
MARSH	PC4	36-38	53.4	75.1
MARSH	PC4	38-40	53.2	74.9
MARSH	PC4	40-42	56.6	77.4
MARSH	PC4	42-44	56.3	77.2
MARSH	PC4	44-46	53.2	74.9
MARSH	PC4	46-48	57.0	77.7
MARSH	PC4	48-50	56.2	77.1
MARSH	PC4	50-52	56.4	77.2
MARSH	PC6	0-2	52.1	74.1
MARSH	PC6	18-20	58.7	78.8
MARSH	PC6	36-38	52.4	74.3
MARSH	PC7	0-2	63.0	81.7
MARSH	PC7	2-4	60.8	80.3
MARSH	PC7	4-6	61.1	80.5
MARSH	PC7	6-8	61.3	80.6
MARSH	PC7	8-10	60.3	79.9
MARSH	PC7	10-12	63.2	81.8
MARSH	PC7	12-14	66.9	84.1
MARSH	PC7	14-16	64.7	82.8
MARSH	PC7	16-18	66.3	83.8
MARSH	PC7	18-20	66.4	83.8
MARSH	PC7	20-22	69.8	85.9
MARSH	PC7	22-24	68.1	84.9
MARSH	PC7	24-26	67.6	84.6
MARSH	PC7	28-30	67.1	84.2
MARSH	PC7	32-34	65.3	83.1
MARSH	PC7	36-38	65.8	83.5
MARSH	PC7	40-42	64.6	82.7
MARSH	PC7	42-44	63.5	82.0
MARSH	PC7	46-48	66.3	83.8

Cruise	Sample ID	Interval (cm)	Water Content (%)	Porosity (%)
MARSH	PC7	50-52	65.9	83.5
MARSH	PC7	54-56	65.4	83.2
MARSH	PC7	62-64	62.1	81.2
MARSH	PC9	0-2	50.7	73.0
MARSH	PC9	2-4	49.8	72.2
MARSH	PC9	4-6	49.4	72.0
MARSH	PC9	6-8	50.8	73.0
MARSH	PC9	28-30	52.7	74.5
MARSH	PC9	54-56	50.1	72.4
MARSH	PC9	56-58	50.2	72.6
MARSH	PC13	0-2	58.9	79.0
MARSH	PC13	2-4	59.3	79.2
MARSH	PC13	4-6	56.2	77.1
MARSH	PC13	6-8	53.8	75.3
MARSH	PC13	8-10	55.7	76.7
MARSH	PC13	10-12	55.5	76.6
MARSH	PC13	12-14	57.8	78.2
MARSH	PC13	14-16	57.6	78.1
MARSH	PC13	16-18	65.9	83.5
MARSH	PC13	18-20	63.8	82.2
MARSH	PC13	20-22	68.6	85.2
MARSH	PC13	22-24	66.8	84.1
MARSH	PC13	24-26	64.2	82.4
MARSH	PC13	26-28	69.3	85.5
MARSH	PC13	28-30	65.8	83.4
MARSH	PC13	32-34	58.2	78.5
MARSH	PC13	36-38	55.0	76.2
MARSH	PC13	40-42	51.7	73.7
MARSH	PC13	44-46	48.0	70.8
MARSH	PC13	48-50	47.5	70.3
MARSH	PC13	60-62	49.0	71.6
MARSH	PC13	62-64	48.9	71.5
MARSH	PC13	70-72	51.1	73.3
MARSH	PC13	80-82	50.1	72.5
MARSH	PC13	88-90	53.9	75.5
MARSH	PC13	90-92	51.7	73.7
MARSH	PC13	92-93.5	50.1	72.4
MARSH	PC14	0-2	55.5	76.6
MARSH	PC14	4-6	43.2	66.6
MARSH	PC14	6-8	43.8	67.2
MARSH	PC14	10-12	45.4	68.5
MARSH	PC14	14-16	46.9	69.9
MARSH	PC14	18-20	46.9	69.9
MARSH	PC14	20-22	46.1	69.2
MARSH	PC14	22-24	45.8	68.9

Cruise	Sample ID	Interval (cm)	Water Content (%)	Porosity (%)
MARSH	PC14	24-26	41.6	65.1
MARSH	PC14	26-28	45.5	68.6
MARSH	PC14	28-30	45.1	68.3
MARSH	PC14	30-32	37.3	61.0
MARSH	PC14	32-34	37.3	61.0
MARSH	PC14	34-36	36.1	59.7
MARSH	PC14	38-40	35.4	59.0
MARSH	PC14	42-44	37.5	61.2
MARSH	PC14	46-48	39.7	63.4
MARSH	PC14	50-52	41.4	65.0
MARSH	PC14	54-56	42.4	65.9
MARSH	PC14	58-60	44.9	68.1
MARSH	PC14	62-64	45.4	68.6
MARSH	PC14	66-68	47.1	70.0
MARSH	PC14	70-72	48.8	71.5
MARSH	PC14	74-76	46.1	69.2
MARSH	PC14	78-80	43.0	66.4
MARSH	PC14	82-84	44.7	67.9
MARSH	PC14	86-88	37.2	60.9
MARSH	PC14	92-94	44.1	67.4
MARSH	PC15	0-2	60.2	79.9
MARSH	PC15	4-6	61.8	80.9
MARSH	PC15	8-10	59.4	79.3
MARSH	PC15	12-14	62.1	81.2
MARSH	PC15	16-18	62.9	81.6
MARSH	PC15	18-20	64.9	82.9
MARSH	PC15	22-24	60.3	79.9
MARSH	PC15	26-28	56.2	77.1
MARSH	PC15	30-32	60.8	80.3
MARSH	PC15	34-36	59.3	79.2
MARSH	PC15	38-40	62.8	81.6
MARSH	PC15	42-44	57.4	78.0
MARSH	PC15	44-46	58.0	78.4
MARSH	PC15	46-48	58.6	78.8
MARSH	PC15	48-50	61.3	80.6
MARSH	PC15	52-54	61.3	80.6
MARSH	PC15	54-56	59.5	79.4
MARSH	PC15	56-58	59.8	79.6
MARSH	PC15	58-60	57.2	77.8
MARSH	PC15	60-62	56.7	77.5
MARSH	PC15	62-64	49.2	71.8
MARSH	PC15	64-66	50.4	72.7
MARSH	PC15	66-68	42.0	65.5
MARSH	PC15	68-70	46.2	69.3
MARSH	PC15	70-72	61.7	80.9
MARSH	PC15	74-76	55.4	76.5
MARSH	PC15	80-82	50.4	72.7

Cruise	Sample ID	Interval (cm)	Water Content (%)	Porosity (%)
MARSH	PC15	84-86	38.8	62.5
MARSH	PC15	90-92	39.2	62.9
MARSH	PC16A	0-2	61.8	80.9
MARSH	PC16A	2-4	57.1	77.8
MARSH	PC16A	4-6	54.9	76.2
MARSH	PC16A	8-10	65.9	83.5
MARSH	PC16A	12-14	67.4	84.5
MARSH	PC16A	14-16	71.4	86.7
MARSH	PC16A	16-18	70.9	86.5
MARSH	PC16A	20-22	71.8	87.0
MARSH	PC16A	24-26	68.4	85.0
MARSH	PC16A	28-30	63.3	81.9
MARSH	PC16A	32-34	48.7	71.4
MARSH	PC16A	36-38	40.9	64.5
MARSH	PC16A	40-42	40.3	63.9
MARSH	PC16A	44-46	42.5	66.0
MARSH	PC16A	48-50	44.7	67.9
MARSH	PC16A	50-52	45.0	68.2
MARSH	PC16A	52-54	44.8	68.1
MARSH	PC16A	56-58	46.3	69.4
MARSH	PC16A	58-60	46.3	69.3
MARSH	PC17	0-2	43.6	67.0
MARSH	PC17	20-22	38.8	62.5
MARSH	PC17	42-44	35.1	58.6
MARSH	PC17	60-62	32.8	56.2
CH02-02	MH-W	0-2	72.1	87.2
CH02-02	MH-W	10-12	53.7	75.3
CH02-02	MH-W	20-22	53.9	75.4
CH02-02	MH-W	40-42	56.2	77.1
CH02-02	MH-W	58-60	50.8	73.0
CH02-02	MH-E	0-2	73.2	87.7
CH02-02	MH-E	2-4	69.3	85.5
CH02-02	MH-E	6-8	62.8	81.6
CH02-02	MH-E	10-12	65.2	83.1
CH02-02	MH-E	14-16	63.2	81.9
CH02-02	MH-E	20-22	61.9	81.0
CH02-02	MH-E	30-32	39.0	62.6
CH02-02	MH-E	40-42	45.7	68.8
CH02-02	MH-E	46-48	44.3	67.6
CH02-02	MH-E	50-52	45.5	68.6
CH02-02	MH-E	52-54	41.7	65.3
CH02-09	257S	4-6	37.9	61.6
CH02-09	257S	20-22	58.2	78.5
CH02-09	257S	38-40	56.2	77.1

APPENDIX E. GRAIN SIZE DATA

Sample ID*	% Gravel	% Sand	% Mud	% Silt	% Clay	Class †
CH01-28 1G	0.16	30.37	69.48	54.7	14.78	sM
2G	65.39	34.01	0.6	nd	nd	sG
3G	0	99.8	0.2	nd	nd	S
4G	0	99.81	0.19	nd	nd	S
9G	22.85	76.09	1.06	nd	nd	S
9G2	46.5	42.24	11.26	5.33	5.93	sG
10G	4.56	41.49	53.95	4.56	49.39	sM
11G	0.96	98.53	0.51	nd	nd	S
12G	0.85	90.36	8.79	0.33	8.46	S
13G	0	99.65	0.35	nd	nd	S
14G	0	92.22	7.78	0.97	6.81	S
15G	2.92	96.84	0.24	nd	nd	S
16G	5.77	23.42	70.81	33.54	37.27	sM
17G	0	92.22	7.78	7.66	0.12	S
18G	21.42	67.00	11.58	4.07	7.51	gS
19G	0	99.93	0.07	nd	nd	S
20G	0	99.94	0.06	nd	nd	S
21G	61.36	30.77	7.87	1.75	6.12	sG
22G	0	13.48	86.52	nd	nd	M
23G	0.03	99.68	0.29	nd	nd	S
24G	5.08	85.7	9.22	nd	nd	S
25G	72.77	23.66	3.57	nd	nd	sG
26G	0	99.38	0.62	nd	nd	S
27G	26.17	62.84	10.99	10.88	0.11	gS
28G	42.46	56.93	0.61	nd	nd	gS
29G	0.08	98.84	1.08	nd	nd	S
30G	6.77	70.74	22.49	nd	nd	mS
31G	42.98	56.38	0.64	nd	nd	gS
32G	2.97	85.57	11.46	nd	nd	S
33G	0	99.06	0.94	nd	nd	S
34G	49.59	48.59	1.82	nd	nd	sG
35G	49.29	32.33	18.38	9.19	9.19	sG
36G	41.93	22.65	35.42	nd	nd	msG
37G	68.18	29.67	2.15	nd	nd	sG
38G	63.56	20.3	16.14	nd	nd	sG
39G	31.88	61.48	6.64	nd	nd	gS
40G	0	3.15	96.85	nd	nd	M
41G	0	21.06	78.94	48.24	30.7	scZ
42G	25.64	32.02	42.34	nd	nd	gsM
43G	0	13.31	86.69	54.75	31.94	cZ
45G	71.48	27.7	0.82	nd	nd	sG
46G	1.37	24.18	74.46	47.38	27.08	sM
47G	0	5.46	94.54	nd	nd	M
48G	4.9	86.97	8.13	nd	nd	S
49G	33.1	65.45	1.45	nd	nd	gS
50G	1.62	97.54	0.84	nd	nd	S
51G	0	13.79	86.21	51.73	34.48	cZ

Sample ID	% Gravel	% Sand	% Mud	% Silt	% Clay	Class
52G	58.98	38.29	2.73	nd	nd	sG
53G	5.51	37.38	57.11	nd	nd	sM
54G	0.71	62.73	36.56	nd	nd	mS
55G	0	54.94	45.06	33.89	11.17	zS
56G	4.03	89.36	6.61	nd	nd	S
57G	78.18	10.25	11.57	nd	nd	G
58G	0	11.91	88.09	63.73	24.36	cZ
59G	0	28.54	71.46	71.14	0.32	sZ
60G	0	43.92	56.08	nd	nd	sM
61G	4.14	94.84	1.02	nd	nd	S
62G	11.01	87.1	1.89	nd	nd	S
63G	0	20.88	79.12	62.17	16.95	sZ
64G	0.86	61.84	37.3	nd	nd	mS
65G	100	0	0	0	0	G
66G	54.14	29.29	16.57	nd	nd	sG
67G	0	5.06	94.94	37.97	56.96	zC
68G	54.11	27.55	18.34	2.62	15.72	sG
69G	72.06	12.88	15.06	2.15	12.91	mG
70G	0	40.03	59.97	29.99	29.99	czS
71G	0.15	81.44	18.41	7.36	11.05	S
72G	24.26	73.44	2.3	nd	nd	gS
73G	6.6	89.17	4.23	2.12	2.12	S
74G	11.19	82.19	6.62	0	6.62	S
75G	0.54	58.64	40.82	13.61	27.21	mS
76G	0.22	88.86	10.92	2.73	8.19	S
77G	0.25	62.65	37.1	12.37	24.73	mS
78G	1.56	92.2	6.24	3.12	3.12	S
79G	5.82	45.68	48.5	35.27	13.23	sM
80G	0	89.55	10.45	6.97	3.48	S
81G	100	0	0	0	0	G
82G	61.2	32.2	6.6	3.26	3.34	sG
83G [‡]	nd	nd	nd	nd	nd	R
84G	55.25	31.94	12.81	8.54	4.27	sG
85G	0	7.87	92.13	50.25	41.88	cZ
86G	100	0	0	0	0	G
87G	0	9.09	90.91	0	90.91	C
88G	0.77	86.41	12.82	nd	nd	S
89G	50.24	28.8	20.96	5.99	14.97	msG
90G	54.45	34.49	11.06	nd	nd	sG
91G	74.59	18.71	6.7	nd	nd	sG
92G	77.85	22.15	0	0	0	G
93G	0	3.31	96.69	nd	nd	M
94G	5.92	5.32	88.76	0	88.76	M
95G	11.32	56.63	32.05	nd	nd	mS
96G	45.19	40.23	14.58	nd	nd	sG
97G	0	5.66	94.34	20.96	73.38	zC
98G	0	29.7	70.3	17.56	52.72	sC
99G	0	20.42	79.58	nd	nd	sM
101G	5.23	70.98	23.79	4.76	19.03	mS

Sample ID	% Gravel	% Sand	% Mud	% Silt	% Clay	Class
102G	0	31.39	68.61	25.73	42.88	szC
103G	6.7	74.67	18.62	0	18.62	mS
104G	0	9.56	90.44	25.84	64.6	zC
105G	0	1.48	98.52	49.26	49.26	zC
106G	0	4.37	95.63	27.32	68.31	zC
107G	0	34.21	65.79	24.67	41.12	szC
108G	8.96	63.38	27.65	0	27.65	mS
109G	0	3.43	96.57	21.46	75.11	zC
110G	0	1.57	98.43	29.53	68.9	zC
111G	11.32	0.96	87.72	31.9	55.82	M
112G	1.85	64.15	34	0	34.73	mS
113G	0	55.75	44.25	0	44.25	cS
114G	0	19.61	80.39	24.12	56.27	zC
115G	0	14.68	85.32	51.19	34.13	zC
116G	0	26.74	73.26	18.32	54.95	sC
117G	0	9.09	90.91	30.3	60.61	zC
118G	62.32	14.3	23.38	6.68	16.7	mG
119G	33.33	23.63	43.04	11.74	31.3	gsM
120G	0	17.42	82.58	7.51	75.08	C
121G	0	26.87	73.13	18.28	54.84	zC
122G	15.17	24.43	60.4	20.13	40.27	sM
123G	0	0.72	99.28	27.08	72.2	zC
124G	84.48	7.9	7.62	1.52	6.1	G
125G [‡]	nd	nd	nd	nd	nd	R
126G	96.12	0.23	3.64	0	3.64	G
127G	0	66.28	33.72	4.82	28.9	cS
128G	0	7.98	92.02	61.35	30.67	cZ
129G	70.61	0.7	28.7	0	28.69	mG
130G	0	6.01	93.99	23.45	70.54	zC
131G [‡]	nd	nd	nd	nd	nd	R
132G	0	4.9	95.1	19.62	75.48	zC
133G	1.17	10.35	88.48	19.54	68.94	M
134G	0	2.8	97.2	28.75	68.45	zC
135G	0	6.39	93.61	21.06	72.55	zC
136G	3.82	23.06	73.13	13.96	59.17	sM
137G	1	78.3	20.7	0	20.7	S
138G	0	40.64	59.36	19.54	39.82	sC
139G	0	21.86	78.14	10.79	67.35	sC
140G	0	2.72	97.28	12.68	84.6	C
141G	19.26	36.88	43.87	4.19	39.67	sM
142G	0	2.98	97.02	22.59	74.42	zC
143G	0	5.72	94.28	21.32	72.96	zC
144G	0	2.52	97.48	20.07	77.41	C
145G	5.4	14.21	80.39	23.82	56.57	M
146G	18.08	1.78	80.14	21.75	58.39	M
147G	0	4.67	95.33	25.51	69.82	zC
148G	41.3	23.75	34.95	7.69	27.26	msG
149G	40.78	26.96	32.26	9.1	23.17	msG
150G	0	3.96	96.04	28.45	67.59	zC

Sample ID	% Gravel	% Sand	% Mud	% Silt	% Clay	Class
151G	0	7.25	92.75	30.86	61.89	zC
152G	0	56.1	43.9	5.27	38.63	cS
153G	0	1.88	98.12	36.5	61.62	zC
154G	11.24	31.72	57.03	21.91	35.12	sM
155G	26.64	28.19	45.17	12.41	32.76	gsM
156G	16.09	64.25	19.66	97.41	0	mS
157G	0	8.45	91.55	35.84	55.71	zC
158G	0	13.97	86.03	41.87	44.15	zC
159G	0	4.19	95.81	45.38	50.44	zC
160G	11.14	2.02	86.84	45.68	41.16	M
161G	0	2.22	97.78	47.42	50.36	zC
162G	0	5.07	94.93	40.64	54.29	zC
163G	0	1.28	98.72	42.42	56.3	zC
164G	0	13.71	86.29	28.95	57.35	zC
165G	0	8.36	91.64	30.35	61.3	zC
166G	0	20.72	79.28	30.69	48.59	szC
167G	3.89	13.79	82.32	33.28	49.04	M
168G	2.32	30.88	66.8	20.2	46.6	sM
169G	0	3.49	96.51	28.8	67.71	zC
170G	0	6.52	93.48	35.58	57.9	zC
171G	0.58	36.06	63.36	17.79	45.57	sM
172G	0.00	20.21	29.90	49.88	79.79	szC
173G	0.00	2.79	22.84	74.37	97.21	zC
174G	1.37	54.12	10.23	34.28	44.51	mS
175G	0.00	4.28	33.50	62.22	95.72	zC
176G	2.55	10.03	27.68	59.74	87.42	sM
177G	0.00	4.16	35.10	60.73	95.84	zC
178G	0.26	73.93	0.00	26.07	25.81	mS
179G	0.43	44.59	49.26	5.71	54.97	sM
180G	51.79	39.27	1.33	7.62	8.94	sG
181G	63.07	4.24	4.46	28.23	32.69	mG
182G	0.3	12.10	33.90	53.69	87.90	M

Sample ID	% Gravel	% Sand	% Mud	% Silt	% Clay	Class
CH09-02						
184G	0.66	66.21	33.12	5.35	27.78	mS
185G	0.00	38.32	61.68	27.15	34.53	czS
186G	0.00	5.45	94.55	34.28	60.27	zC
187G	0.00	29.54	70.46	23.40	47.06	szC
188G	16.67	18.45	64.88	22.01	42.87	sM
190G	0.00	5.80	94.20	26.86	67.34	zC
191G	0.00	0.44	99.56	93.18	6.38	Z
192G	73.14	15.95	10.90	0.54	10.37	sG
193G1	0.00	32.18	67.82	16.36	51.45	sC
193G2	0.00	35.52	64.48	18.64	45.85	sC
194G	62.51	20.90	16.59	3.00	13.59	sG
195G	1.02	81.72	17.26	0.95	16.31	s
196G	45.73	13.79	40.48	14.11	26.37	mG
197G	0.00	58.66	41.34	7.35	33.99	cS
198G	12.35	49.50	38.15	11.38	26.77	mS
199G	0.00	6.95	93.05	39.45	53.60	zC
200G	88.14	3.68	8.17	1.46	6.71	G
201G	64.43	22.95	12.63	1.14	11.48	sG
202G [‡]	nd	nd	nd	nd	nd	G
203G	51.60	33.94	14.47	1.82	12.64	sG
204G	0.00	18.72	81.28	32.48	48.80	zC
205G	0.00	9.68	90.32	22.54	67.78	zC
206G	22.67	57.59	19.74	1.82	17.92	gmS
207G	72.23	18.40	9.37	1.01	8.35	sG
208G	0.00	4.91	95.09	27.37	67.73	zC
210G	0.00	13.50	86.50	nd	nd	zC
211G	0.00	1.70	98.30	21.91	76.39	C
212G	0.17	29.36	70.48	15.21	55.26	sM
213G	6.71	22.39	70.90	26.41	44.49	sM
214G	0.00	14.78	85.22	31.59	53.63	zC
215G	0.56	79.50	19.94	1.08	18.86	S
216G	0.00	82.55	17.45	0.00	17.45	S
217G	50.44	31.92	17.64	2.19	15.45	sG
218G	0.00	5.29	94.71	23.80	70.92	zC
219G	0.00	12.39	87.61	38.28	49.32	zC
220G	1.64	73.71	24.65	3.78	20.86	mS
221G	0.00	4.99	95.01	38.79	56.22	zC
222G	67.35	22.38	10.27	0.83	9.44	sG
223G	57.35	28.20	14.45	2.00	12.45	sG
224G	0.00	7.02	92.98	33.78	59.20	zC
225G	3.81	79.22	16.97	nd	nd	S
226G [‡]	nd	nd	nd	nd	nd	sM
227G	42.59	36.40	21.01	3.96	17.05	msG

Sample ID	% Gravel	% Sand	% Mud	% Silt	% Clay	Class
228G	0.00	5.13	94.87	32.64	62.22	zC
229G	0.00	6.12	93.88	34.44	59.44	zC
230G	0.00	39.78	60.22	22.33	37.90	czS
230G	83.06	0.12	16.83	1.87	14.96	G
232G	0.00	16.96	83.04	23.31	59.73	zC
233G	0.00	1.04	98.96	30.86	68.10	zC
235G	0.00	73.16	26.84	3.19	23.65	cS
236G	0.59	34.66	64.74	19.90	44.84	sM
238G	0.00	86.67	13.33	0.44	12.89	S
239G	0.00	19.06	80.94	nd	nd	M
245G	4.82	71.78	23.40	5.61	17.79	mS
247G	0.00	20.23	79.77	18.95	60.82	sC
248G	0.00	43.50	56.50	13.40	43.10	cS
249G	0.00	2.34	97.66	86.43	11.23	Z
250G	0.02	21.97	78.01	74.08	3.93	sM
254G	0.00	2.82	97.18	23.44	73.74	zC
255G	0.00	3.82	96.18	25.99	70.20	zC
256G	0.00	81.11	18.89	1.40	17.49	S
258G	0.00	50.41	49.59	11.92	37.67	cS
259G	5.31	69.09	25.60	3.99	21.61	mS
260G	10.55	59.20	30.25	7.78	22.48	mS
263G [‡]	nd	nd	nd	nd	nd	R
264 top	0.95	78.02	21.03	1.03	20.00	S
264 bot	0.00	3.72	96.28	21.70	74.57	zC
265G	1.43	49.16	49.41	14.14	35.27	mS
272G2	0.39	64.06	35.55	5.17	30.38	mS
272G1	0.00	27.84	72.16	17.86	54.29	scZ
273G	2.35	81.55	16.09	0.19	15.90	S
275G	0.00	62.58	37.42	10.68	26.74	cS
276G [‡]	nd	nd	nd	nd	nd	SH
277G	3.91	84.50	11.58	0.00	12.19	S
278G	0.00	73.88	26.12	5.84	20.28	cS
279G	2.15	81.13	16.72	1.91	14.81	S
280G	0.00	69.72	30.28	6.62	23.66	cS
281G	0.00	54.76	45.24	13.24	32.01	cS
282G	0.00	45.29	54.71	20.00	34.71	cS
283G	0.00	80.19	19.81	0.36	19.45	S
285G	0.00	29.15	70.85	20.73	50.12	scZ
286G1	1.35	55.73	42.92	12.78	30.14	mS
286G2	1.00	46.20	52.80	13.21	39.58	sM
287G	0.00	49.02	50.98	18.34	32.64	cS
288G	0.00	60.20	39.80	13.94	25.86	cS
289G	0.00	77.84	22.16	4.67	17.50	cS
290G	0.12	76.75	23.13	3.74	19.39	S

Sample ID	% Gravel	% Sand	% Mud	% Silt	% Clay	Class
291G	16.34	70.33	13.32	0.00	13.76	gS
292G	0.00	70.67	29.33	12.33	17.00	cS
293G	0.00	68.96	31.04	2.77	28.27	cS
295G	0.00	80.20	19.80	0.00	19.80	S
296G	0.35	76.14	23.52	1.65	21.86	S
297G	2.72	58.16	39.12	7.79	31.33	mS
298G	0.75	70.92	28.33	0.79	27.54	mS

* See Appendix C for sample locations

† G, gravel; g, gravelly; S, sand; s, sandy; M, mud; m, muddy; Z, silt; z, silty; C, clay; c, clayey; R, rock; SH, shell

‡ No analysis performed; size class based on field observation

nd=not determined

APPENDIX F. Cs-137 and Pb-210 ACTIVITIES

Core [†]	Interval (cm)	Cs-137 (dpm/g) [‡]	Error (dpm/g)
C1	14-15	0.016	0.008
C1	22-23	0.008	0.007
C1	48-50	0.007	0.003
C2	0-1	0.029	0.013
C2	1-2	nd	-
C2	22-23	nd	-
C2	50-52	nd	-
C4	0-1	0.012	0.008
C4	1-2	0.001	0.004
C4	20-21	nd	-
C4	50-52	nd	-
C7	0-1	nd	-
C7	10-11	nd	-
C7	25-26	0.008	0.006
C7	50-52	nd	-
C8	0-1	0.131	0.024
C8	1-2	0.082	0.022
C8	2-3	0.079	0.022
C8	3-4	0.061	0.015
C8	19-20	0.039	0.009
C8	47-49	0.038	0.013
C8	57-59	0.005	0.005
C9	0-1	0.091	0.027
C9	1-2	0.057	0.015
C9	2-3	nd	-
C9	3-4	nd	-
C9	20-22	0.075	0.009
C9	50-52	0.019	0.007
C14b	0-2	0.075	0.023
C14b	2-4	0.057	0.013
C14b	4-6	0.051	0.012
C14b	6-8	0.072	0.012
C14b	8-10	0.018	0.006
C14b	10-12	0.059	0.011
C14b	12-14	0.041	0.009
C14b	14-16	nd	-
C14b	16-18	nd	-
C14b	18-20	0.105	0.020
C14b	20-22	0.082	0.012
C14b	22-24	0.063	0.014
C14b	24-26	0.021	0.007

Core	Interval (cm)	Cs-137 (dpm/g) [‡]	Error (dpm/g)
C14b	26-28	0.075	0.017
C14b	28-30	0.095	0.014
C14b	30-32	0.012	0.009
C14b	32-34	0.011	0.005
C14b	34-36	0.058	0.014
C14b	38-40	0.026	0.010
C14b	42-44	0.053	0.011
C14b	46-48	0.090	0.019
C14b	50-52	0.085	0.018
C14b	52-54	0.095	0.024
C14b	54-56	0.210	0.028
C15a	0-2	0.067	0.025
C15a	32-34	0.312	0.031
C15a	34-36	0.219	0.031
C15a	36-38	0.024	0.005
C15a	38-40	0.157	0.028
C15a	40-42	0.155	0.029
C15a	42-44	0.250	0.030
C15a	44-46	0.203	0.028
C15a	46-48	0.204	0.029
C15a	48-50	0.081	0.030
C15a	50-52	0.132	0.030
C15a	52-54	0.300	0.030
C15a	54-56	0.201	0.030
C15a	56-58	0.192	0.029
C15a	58-60	0.131	0.033
C15a	60-62	0.153	0.031
C15a	62-64	0.131	0.033
C15a	64-66	0.221	0.033
C15a	66-68	0.100	0.024
C16b	0-1	0.018	0.009
C16b	1-2	0.072	0.014
C16b	2-3	0.038	0.013
C16b	3-4	0.072	0.014
C16b	4-6	0.045	0.009
C16b	6-8	0.000	0.000
C16b	8-10	0.024	0.007
C16b	10-12	0.005	0.004
C16b	12-14	0.121	0.018
C16b	14-16	0.099	0.020
C16b	16-18	0.104	0.018
C16b	18-20	0.052	0.016
C16b	20-22	0.040	0.014
C16b	22-24	0.090	0.018
C16b	24-26	0.071	0.019
C16b	26-28	0.085	0.020

Core	Interval (cm)	Cs-137 (dpm/g)‡	Error (dpm/g)
C16b	28-30	0.080	0.013
C16b	30-32	0.089	0.019
C16b	32-34	0.105	0.018
C16b	34-36	0.054	0.017
C16b	36-38	0.033	0.015
C16b	38-40	0.084	0.021
C16b	40-42	0.116	0.020
C16b	42-44	0.230	0.025
C16b	44-46	0.124	0.019
C16b	46-48	0.083	0.016
C16b	48-50	0.137	0.020
C16b	50-52	0.028	0.014
C16b	52-54	0.050	0.016
C16b	54-56	0.085	0.015
PC4	0-2	0.022	0.016
PC4	2-4	0.148	0.020
PC4	4-6	0.220	0.021
PC4	6-8	0.095	0.018
PC4	8-10	0.207	0.019
PC4	10-12	0.205	0.021
PC4	12-14	0.133	0.018
PC4	14-16	0.185	0.027
PC4	16-18	0.126	0.019
PC4	18-20	0.318	0.025
PC4	20-22	0.181	0.024
PC4	22-24	0.190	0.027
PC4	24-26	0.127	0.017
PC4	26-28	0.142	0.018
PC4	28-30	0.121	0.016
PC4	30-32	0.168	0.024
PC4	32-34	0.173	0.018
PC4	34-36	0.141	0.022
PC4	36-38	0.119	0.018
PC4	38-40	0.125	0.020
PC4	40-42	0.188	0.025
PC4	42-44	0.148	0.016
PC4	44-46	0.107	0.019
PC4	46-48	0.085	0.017
PC4	48-50	0.093	0.024
PC4	50-52	0.059	0.018
PC7	0-2	0.653	0.033
PC7	2-4	0.234	0.029
PC7	4-6	0.150	0.016
PC7	6-8	0.121	0.018
PC7	8-10	0.149	0.019
PC7	10-12	0.089	0.015

Core	Interval (cm)	Cs-137 (dpm/g)‡	Error (dpm/g)
PC7	12-14	0.006	0.002
PC7	14-16	nd	-
PC7	16-18	0.100	0.017
PC7	18-20	0.216	0.027
PC7	20-22	0.063	0.014
PC7	22-24	0.170	0.022
PC7	24-26	0.202	0.022
PC7	28-30	0.123	0.018
PC7	32-34	0.069	0.013
PC7	36-38	nd	-
PC7	40-42	nd	-
PC7	42-44	nd	-
PC7	46-48	nd	-
PC7	50-52	nd	-
PC7	54-56	nd	-
PC7	62-64	nd	-
PC13	14-16	0.243	0.021
PC13	16-18	0.192	0.026
PC13	18-20	0.160	0.025
PC13	22-24	0.233	0.028
PC13	26-28	0.545	0.036
PC13	30-32	0.215	0.027
PC13	32-34	0.308	0.028
PC13	34-36	0.238	0.024
PC13	36-38	0.071	0.013
PC13	38-40	nd	-
PC13	42-44	0.057	0.015
PC13	46-48	nd	-
PC13	54-56	nd	-
PC14	0-2	0.253	0.047
PC14	4-6	0.349	0.055
PC14	6-8	0.547	0.052
PC14	10-12	0.389	0.062
PC14	14-16	0.677	0.076
PC14	18-20	0.657	0.064
PC14	20-22	0.787	0.065
PC14	22-24	0.703	0.062
PC14	24-26	0.734	0.058
PC14	26-28	0.246	0.045
PC14	28-30	0.296	0.047
PC14	30-32	0.021	0.017
PC14	32-34	nd	-
PC14	34-36	0.002	0.003
PC14	38-40	0.044	0.024
PC14	42-44	0.002	0.003
PC14	46-48	0.040	0.022

Core	Interval (cm)	Cs-137 (dpm/g)‡	Error (dpm/g)
PC14	50-52	nd	0.000
PC14	54-56	nd	-
PC14	58-60	nd	0.000
PC14	62-64	nd	0.000
PC14	66-68	0.163	0.038
PC14	70-72	0.009	0.009
PC14	74-76	0.572	0.060
PC14	78-80	0.387	0.050
PC14	82-84	0.060	0.029
PC14	86-88	nd	-
PC14	92-94	nd	-
PC15	0-2	0.230	0.040
PC15	4-6	0.221	0.049
PC15	8-10	0.341	0.061
PC15	12-14	0.324	0.056
PC15	16-18	0.378	0.049
PC15	18-20	0.348	0.055
PC15	22-24	0.377	0.051
PC15	26-28	0.387	0.057
PC15	30-32	0.477	0.047
PC15	34-36	0.598	0.059
PC15	38-40	0.842	0.065
PC15	42-44	0.773	0.060
PC15	44-46	0.736	0.062
PC15	46-48	1.007	0.067
PC15	48-50	0.678	0.069
PC15	52-54	0.699	0.067
PC15	54-56	0.921	0.068
PC15	56-58	0.993	0.071
PC15	58-60	1.142	0.072
PC15	60-62	1.286	0.075
PC15	62-64	1.123	0.069
PC15	64-66	0.573	0.059
PC15	66-68	0.110	0.041
PC15	68-70	nd	-
PC15	70-72	0.015	0.027
PC15	74-76	nd	-
PC15	80-82	nd	-
PC15	84-86	0.059	0.034
PC15	90-92	0.024	0.026
PC16	0-2	2.035	0.001
PC16	2-4	1.999	0.001
PC16	4-6	2.010	0.001
PC16	8-10	1.147	0.001
PC16	12-14	0.400	0.001
PC16	14-16	nd	-

Core	Interval (cm)	Cs-137 (dpm/g) [‡]	Error (dpm/g)
PC16	20-22	nd	-
PC16	32-24	nd	-
PC16	40-42	nd	-
PC16	44-46	nd	-
PC16	58-60	nd	-
MHW	0-2	0.226	0.045
MHW	10-12	0.119	0.026
MHW	20-22	0.062	0.032
MHW	40-42	0.050	0.037
MHW	58-60	0.131	0.040
MHE	2-4	0.102	0.023
MHE	10-12	0.097	0.024
MHE	14-16	0.128	0.022
MHE	20-22	0.184	0.028
MHE	30-32	0.040	0.014
MHE	40-42	0.150	0.027
MHE	46-48	nd	-
111S	8-10	0.051	0.019
111S	22-24	0.171	0.026
111S	34-36	0.133	0.026
144S1	0-2	0.089	0.023
144S1	28-30	0.127	0.023
144S1	58-60	0.060	0.024
177S	6-8	nd	-
177S	24-26	nd	-
177S	40-42	0.013	0.011
257S	4-6	0.056	0.56
257S	20-22	nd	nd
257S	38-40	0.039	0.039

[†] See Appendix C for core locations and details

[‡] Minimum detectible activity (MDA) = 0.05 dpm/g

nd= non-detectible (below MDA)

Core	Interval (cm)	xsPb-210 (dpm/g)	Error (dpm/g)
PC-14	0-2	4.16	0.40
PC-14	4-6	2.80	0.35
PC-14	6-8	2.22	0.33
PC-14	10-12	1.51	0.30
PC-14	14-16	2.21	0.35
PC-14	18-20	1.95	0.31
PC-14	20-22	1.30	0.28
PC-14	22-24	1.09	0.27
PC-14	24-26	1.34	0.28
PC-14	26-28	1.18	0.26
PC-14	28-30	0.63	0.25
PC-14	30-32	0.98	0.24
PC-14	32-34	0.57	0.24
PC-14	34-36	0.80	0.21
PC-15	0-2	5.66	0.72
PC-15	4-6	4.76	0.77
PC-15	8-10	2.27	0.67
PC-15	12-14	3.11	0.69
PC-15	16-18	3.76	0.77
PC-15	18-20	4.52	0.71
PC-15	22-24	3.09	0.63
PC-15	26-28	2.40	0.57
PC-15	30-32	2.38	0.57
PC-15	34-36	1.27	0.55
PC-15	38-40	2.28	0.63
PC-15	42-44	1.35	0.52
PC-15	44-46	1.42	0.54
PC-15	46-48	1.43	0.56
PC-15	48-50	0.96	0.55
PC-15	52-54	1.01	0.53
PC-15	56-58	0.46	0.45
PC-15	58-60	0.69	0.49
PC-15	60-62	0.50	0.45
PC-4	0-2	3.12	0.26
PC-4	2-4	2.54	0.19
PC-4	4-6	2.57	0.20
PC-4	6-8	2.21	0.19
PC-4	8-10	2.19	0.18
PC-4	10-12	3.28	0.21
PC-4	12-14	2.20	0.18
PC-4	14-16	2.93	0.22
PC-4	16-18	2.57	0.19
PC-4	18-20	2.02	0.21
PC-4	20-22	2.46	0.21
PC-4	22-24	2.21	0.22

Core	Interval (cm)	Pb-210 (dpm/g)	Error (dpm/g)
PC-4	28-30	0.93	0.1300
PC-4	32-34	1.71	0.16
PC-4	34-36	1.11	0.15
PC-4	42-44	1.31	0.14
PC-13	14-16	2.04	0.22
PC-13	16-18	3.17	0.26
PC-13	18-20	1.62	0.24
PC-13	20-22	1.73	0.24
PC-13	22-24	2.13	0.25
PC-13	24-26	1.97	0.24
PC-13	26-28	2.01	0.24
PC-13	28-30	1.15	0.22
PC-13	30-32	1.44	0.23
PC-13	32-34	2.09	0.23
PC-13	34-36	0.64	0.18
PC-13	36-38	1.13	0.20
PC-13	38-40	1.31	0.19
PC-13	42-44	0.68	0.20
PC-13	46-48	1.05	0.20
PC-13	54-56	0.39	0.18
MHE	2-4	1.94	0.25
MHE	10-12	3.32	0.29
MHE	14-16	3.67	0.30
MHE	20-22	2.47	0.26
MHE	30-32	1.13	0.19
MHE	40-42	2.09	0.25
MHE	46-48	1.00	0.21
MHE	52-54	1.47	0.25
C-14b	0-2	3.31	0.35
C-14b	2-4	1.42	0.23
C-14b	4-6	0.69	0.22
C-14b	6-8	1.72	0.23
C-14b	8-10	1.84	0.20
C-14b	10-12	2.42	0.23
C-14b	12-14	2.14	0.25
C-14b	14-16	1.18	0.23
C-14b	16-18	1.39	0.18
C-14b	18-20	2.82	0.33
C-14b	20-22	3.25	0.26
C-14b	22-24	1.70	0.25
C-14b	24-26	1.68	0.22
C-14b	26-28	2.74	0.32
C-14b	28-30	2.80	0.28
C-14b	30-32	2.48	0.30

Core	Interval (cm)	Pb-210 (dpm/g)	Error (dpm/g)
C-14b	32-34	2.38	0.27
C-14b	34-36	1.83	0.26
C-14b	38-40	0.84	0.18
C-14b	42-44	0.94	0.19
C-14b	46-48	2.18	0.31
C-14b	50-52	2.95	0.34
C-14b	52-54	4.37	0.43
C-14b	54-56	5.75	0.47